

# Development of electrochemical microfluidic biosensing strategies for microbial detection

Dissertation zur Erlangung des Doktorgrades der Naturwissenschaften

(Dr. rer. nat.)

an der Fakultät Chemie und Pharmazie

der Universität Regensburg

Deutschland



vorgelegt von

**Christian Griesche**

aus Ingolstadt

im Jahr **2021**

Die vorliegende Dissertation entstand in der Zeit von Juni 2017 bis Juni 2021 am Institut für Analytische Chemie, Chemo- und Biosensorik der Universität Regensburg.

Die Arbeit wurde angeleitet von Prof. Dr. Antje J. Bäumner.

Promotionsgesuch eingereicht am: 09.06.2021

Kolloquiumstermin: 22.07.2021



## Acknowledgements

First of all. I want to thank **Prof. Dr. Antje J. Bäumner** for providing me with this interesting and versatile topic, valuable discussions and continuous support especially in cases in which my research did not work out as planned.

Furthermore, I want to thank **Prof. Dr. Sam R. Nugen** for the possibility to work in his lab, **Hannah S. Zurier**, and **Brenda G. Werner** for their continuous help at Cornell University.

Also, I want to thank **Patrick Geier, Thomas Köwer, John Galligan, Kilian Höcherl** and **Michael Schaffer** for their work during their bachelor theses or internships.

I furthermore want to thank **Arne Behrent** for his collaboration in the initial work on LIG, **Marcel Simsek** for providing me with SEM images, and **Vanessa Tomanek** for numerous beautiful drawings and her assistance when working with bacteria.

As well I thank my lab-mates **Simone Rink** and **Florian Gerstl** for making the long hours in the lab enjoyable even when progress was slow. I also want to thank all other colleagues contributing to an excellent atmosphere in the working group.

No less, I want to thank especially **my parents** for their invaluable support and their love.



## **Declaration of Collaborations**

Most of the theoretical and experimental work presented in this thesis was conducted solely by the author. However, parts of the results were gained in collaboration with other researchers, which are stated in this section in accordance with §8 Abs. 1 Satz 2 Punkt 7 of the “Ordnung zum Erwerb des akademischen Grades eines Doktors der Naturwissenschaften (Dr. rer. Nat.) an der Universität Regensburg vom 18. Juni 2009”.

### **Biosensors to support sustainable agriculture and food safety (Chapter 1)**

The literature search and writing of the review was done by Antje J. Baeumner and the author. The author wrote the first draft of the manuscript. Antje J. Baeumner revised the manuscript. Antje J. Baeumner is corresponding author.

### **Electrochemical lab-on-a-chip systems (Chapter 2)**

The concept for the review article, including this chapter, was developed by Nongnoot Wongkaew and Antje J. Baeumner. The literature search and writing of this chapter was done by Nongnoot Wongkaew, Antje J. Baeumner and the author. The author wrote the first draft of this chapter. Nongnoot Wongkaew, Marcel Simsek and Antje J. Baeumner revised the manuscript. Antje J. Baeumner is corresponding author.

### **Substrate-Independent Laser-Induced Graphene Electrodes for Microfluidic Electroanalytical Systems (Chapter 3)**

Antje J. Baeumner and the author planned the experiments. The author did most of the experimental work. Kilian Hoecherl helped with the microfluidic electrochemical characterization of LIG and tLIG. The author wrote the first draft of the manuscript. Antje J. Baeumner and Kilian Hoecherl revised the manuscript. Antje J. Baeumner is corresponding author.

### **Electrochemical detection of *Escherichia coli* via genetically modified bacteriophages (Chapter 4)**

Sam R. Nugen and Antje J. Baeumner developed the concept for this work. Antje J. Baeumner and the author planned the detailed experiments. The author did most of the experimental work. Hannah S. Zurier prepared the *E. coli* lysate. Brenda G. Werner performed initial experiments on the electrochemical detection. The author wrote the first draft of the manuscript. Sam R. Nugen and Hannah S. Zurier wrote the experimental part on bacteriophages, bacterial cultures, and *E. coli*

infection. Hannah S. Zurier, Sam R. Nugen and Antje J. Baeumner revised the manuscript. Antje J. Baeumner is corresponding author.

**Liposome-based POCT sensors for the detection of beta-hemolytic *Streptococcus pyogenes* (Chapter 5)**

Antje J. Baeumner and the author planned the experiments. The author did most of the experimental work. Michael Schaffer helped with electrochemical measurements. The author wrote the first draft of the manuscript. Antje J. Baeumner revised the manuscript.

## Contents

Summary .....	1
Zusammenfassung.....	3
Introduction and Structure of the Thesis .....	6
1 Biosensors to support sustainable agriculture and food safety .....	10
1.1 Introduction.....	11
1.1.1 Contamination of Food .....	13
1.1.1.1 Contaminants in food.....	13
1.1.1.2 Food Fraud .....	17
1.1.2 Sustainable Agriculture .....	19
1.1.3 Biosensors .....	19
1.1.3.1 Definition.....	19
1.1.3.2 Biorecognition elements .....	19
1.2 Biosensors within the food supply chain .....	21
1.3 Biosensors in food safety .....	22
1.3.1 Bacteria .....	22
1.3.2 Veterinary Drugs.....	26
1.3.3 Mycotoxins .....	27
1.3.4 Pesticides .....	27
1.3.5 Other contaminants.....	28
1.4 Food Fraud .....	29
1.5 Biosensors supporting sustainable agriculture .....	30
1.6 Biosensors supporting livestock and animal health .....	34



1.7 Conclusion and Future Perspective .....	38
1.8 References.....	40
2 Electrochemical Lab-on-a-Chip Systems.....	51
2.1 Definition.....	51
2.2 Design of lab-on-a-chip systems .....	51
2.2.1 Materials and fabrication .....	51
2.2.2 Integration of Sample Preparation .....	52
2.2.3 On-chip electrochemistry.....	55
2.3 References.....	59
3 Substrate-Independent Laser-Induced Graphene Electrodes for Microfluidic Electroanalytical Systems .....	64
3.1 Introduction.....	65
3.2 Experimental Section .....	67
3.2.1 Reagents.....	67
3.2.2 Laser-Induced Graphene (LIG).....	67
3.2.2.1 Infiltration Transfer of Laser-Induced Graphene to PDMS.....	67
3.2.2.2 Pressure-Driven Transfer of Laser-Induced Graphene to PMMA (tLIG) .....	67
3.2.3 Microfluidic Setup.....	68
3.2.3.1 Fabrication of Microfluidic Channels with Indirect Bonding using Adhesive Tape .....	68
3.2.3.2 Fabrication of Microfluidic Channels with Solvent Bonding of Polyimide to PMMA Microfluidic Channels .....	68
3.2.4 LIG Characterization.....	69
3.2.4.1 Sheet Resistance.....	69

3.2.4.2 Contact Angle .....	69
3.2.4.3 Electrode Morphology .....	69
3.2.4.4 Raman Spectroscopy.....	69
3.2.5 Electrochemical Measurements .....	69
3.2.5.1 Cyclic Voltammetry .....	69
3.2.5.2 Square Wave Voltammetry .....	70
3.2.5.3 Amperometry .....	70
3.2.5.4 Detection of Alkaline Phosphatase .....	70
3.3 Results and Discussion .....	70
3.3.1 Laser-Induced Graphene Electrodes in Microfluidics .....	76
3.3.2 Detection of Alkaline Phosphatase .....	79
3.4 Conclusions.....	80
3.5 References.....	81
3.6 Supporting Information .....	84
4 Electrochemical detection of <i>Escherichia coli</i> via genetically modified bacteriophages.....	93
4.1 Introduction.....	94
4.2 Material and Methods .....	95
4.2.1 Reagents and Materials .....	95
4.2.2 Bacteriophage and Bacterial Cultures.....	96
4.2.3 Assay Procedure .....	96
4.2.4 Statistical evaluation.....	97
4.3 Results and Discussion .....	98
4.4 Conclusion .....	103

4.5 References.....	105
4.6 Supporting Information .....	108
5 Liposome-based POCT sensors for the detection of beta-hemolytic Streptococcus pyogenes.....	112
5.1 Introduction.....	113
5.2 Material and Methods .....	114
5.2.1 Materials and Bacterial Strains.....	114
5.2.2 Liposome preparation.....	115
5.2.3 Preparation of laser-induced graphene electrodes.....	115
5.2.4 Electrochemical measurements .....	115
5.3 Results and Discussion .....	116
5.4 Conclusion .....	119
5.5 References.....	121
5.6 Supporting Information .....	123
6 Conclusions and Future Perspective .....	124
6.1 References .....	128
Curriculum Vitae.....	130
Publications.....	132
Presentations .....	133
Eidesstattliche Erklärung .....	134



### Summary

Access to safe and nutritious food is mandatory for sustaining life and promoting health. While contaminated food directly is connected to illness and death food safety also is closely linked to nutrition and food security, whereby a safe food supply chain is supporting national economies, trade, and tourism. Modern challenges in the food supply include a growing world population, globalization as well as climate change, or soil degradation. While these changes affect everyone, the developing world is predominantly affected by unsafe food while suffering from a lack of infrastructure especially expensive equipment and trained personnel. To overcome these challenges biosensors are identified as promising tools to enable the monitoring of food along the whole food supply chain with the ease of their integration into mobile solutions. The fields of electrochemistry, microfluidics, and biosensors complement one another in this objective with special emphasis on novel electrode materials and detection strategies for the design of highly sensitive, reliable but cost-efficient biosensors.

#### **Substrate-independent laser-induced graphene electrodes**

Discovered in 2014 laser-induced graphene (LIG), directly derived from polyimide films, is particularly interesting with the ease of its production in contrast to other materials from the graphene family. While the growing number of publications on electrochemical sensors represent this interest the inertness of the polyimide substrate limits its integration into microfluidic devices. In addition to already established transfer techniques, a pressure-driven transfer of LIG to thermoplastic polymeric substrates was developed and the derived transferred laser-induced graphene (tLIG) was compared with LIG. Morphologically and chemically the surface of tLIG and LIG differed whereby tLIG showed a much smoother surface, resulting in a much lower electrochemically active surface area, a higher sheet resistance, and a slightly decreased electron transfer rate. Additionally, the graphene characteristic Raman 2D peak was not maintained after transfer. Besides all morphological differences, in amperometric detection both LIG compounds performed equally well for the detection of *p*-aminophenol, ruthenium (III) hexamine, and potassium ferrocyanide. A microfluidic chip was fabricated using adhesive tape for the indirect binding using a poly(methyl methacrylate) (PMMA) microfluidic channel. Channel height and flow rate were optimized towards the sensitive amperometric detection of *p*-aminophenol, the product of the enzymatic conversion of *p*-aminophenyl phosphate by alkaline phosphatase. Alkaline phosphatase, commonly detected as a biomarker or used as a biosensing amplification system, was detected with a limit of detection of  $0.3 \text{ U L}^{-1}$  requiring a sample volume of only  $40 \mu\text{L}$ .

### **Bioassays for microbial detection**

For the detection of *Escherichia coli* (*E. coli*) an electrochemical bioassay based on the utilization of genetically modified bacteriophages (phages) was developed. A lytic T7 phage was engineered to overexpress alkaline phosphatase (ALP) fused to a cellulose-specific carbohydrate-binding module after the infection of viable *E. coli* cells within 30 min incubation. Before the electrochemical detection, the expressed ALP is concentrated out of the media, by its affinity tag, simply by filtration of the bacteria lysate through cellulose. The amount of immobilized ALP directly correlates to the original bacteria concentration and is utilized for the enzymatic conversion of a substrate and the following electrochemical detection of the generated product. The enzymatic substrates *p*-aminophenyl phosphate (pAPP) and *p*-nitrophenyl phosphate (pNPP) were tested whereby pAPP outperformed pNPP for the electrochemical detection of the resulting product with screen-printed carbon electrodes. The enzymatic reaction was optimized with respect to pH, reaction time, reaction temperature, and substrate concentration resulting in a limit-of-detection of  $10^3$  CFU mL<sup>-1</sup> within just 2 h. The simplicity of the bioassay, its low cost, and its ruggedness against matrix interferences displays the potential for the application in various complex sample matrices especially in resource-limited areas. Hereby the sensitivity can be enhanced by the cultivation of the bacteria before phage infection or the processing of higher sample volumes or even further by a combination of both approaches.

*Streptococcus pyogenes* (*S. pyogenes*) are usually detected by their beta-hemolytic activity with cultivation on a blood agar plate in laboratory diagnosis. Besides the requirement of trained personnel, the detection is time-consuming and limits the timely decision on the right medical treatment. Liposomes, as erythrocyte surrogates, were exploited for the detection of *S. pyogenes* by utilizing their beta-hemolytic activity. Liposomes, composed of phospholipids and cholesterol, are synthesized by the reverse-phase evaporation method and encapsulate electrochemical active potassium ferrocyanide. Hereby the liposome size was directly controlled with the applied membranes, with various pore sizes, at the extrusion. The detection principle relies on the lysis of the liposomes by exotoxins of *S. pyogenes* and the electrochemical detection of the released potassium ferrocyanide using LIG electrodes. After 7 h of cultivation, *S. pyogenes* was detected within 15 min. The limits of detection were  $10^2$  to  $10^3$  CFU mL<sup>-1</sup> whereby larger liposomes (hydrodynamic diameter 700 nm and 340 nm, respectively) were found to be slightly more sensitive compared to smaller liposomes (180 nm hydrodynamic diameter). Furthermore, the specificity of the detection for beta-hemolysis was verified with non-hemolytic *E. coli* and heat-inactivated *S. pyogenes*.

### Zusammenfassung

Der Zugang zu gesunden und nahrhaften Lebensmitteln ist zwingend erforderlich, um Leben zu erhalten und die Gesundheit zu fördern. Während direkte Folgen von kontaminierter Nahrung Krankheit und auch Todesfälle beinhalten, besteht auch eine Verbindung zwischen Lebensmittelsicherheit und Ernährung sowie der Ernährungssicherung. Hierbei unterstützt eine gesicherte Lebensmittelversorgung für nationale Wirtschaften, Handel und Tourismus. Moderne Herausforderungen in der Lebensmittelversorgung beinhalten eine steigende Weltbevölkerung, die zunehmende Globalisierung, den Klimawandel und die, sich zunehmend verschlechternde, Bodenqualität. Obwohl diese Änderungen jeden betreffen sind, insbesondere Entwicklungsländer von den Folgen fehlender Lebensmittelsicherheit, aufgrund fehlender Infrastruktur, teurer Laborausstattung und qualifiziertem Personal, betroffen. Biosensoren wurden als vielversprechende Werkzeuge identifiziert, um diese Herausforderungen zu meistern. Ihre Integrierbarkeit in portable Geräte ermöglicht die Überwachung von Lebensmitteln entlang der gesamten Lebensmittelkette. Die Fachgebiete Elektrochemie, Microfluidik und Biosensoren ergänzen sich hierbei. Insbesondere neue Elektrodenmaterialien und Nachweisstrategien sind hierbei der Schlüssel für die Entwicklung von hochsensitiven, verlässlichen und kostengünstigen Biosensoren.

#### **Substratunabhängige *laser-induced graphene* Elektroden**

Das 2014 entdeckte *laser-induced graphene* (LIG) kann direkt aus Polyimidfolien gewonnen werden. Aufgrund dieser einfachen Fabrikation ist LIG von besonderem Interesse, da es sich hierdurch von anderen Graphenmaterialien unterscheidet. Während die zunehmende Anzahl von Publikationen an elektrochemischen LIG-Sensoren dieses Interesse unterstreicht, ist die Integration von Polyimide in mikrofluidische Detektionssysteme erschwert durch seine Lösungsmittelbeständigkeit und thermische Stabilität. Zusätzlich zu bestehenden Transferstrategien wurde ein neues, auf Druck basierendes, Transferverfahren für den Transfer von LIG auf Thermoplaste entwickelt. Die morphologischen und elektrochemischen Eigenschaften des transferierten LIG (tLIG) wurden untersucht und mit LIG verglichen. Hierbei weist tLIG eine weniger poröse Oberfläche im Vergleich mit LIG auf. tLIG weist eine geringere aktive Elektrodenoberfläche, einen höheren Flächenwiderstand und geringfügig verringerte Elektronentransferraten auf. Zusätzlich bleibt der, für Graphen, charakteristische 2D -Peak im Ramanspektrum nicht während des Transfers erhalten. Trotz aller morphologischen Unterschieden sind die Ergebnisse in amperometrischen Messungen für beide LIG-Materialien vergleichbar für die Analyten p-Aminophenol, Hexaamineruthenium(III) und Kaliumhexacyanoferrat(II). Mittels doppelseitiger Klebebänder wurden mikrofluidische Chips,

unter Verwendung von Polymethylmethacrylat (PMMA), hergestellt. Der Einfluss der Höhe des mikrofluidischen Kanals und der Fließgeschwindigkeit der Probenlösung wurde für die nachweisstarke Bestimmung von *p*-Aminophenol, dem Reaktionsprodukt der enzymatischen Umsetzung von *p*-Aminophenolphosphat mittels alkaliner Phosphatase, optimiert. Alkaline Phosphatase ist zum einen ein häufig detektierter Biomarker und andererseits zur enzymatischen Signalverstärkung in der Biosensorik. In dem entwickelten mikrofluidischen System konnte alkaline Phosphatase mit einem Detektionslimit von  $0.3 \text{ U L}^{-1}$ , unter Verwendung von  $40 \mu\text{L}$  Probelösung, detektiert werden.

### **Bakteriellen Nachweis durch Bioassays**

Zur Bestimmung von *Escherichia coli* (*E. coli*) wurde ein elektrochemischer Bioassay unter der Verwendung von genetisch veränderten Bakteriophagen entwickelt. Eine lytische T7 Bakteriophage wurde gentechnisch verändert um alkaline Phosphatase (ALP), die ein für Zellulose spezifischen Kohlenhydrat-Bindungsmodul beinhaltet, zu exprimieren. Hierbei wird ALP innerhalb von 30 min nach der Infektion von vitalen *E. coli* Zellen freigesetzt. Der Affinitäts-Tag ermöglicht die einfache Anreicherung von ALP auf Zellulose durch Filtration des Mediums, nach Lyse der Bakterien, vor der elektrochemischen Bestimmung. Die Menge an immobilisierter ALP korreliert hierbei direkt mit der ursprünglichen *E. coli* Konzentration und wird für die enzymatische Umsetzung eines Enzymsubstrats und der folgenden elektrochemischen Detektion des Produkts verwendet. Hierzu wurden die Substrate *p*-Nitrophenolphosphat (pNPP) und *p*-Aminophenolphosphat (pAPP) getestet wobei pAPP eine nachweisstärkere Detektion mittels *screen-printed carbon electrodes* ermöglicht. Die enzymatische Reaktion wurde unter Einbeziehung von pH-Wert, Reaktionszeit, Reaktionstemperatur und Substratkonzentration optimiert, wodurch eine untere Nachweisgrenze von  $10^3 \text{ CFU mL}^{-1}$  *E. coli* innerhalb von 2 h mit dem entwickelten Bioassay erreicht wurde. Die Einfachheit des Bioassays kombiniert mit geringen Kosten und die hohe Robustheit gegenüber störenden Matrixeffekten zeigt das Potential für zukünftige Anwendungen, insbesondere in Gebieten mit beschränkten Ressourcen. Durch die Kultivierung von Bakterien vor der Infektion mit Bakteriophagen oder die Filtration von größeren Volumina, sowie eine Kombination beider Strategien kann die Sensitivität der Detektion weiter verbessert werden.

In der Labordiagnostik wird zum Nachweis von *Streptococcus pyogenes* (*S. pyogenes*), mittels Kultivierung auf Blutagar, deren Beta-Hämolyse genutzt. Neben der Notwendigkeit von qualifiziertem Personal ist diese Nachweismethode sehr zeitaufwändig und begrenzt die zeitige Einbeziehung der Ergebnisse für medizinische Behandlungen. Liposome, als Stellvertreter für Erythrozyten, wurden für den Nachweis von *S. pyogenes*, aufgrund ihrer Beta-Hämolyse, genutzt. Liposome, zusammengesetzt aus Phospholipiden und Cholesterol, wurden mittels



Rückphasenverdampfung synthetisiert wobei elektrochemisch aktives Kaliumhexacyanoferrat(II) eingeschlossen wurde. Hierbei wurde die Größe der Liposome durch die Verwendung von Membranen mit unterschiedlichen Porengrößen, während der Extrusion, kontrolliert. Die Detektionsstrategie basiert auf der Lyse von Liposomen durch, von *S. pyogenes* produzierten, Exotoxine und der anschließenden elektrochemischen Bestimmung von freigesetztem Kaliumhexacyanoferrat(II) unter Verwendung von LIG Elektroden. Nach 7 h Kultivierung konnte *S. pyogenes* innerhalb von 15 min detektiert werden wobei untere Nachweisgrenzen von  $10^2$  CFU mL<sup>-1</sup> bis  $10^3$  CFU mL<sup>-1</sup> erreicht wurden. Größere Liposome mit hydrodynamischen Durchmessern von 700 nm und 340 nm erwiesen sich hierbei ein wenig nachweisstärker im Vergleich zu Liposomen mit einem hydrodynamischen Durchmesser von 180 nm. Die Sensitivität des Nachweises von Beta-Hämolyse wurde anhand von nicht-hämolysierenden *E. coli* und hitzedeaktivierten *S. pyogenes* gezeigt.

## Introduction and Structure of the Thesis

This thesis describes the preparation, characterization, and (bio)analytical application of microfluidic chips incorporating laser-induced graphene electrodes for electrochemical sensing and the development of advanced biosensing principles for fast and inexpensive microbial detection with special consideration of novel reporter probes for the possible implementation in sensitive, miniaturized and cost-efficient mobile sensors.

Since the invention of the first biosensor by Clark and Lyons in 1962 [1] subsequent research on biosensors has contributed to tremendous advances in multiple scientific and technological areas with an emphasis on healthcare and medical areas, environmental areas, and the food industry [2]. Throughout the decades the combination of various biorecognition elements and transducers has led to numerous biosensor platforms for countless analytes and biosensors have been identified as powerful tools for highly sensitive, specific, rapid, and inexpensive detection. Food contaminants, including harmful bacteria, viruses, parasites, or chemical substances, are related to more than 200 diseases and 600 million sick people worldwide every year with the developing world been affected particularly severely [3]. Already existing and ongoing challenges in ensuring food safety are the globalization of the food market, climate change, and a growing world population and require effort to monitor food along the food chain and sustainable agricultural practices. **Chapter 1** gives an overview of the latest biosensor developments addressing food safety and the affiliated areas of sustainable agriculture and food fraud. The major trends that can be observed within the latest biosensor development are the integration and combination of novel materials, with a focus on nanomaterials, to long-time established sensors as well as the increasing use of synthetic aptamers as biorecognition element [4].

Being ideal tools for simple, quick and affordable analysis the miniaturization of biosensors miniaturization is key for their application in point-of-care applications or the detection on-field whereby electrochemically is particularly suited. While the miniaturization of sensing electrodes, in general, does not compromise detection limits downscaled electrochemical components can be produced with advanced microfabrication technologies with low production cost and operated with low-power requirements [5]. In recent years the convergence of biosensors, electrochemistry, and microfluidics has formed new application areas including lab-on-a-chip formats [6]. **Chapter 2** highlights electrochemical lab-on-a-chip systems with a focus on the variety and fabrication of applied microfluidic substrates and electrode materials.

Being key for the sensitivity of the electrochemical detection in lab-on-chip devices the working electrode material ideally exhibits a favorable redox behavior towards the respective analyte [7].

The most commonly used electrode materials are carbon electrodes and novel metals like gold and platinum with their long-established thin-film and thick-film fabrication techniques. In the last decades, the steadily growing graphene hype led to the development of numerous novel electrode materials [8]. Among that novel, carbon materials laser-induced graphene (LIG) is predestined as electrode material for microfluidic chips due to its excellent electrochemical properties and simple one-step fabrication using commercial polyimide films enabling roll-to-roll manufacturing [9]. To overcome the challenging integration of inert polyimide into polymeric microfluidic chips transfer strategies of LIG to PMMA and the integration into microfluidic chips are described (**Chapter 3**). LIG and transferred LIG (tLIG) are characterized electrochemically off-chip using common redox-markers ruthenium hexamine and potassium ferrocyanide. The performance of electrochemical microfluidic chips is optimized towards the detection of alkaline-phosphatase regarding the channel height and flow rate.

**Chapter 4** describes a novel electrochemical bioassay format for the detection of *Escherichia coli* (*E. coli*). For this purpose, bacteriophages, genetically engineered to overexpress alkaline phosphatase (ALP), are utilized as biorecognition elements. In contrast to commonly used aptamers and antibodies, bacteriophages can distinguish between dead and alive bacteria. Solely viable *E. coli* are infected by the bacteriophages and produce ALP fused with a cellulose affinity tag. Automated filtration through cellulose disc captures and concentrates the expressed alkaline phosphatase. Hereby the amount of captured alkaline phosphatase directly correlates with the number of viable *E. coli* and is quantified by the electrochemical detection of enzymatically generated *p*-aminophenol using *p*-aminophenyl phosphate as enzymatic substrate. The sensitivity of the assay was optimized to pH, temperature, reaction time, and substrate concentration of the enzymatic reaction.

Liposomes – artificial vesicles consisting of a hydrophobic bilayer separating the inner hydrophilic cavity from the outer hydrophilic medium – were described first by the group of Bangham in 1964 and originally used as a model for biological cell membranes [10]. Today liposomes are widely used as versatile tools for drug delivery [11] as well as in analytical bioassays as powerful signal amplifiers [12]. **Chapter 5** describes the electrochemical detection of  $\beta$ -hemolytic *Streptococcus pyogenes* (*S. pyogenes*). *S. pyogenes* produces exotoxins that lyse red blood cells. Used as cell substitutes liposomes, encapsulating electrochemical active potassium ferrocyanide, are lysed in the presence of  $\beta$ -hemolytic *S. pyogenes* and the encapsulated potassium ferrocyanide is released. The number of lysed liposomes and the amount of released potassium ferrocyanide is found to directly correlate with the bacterial concentration and is quantified amperometrically using LSG electrodes. The time-dependency and concentration-dependency of the bacteria-

liposome interaction were investigated for liposomes of different sizes and the specificity of liposome lysis was verified using non-hemolytic *E. coli* and heat-inactivated *S. pyogenes*.

In **Chapter 6** the results and insights of this thesis are discussed with respect to the main advantages but also drawbacks of electrochemical biosensors with special emphasis on combination with the utilized detection principles. Furthermore, this chapter addresses the future challenges and perspectives of biosensor applications.

## References

- [1] L.C. Clark Jr., C. Lyons, ELECTRODE SYSTEMS FOR CONTINUOUS MONITORING IN CARDIOVASCULAR SURGERY, *Ann. N. Y. Acad. Sci.* 102 (1962) 29–45. <https://doi.org/https://doi.org/10.1111/j.1749-6632.1962.tb13623.x>.
- [2] V. Zucolotto, Specialty Grand Challenges in Biosensors, *Front. Sensors.* 1 (2020) 3. <https://doi.org/10.3389/fsens.2020.00003>.
- [3] WHO | WHO estimates of the global burden of foodborne diseases, WHO. (2019). [http://www.who.int/foodsafety/publications/foodborne\\_disease/fergreport/en/](http://www.who.int/foodsafety/publications/foodborne_disease/fergreport/en/) (accessed February 28, 2021).
- [4] K. Zhang, H. Li, W. Wang, J. Cao, N. Gan, H. Han, Application of Multiplexed Aptasensors in Food Contaminants Detection, *ACS Sensors.* 5 (2020) 3721–3738. <https://doi.org/10.1021/acssensors.0c01740>.
- [5] F.M. Matysik, Miniaturization of electroanalytical systems, *Anal. Bioanal. Chem.* 375 (2003) 33–35. <https://doi.org/10.1007/s00216-002-1635-x>.
- [6] D.G. Rackus, M.H. Shamsi, A.R. Wheeler, Electrochemistry, biosensors and microfluidics: a convergence of fields, *Chem. Soc. Rev.* 44 (2015) 5320–5340. <https://doi.org/10.1039/c4cs00369a>.
- [7] J. Wang, Electrochemical detection for microscale analytical systems: A review, *Talanta.* 56 (2002) 223–231. [https://doi.org/10.1016/S0039-9140\(01\)00592-6](https://doi.org/10.1016/S0039-9140(01)00592-6).
- [8] E.M. Kirchner, T. Hirsch, Recent developments in carbon-based two-dimensional materials: synthesis and modification aspects for electrochemical sensors, *Microchim. Acta.* 187 (2020) 1–21. <https://doi.org/10.1007/s00604-020-04415-3>.
- [9] N. Kurra, Q. Jiang, P. Nayak, H.N. Alshareef, Laser-derived graphene: A three-dimensional printed graphene electrode and its emerging applications, *Nano Today.* 24 (2019) 81–102. <https://doi.org/10.1016/j.nantod.2018.12.003>.
- [10] A.D. Bangham, R.W. Horne, Negative staining of phospholipids and their structural modification by surface-active agents as observed in the electron microscope, *J. Mol. Biol.* 8 (1964) 660–668. [https://doi.org/10.1016/S0022-2836\(64\)80115-7](https://doi.org/10.1016/S0022-2836(64)80115-7).
- [11] B.S. Patti, V. V. Chupin, V.P. Torchilin, New Developments in Liposomal Drug Delivery, *Chem. Rev.* 115 (2015) 10938–10966. <https://doi.org/10.1021/acs.chemrev.5b00046>.

- [12] J. Sforzi, L. Palagi, S. Aime, Liposome-based bioassays, *Biology (Basel)*. 9 (2020) 1–28.  
<https://doi.org/10.3390/biology9080202>.

# 1 Biosensors to support sustainable agriculture and food safety

## Highlights

- The most current biosensors for food safety and food fraud are reviewed
- Biosensors supporting sustainable agriculture and livestock are highlighted
- The future role of biosensors for improving food safety is discussed

## Abstract

Food safety affects everyone worldwide and will remain a global challenge to human health in the foreseeable future requiring the rapid, sensitive, efficient and inexpensive detection of food contaminants. Biosensors have long been investigated to be part of a solution. In fact, current research trends of nanoscale science and technology, efforts of miniaturization and connectivity enabled through the internet of things boost biosensors' capabilities to a degree that they surely will play a major part of the answer to this global challenge. Surprisingly though, the adaption of such biosensors to function along the entire food value chain and hence also include important aspects of sustainable agriculture and food fraud has been neglected so far. In this review, the latest developments of biosensors addressing these issues are presented for the years 2015 – 2019 and point toward important new strategies needed to truly ensure safe food in a sustainable global market.

## Keywords

biosensors, food safety, food fraud, sustainable agriculture, livestock monitoring, wearable sensors

---

**This chapter has been published.**

Christian Griesche, Antje J. Baeumner, *Trends in Analytical Chemistry*, **2020** (128) 115906. DOI: <https://doi.org/10.1016/j.trac.2020.115906>

**Author contributions:** The literature search and writing of the review was done by CG and AJB. CG wrote the first draft of the manuscript. AJB revised the manuscript. AJB is corresponding author.

## Abbreviations

EIS	electrochemical impedance spectroscopy
ELISA	enzyme-linked immunosorbent assay
FAO	Food and Agriculture Organization of the United Nations
GMO	genetically modified organism
ICSDP	isothermal circular strand displacement polymerization
IUPAC	International Union of Pure and Applied Chemistry
LAMP	loop-mediated isothermal amplification
LOD	Limit of Detection
OTA	Ochratoxin A
PCR	polymerase chain reaction
PNA	peptide nucleic acid
SERS	surface-enhanced Raman scattering
SPR	surface plasmon resonance
ssDNA	single-stranded DNA
TTI	time-temperature integrators
UCNP	upconverting nanoparticle
USD	United States dollar
USDA	United States Department of Agriculture
VOC	volatile organic compound
WHO	World Health Organization

## 1.1 Introduction

Access to safe and nutritious food not only is key to sustaining life and promoting good health but also underpins sustainable development by supporting national economies [1]. This effect of safe food was often underestimated due to underreporting and difficulty to establish a causation between contaminated food, until the WHO Foodborne Disease Burden Epidemiology Reference

Group (FERG) published their report “WHO estimates of the global burden of foodborne diseases” in 2015. [1][2] Just 31 foodborne hazards causing 32 diseases were included in this report being responsible for 600 million foodborne illnesses and 420,000 deaths in one year. According to the WHO’s findings the burden of foodborne diseases is differently distributed by age and location. Especially children under the age of 5 and low-income subregions of e.g. Africa or South East Asia, suffer from foodborne diseases [2].

As food safety clearly has to be increased for the developing world, ensuring food safety also is a continuous challenge everywhere else. This need becomes obvious as constant or even increasing number of food recalls are seen among developed countries in this decade. In the US the number of food recalls increased by 10% from 2013 to 2018 [3] while in Germany the warnings on dangerous food were more than doubled in the same period [4].

The world’s growing population, leading to increasing demands of food and being linked to the industrialization and intensification of agriculture and animal husbandry, results in both challenges and opportunities for safe food. Other factors contributing to emerging risks are caused by the climate change and in globalization. Higher temperatures are predicted to modify food safety risks during production, storage and distribution, while the globalization leads to a longer and more complex food chain, often passing several borders. [1][5] The lack of keeping track of food from field to plate became obvious in the European *E. Coli* outbreak with its center in Germany in 2011 resulting in more than 50 deaths. Due to insufficient monitoring of the food chain the outbreak was wrongly attributed to imported cucumbers in a first action. This led to huge economic loss in producing countries and insecurity among costumers before the outbreak was finally attributed to sprouts and even one year after the outbreak the identity of source remained a controversy [6].

The relevance of biosensors for ensuring food safety is shown by a projected market growth from 17 billion dollars in 2018 to 24.6 billion dollars in 2023 [7]. Consequently, biosensors in their applications to food safety are a research field of growing interest with rising numbers of publications (Fig. 1A) including a range of reviews covering topics including those focusing on specific analytes or detection methods to those that provide a comprehensive overview of recent publications. This review will focus on publications of the last two years regarding the detection of food contaminants and highlight biosensor development of 2015 – 2019 that supports food safety throughout the entire food chain.



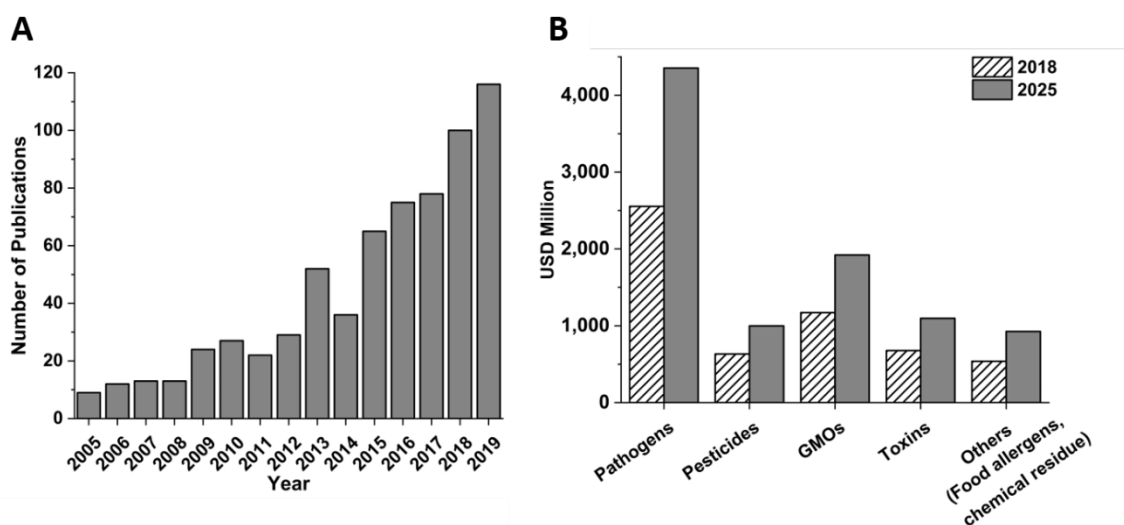


Fig. 1 **A** Number of publications from 2005 to 2019 for biosensors for food safety (results according to Web of science for “biosensor” + “food safety”) **B** Volume of the north american food safety testing market by contaminants, estimated for 2018 and 2025, adapted from ref [8].

### 1.1.1 Contamination of Food

#### 1.1.1.1 Contaminants in food

In the “General Standard for Contaminants and Toxins in Food and Feed” the WHO, together with the Food and Agriculture Organization of the United Nations (FAO) define a contaminant as any substance not being intentionally added to food or feed and being present as a result of the production, manufacture, processing, preparation, treatment, packing, packaging transport or holding or being present due to environmental contamination [9]. The Codex Alimentarius Commission set maximum limits for mycotoxins, metals, radionuclides and other organic chemicals. While other contaminants as pesticide residues, residues of veterinary drugs, microorganisms, microbial toxins and residues of processing aids are excluded due to being in the terms of other committees. In addition to above mentioned contaminants publications for the detection of food allergens are included as the prevalence of food allergy, especially in developed countries, are increasingly resulting in a growing health burden [10]. For all categories of analytes, except radionuclides, biosensors were published in 2018 and 2019 and are summarized in table 1, sorted by analytes and providing information about the used biorecognition elements, the used detection technique, the assay time and their limits of detection (LOD). The same trend on the analyte choice from researchers could be observed when monitoring a longer period [11].

Table 1: Reviewed biosensors for the detection of food contaminants sorted by contaminants with utilized biorecognition element, detection method, assay time, food sample, pretreatment and limit of detection (LOD).

Category	Analyte	Biorecognition element	Detection method	Assay time	Food sample	Pretreatment	LOD	ref
Microorganism	<i>E. Coli O157:H7</i>	Aptamer	SERS	20 min	ground beef	1	10 <sup>1</sup> CFU/mL (culture medium)	[31]
	<i>E. Coli O157:H7</i>	Aptamer	Colorimetric	>15 min	ground beef	1	10 <sup>3</sup> CFU/mL (ground beef) 25 CFU/mL (culture medium)	[32]
	<i>E. Coli</i>	Bacteriophage	Refractive Index	7 min	-	2a	233 CFU/mL (ground beef)	[33]
	<i>E. Coli O157:H7</i>	ssDNA	Piezoelectric	≈ 1 h	milk	10, 4	10 <sup>3</sup> CFU/mL	[34]
	<i>Vibrio parahaemolyticus</i>						3.254 x 10 <sup>-18</sup> mol/L (DNA)	
	<i>Salmonella choleraesuis</i>						6.463 x 10 <sup>-18</sup> mol/L (DNA)	
	<i>Staphylococcus aureus</i>						6.865 x 10 <sup>-18</sup> mol/L (DNA)	
	<i>Listeria monocytogenes</i>						8.696 x 10 <sup>-18</sup> mol/L (DNA)	
	<i>Shigella dysenteriae</i>						1.824 x 10 <sup>-18</sup> mol/L (DNA)	
	<i>Salmonella Typhimurium</i>	Aptamer	Electrochemical	≈ 4 h	-	2a	15.385 x 10 <sup>-18</sup> mol/L (DNA)	[35]
	<i>Salmonella Typhimurium</i>	Antibody	Electrochemical	≈ 3 h	-	2a	8 CFU/mL	[36]
	<i>Salmonella typhimurium</i>	Antibody	Fluorescence	2 h	apple juice	5	833 – 1000 Cells/mL	[37]
	<i>Salmonella typhimurium</i>	PNA	Colorimetric	≈ 30 min	milk	3, 6	58 CFU/mL	[38]
	<i>Salmonella typhimurium</i>	Antibody	Electrochemical	125 min 155 min	skim milk	-	4 CFU/mL 10 CFU/min	[39]
	<i>Salmonella enteritidis</i>	Antibody	Colorimetric	20 min	whole milk water, watermelon juice, salads	7b 2b	10 <sup>2</sup> CFU/mL	[40]
	<i>Salmonella Enteritidis</i>	Antibody	Colorimetric	11 min	water, pork, tomato	2b	80 CFU/mL	[41]
	<i>Salmonella Typhimurium</i>	Antibody	Piezoelectric	≈ 2 h	chicken meat	1, 9, 7b	10 <sup>6</sup> CFU/mL	[42]
	<i>Salmonella Typhimurium</i>	Antibody	SPR	> 16 h	chicken rinse	9	6.8 CFU/mL	[43]
	<i>Salmonella typhimurium</i> , <i>Listeria monocytogenes</i>	Antibody	SERS	> 15 min	milk	2b	75 CFU/mL	[44]
	<i>Listeria monocytogenes</i>	Antibody	Electrochemical	≈ 1 h	milk	5	75 CFU/mL 22 CFU/mL (buffer) 5.5 CFU/mL (milk)	[45]

Category	Analyte	Biorecognition element	Detection method	Assay time	Food sample	Pretreatment	LOD	ref
	<i>Vibrio parahaemolyticus</i>	ssDNA	Fluorescence	> 2 h	-	3, 2a	$0.067 \times 10^9$ mol/L (DNA) = 10 CFU/mL	[46]
	<i>Staphylococcus aureus</i>	Antibody	Refractive Index	30 min	-	2a	224 CFU/mL	[47]
<b>Mycotoxins</b>	Aflatoxin M <sub>1</sub>	Antibody	Electrochemical	> 2.5 h	milk	2b	$0.02 \times 10^6$ g/L = $6 \times 10^{11}$ mol/L	[48]
	Aflatoxin M <sub>1</sub>	Aptamer	Fluorescence	>1.25 h	milk powder	1, 10, 7a, 11	$0.05 \times 10^6$ g/kg	[49]
	Ochratoxin A	Aptamer	Electrochemical	-	watermelon	2b	$5.2 \times 10^{12}$ g/L = $13 \times 10^{-15}$ mol/L	[50]
	Ochratoxin A	Aptamer	Electrochemical	Real-time	iced coffee	-	-	[51]
<b>Pesticides</b>	Malathion	Aptamer	Electrochemical	> 4 h	cauliflower, cabbage	2b	$0.5 \times 10^9$ g/L = $1.5 \times 10^{-12}$ mol/L	[52]
	Malathion	Enzyme (Acetylcholin-esterase)	Electrochemical	≈ 15 min	water	-	$0.92 \times 10^{12}$ mol/L	[53]
	Monocrotophos	Enzyme (Acetylcholin-esterase)	Electrochemical	≈ 15 min	cabbage, lettuce, leak	1, 7a, 8	$3.2 \times 10^{11}$ mol/L	[54]
	Monocrotophos	Enzyme (Acetylcholin-esterase)	Electrochemical	≈ 15 min	potted plants	1	$3.3 \times 10^{11}$ mol/L	[55]
	Carbaryl	Enzyme (Acetylcholin-esterase)	Electrochemical	≈ 5 min	tomato	2b	$1.9 \times 10^9$ mol/L	[56]
	Carbaryl	Antibody	Piezoelectric	≈ 1.5 h	honey	5	$0.118 \times 10^6$ g/L (buffer) = $5.86 \times 10^{-10}$ mol/L $0.035 \times 10^6$ g/L (honey) = $1.74 \times 10^{-10}$ mol/L	[57]
	Chlorpyrifos	Antibody	SPR	10 min	maize, cabbage, apple, medlar	2b	$0.056 \times 10^6$ g/L = $1.6 \times 10^{-10}$ mol/L	[58]

Category	Analyte	Biorecognition element	Detection method	Assay time	Food sample	Pretreatment	LOD	ref
Veterinary drugs	Chloramphenicol	Antibody	Chemiluminescence	1.5 h	milk	7c	$2.86 \times 10^{-9}$ g/L = $8.85 \times 10^{-12}$ mol/L	[59]
	Sulfadiazine						$0.22 \times 10^{-6}$ g/L = $8.79 \times 10^{-10}$ mol/L	
	Neomycin						$0.03 \times 10^{-3}$ g/L = $4.88 \times 10^{-8}$ mol/L	
Metals	Kanamycin	Aptamer	Fluorescence	30 min	milk	2b	$1.0 \times 10^{-9}$ g/L	[60]
	Pb <sup>2+</sup>	DNAzyme	Fluorescence	20 min	water		$0.16 \times 10^{-9}$ mol/L	[61]
Packaging component	Bisphenol A	Enzyme (Tyrosinase)	Electrochemical	≈ 5 min	olive oil, chips	10	$1.80 \times 10^{-6}$ g/L = $7.88 \times 10^{-9}$ mol/L	[62]
	Bisphenol A	Antibody	Colorimetric	10 min	-	2a	10 ppb = $4.38 \times 10^{-8}$ mol/L	[63]
Allergens	Tropomyosin (shellfish)	Antibody	Circular Dichroism Spectroscopy	-	shellfish	1, 10	$21 \times 10^{-9}$ g/L	[64]
Other	Melamine	Antibody	SPR	≈ 10 min	milk	5, 7c	$1.3 \times 10^{-6}$ g/L = $1.0 \times 10^{-8}$ mol/L	[65]
	Melamine	Antibody	Electrochemical	2.5 h	dairy products	2b	$1.2 \times 10^{-11}$ mol/L	[66]
	1) Homogenisation (with buffer) 2) Proof of concept(a) spiked buffer (b) spiked extracts 3) DNA extraction 4) Filtration 5) Dilution 6) DNA amplification 7) Centrifugation (a) remove solids (b) suspend pellet (c) ultrafiltration-centrifugation 8) standard addition 9) Culturing 10) Extraction 11) Preconcentration							

The largest number of biosensors is developed towards the sensitive detection of food contaminants whereby research interests highly correlate with market interest (Fig. **1B**) as the biggest number of publications focuses on the detection of microorganism, followed by mycotoxins, pesticides and veterinary drugs [8,12].

### 1.1.1.2 Food Fraud

Today, with longer, more complex food chains the risk of food fraud for economic gain by producers, manufacturers, distributors or retailers is gaining increasing attention [13]. Primarily, food fraud is considered to be an economic issue instead of being a concern of food safety. However, by the adulteration of food the original composition is changed by dilution, substitution of ingredients, adding of other ingredients or modifying original ingredients, only the criminal is aware of the foods' composition. Consequently, with their focus on economic gain and evading quality assurance and control systems public health risks of adulterated food often is unknown and can have dramatic consequences. By example, before 2007 melamine was not considered to be a potential contaminant or adulterant for food safety. With the incidents in 2007, contaminated pet food in the US and Canada, and 2008, milk adulterated with melamine in China, the risk of food adulteration for consumers became obvious so that melamine is listed as food contaminant in the Codex Alimentarius for "General Standards for Contaminants and Toxins in Food and Feed" today [9]. Between 1980 and 2010 the most food fraud incidents were reported for olive oil, milk, honey, saffron, orange juice, coffee, apple juice and fish [13]. Biosensor developments for the detection of food frauds are summarized in table 2. Recent biosensor developments mainly focus on the identification of meat and fish, followed by urea and single publications on the identification of wine or manuka honey.

**Table 2** Reviewed biosensors for the detection of food fraud and adulteration sorted by analyte with utilized biorecognition element, detection method, assay time, food sample, pretreatment and limit of detection (LOD).

Analyte	Biorecognition element	Detection method	Assay time	Food sample / Pretreatment	LOD	ref
Leaf, Must, Wine <i>Vitis vinifera</i> (DNA)	DNA	Refractive Index	-	1, 2	-	[91]
Meat species (8)	DNA	Colorimetric	30 min (after PCR amplification)	1, 2	$0.5 \times 10^{-12}$ g; 0.001%	[84]
Atlantic cod, pacific cod, Alaska pollock and ling	Antibody	Colorimetric	5 min (after PCR amplification)	1, 2	$50 \times 10^{-11}$ g - $50 \times 10^{-12}$ g	[85]
Mammal meat identification (15 mammalian species, 7 other meat varieties)	Antibody	Colorimetric	5 min (after LAMP amplification)	1, 2	$10 \times 10^{-12}$ g (cow)	[86]
Pork	Antibody	Electrochemical	2 h (direct) 20 min (competitive)	3	0.1%	[92]
Pork	DNA	Colorimetric	30 min	4	$0.1 \times 10^{-6}$ mol/L (DNA)	[93]
Urea	Enzyme	Electrochemical	2 min	milk / 5, 6	$1 \times 10^{-3}$ mol/L	[87]
Urea	Enzyme (Urease)	Electrochemical	-	4	$1.8 \times 10^{-6}$ mol/L	[94]
Urea	Enzyme	Electronical	3 min	4	$1 \times 10^{-6}$ mol/L	[95]
Urea	Enzyme	Electrochemical	20 min	milk	$1 \times 10^{-12}$ mol/L $3 \times 10^{-12}$ mol/L	[88]
Melamine						
Leptosperin (marker for manuka honey)	Antibody	Colorimetric	20 min	manuka honey / 6	$0.014 \times 10^{-6}$ mol/L	[89]
1) DNA extraction	4) Proof of concept (spiked buffer)					
2) DNA amplification	5) Filtration					
3) Protein extraction	6) Dilution					

### 1.1.2 Sustainable Agriculture

According to the United States Department of Agriculture (USDA), sustainable agriculture practices are intended to protect the environment, expand the Earth's natural resource base and maintain and improve soil fertility [14]. With an ongoing growth of the world population agriculture has to fulfill the needs of present and future generations. Today, commercial agriculture is often unsustainable because of its negative impact on natural resources and the environment with high amounts of degraded farmland, loss of genetic diversity in crops, overfishing and forests being converted into other land use [15]. Topics within sustainable agriculture are wide spread among producers, politicians, distributors and consumers ranging from water use efficiency, water quality management, soil nutrient management, zero-emission freight transport, addressing of food insecurity, biofuels, conservation tillage, food waste management, integrated pest management, nutrition and food systems education, biological integrated farming systems, food labeling/certifications to global sustainable sourcing of commodities [16]. The deployment of sensor technology including biosensors is possible within several of these topics. Most likely (bio)sensors can be advantageous in addressing food insecurity, monitoring and thereby managing water and soil quality, which can reduce the overuse of fertilizers and pesticides. Biosensors could also be helpful for integrated pest management among crops and livestock by continuous monitoring or early detection of diseases avoiding the outbreak.

### 1.1.3 Biosensors

#### 1.1.3.1 Definition

The International Union of Pure and Applied Chemistry (IUPAC) defines a biosensor as "a device that uses specific biochemical reactions mediated by isolated enzymes, immunosystems, tissues, organelles, or whole cells to detect chemical compounds usually by electrical, thermal or optical signals" [17]. In addition to biosensors following the IUPAC definition bioprobes being single-use devices, e.g. lateral flow assay, are included in this review.

#### 1.1.3.2 Biorecognition elements

The most reviewed biosensors for the detection of contaminants, food fraud or pathogens utilized antibodies, aptamers, nucleic acids and enzymes as biorecognition element. Occasionally, other proteins, viruses or bacteriophages are applied within biosensors.

**Antibodies** are a common used recognition element in immunoassays to separate the desired analyte from the sample matrix by specific binding. The high binding constants of antibodies are,

to-date, not realized with other recognition elements, making them irreplaceable in numerous established assays as well as in the development of new sensitive detection strategies. In the here reviewed literature, antibodies are utilized in the detection for food contaminants such as microorganism, mycotoxins, veterinary drugs and allergens. In the detection of food fraud or agricultural pathogens antibodies against specific labels introduced in the duplicated DNA strands, e.g. carboxyfluorescein, are used instead of target-specific antibodies.

**Aptamers** are a well-known alternative to antibodies with an increased use as biorecognition element in the scientific community since the 2000s. The growing interest is founded in their production, not relying on animals or cells, and their high batch-to-batch reproducibility making them inexpensive to synthesize compared with antibodies. Aptamers also display prolonged shelf life, are stable under non-physiological conditions and can be flexibly modified to improve their functionality. Especially for the detection of small molecules the use of aptamers is advantageous over their analogue antibodies [18]. This advantage is displayed in the here reviewed literature where aptamers are the biorecognition element of choice for the detection of the mycotoxins and are also utilized in the assays for the detection of microorganism, veterinary drugs and pesticides.

**Nucleic Acids** are widely used as specific biorecognition elements in traditional DNA hybridization assays with examples for the detection of microorganism in the here reviewed literature. Within the field of food safety the rare use of DNA analysis is in part caused by the need of additional sample preparation steps which are unnecessary using antibodies or aptamers. Within the needed sensitive detection of agricultural pathogens, like viruses, funghi or bacteria species, or the identification of alien species in the case of food fraud DNA hybridization assays (not sensors) are more common after DNA amplification.

**Enzymes** are widely used as labels in immunoassays to catalyze chemical reactions resulting in the formation of colored or fluorescent dyes or electrochemically active marker molecules. In addition enzymes can be utilized as biorecognition elements. Here, enzymes can be used as target-specific biorecognition element for the direct detection of an enzymatic substrate. On the other hand, enzymes can be used for the unspecific detection of numerous inhibitory molecules by monitoring the enzyme activity.

**Bacteriophages**, viruses that infect and replicate within bacteria can be used as a biorecognition element for the detection of bacterial cells by their specific binding to receptors. In addition to their high specificity towards the bacterial target bacteriophages can distinguish between dead and alive bacterial cells, an often-missing feature in antibody-based assays.



## 1.2 Biosensors within the food supply chain

All parties involved in the food chain are interested to ensure food safety but are subjected to different restrictions in their scope of action. Agricultural products are usually processed before being distributed to retailers before ending at the consumers (see Fig. 2). All parties during the food chain should be concerned in ensuring that produced food is not tainted with any contaminant above the maximum level and does not underly food fraud (chapter 1.4). In addition, especially farmers are interested in maintaining healthy productive crops and soils (chapter 1.5) as well as livestock (chapter 1.6). The ideal biosensor fulfilling a farmer's needs is easy-to-use, requires no sample preparation and is designed for the in-field handling. In contrast to the farmer, food manufacturers usually have the opportunity for testing under laboratory conditions by technically trained personnel. To ensure an uninterrupted manufacturing process fast analysis time of the food samples are key.

In direct contrast, the possibilities of testing for the customer and during retailing are strongly limited. Therefore, the integration of (bio)sensors into food packaging is of great interest resulting in smart or intelligent packaging. For example, smart packaging enables tracking of changes in food freshness by the detection of markers, bacteria or temperature changes. Commercially available biosensors for the detection of bacteria based on antibody recognition are available under the trade names Food Sentinal System™ (SIRA Technologies Inc.) and ToxinGuard™ (Toxin Alert Inc.) [19–21]. Biosensor-based time-temperature integrators (TTI) are also commercially available. The Vitsab L5-8 Smart TTI Seafood Label is based on the time dependence of an enzymatic reaction which is activated by mixing the enzyme and the enzymatic substrate [22]. In the case of Cryologs (eO)® TTI is determined based on the pH changes caused by microbial growth [23]. Biological reactions, such as enzymatic autolysis and microbial growth, and oxidation are the main causes of meat spoilage. Thus, such biosensor TTI are advantageous over other types of TTI sensors or indicators [24]. However, it must be pointed out that research for TTI, and the detection of O<sub>2</sub>, CO<sub>2</sub> and volatile compounds directly in packaging focusses primarily on indicators and sensors, as biosensors simply are too expensive for this application [24]. Nonetheless, Yousefi *et al.* have recently demonstrated a noteworthy exception. They developed a fluorescent turn-on biosensor based on DNAzymes and proven its functionality after attachment of the DNAzyme to a cyclo-olefin polymer [25]. Other biosensors stated for monitoring of food freshness are electrochemical biosensors based on enzymes which are reported for metabolites like glucose, lactic acid or biogenic amines [26–28]. However, again, high costs and the challenging integration into packaging makes their application for smart packaging rather impractical. Their use is more likely applicable for

quality control laboratories of manufacturers, distributors or local authorities. A more detailed overview about (bio)sensor developments for smart/intelligent packaging is given in lately published reviews [21,24,29,30]. It should finally be noted that local authorities should also be concerned about testing food during throughout the food chain. For example, at border patrols fast in-field useable biosensors would be advantageous to avoid delivery delays but protect costumers of harmful products. As more time-consuming laboratory tests identify a harmful food product, its successful tracking and ease of identification throughout the whole food chain is key to limit the negative effects on public health.



Fig. 2: Food supply chain with involved parties from the raw materials to costumer.

### 1.3 Biosensors in food safety

#### 1.3.1 Bacteria

Literature review of the most recent years shows that bacteria detection strategies are mainly based on specific recognition by antibodies or aptamers. Antibodies clearly dominated, which suggests that research effort into the development of new aptamers for bacterial detection was amiss. Here, the group of Stanciu was a notable exception using one anti-*E. coli* aptamer in two sandwich format biosensors. Beside readouts with established methods like spectroscopy, fluorescence or electrochemistry less popular detection techniques are also reported. Surprisingly in the reviewed literature only a single biosensor is developed towards multiplexing, which clearly misses the current trend in other biosensor fields such as those for medical diagnostics, and also

the need requested by the end-users. Also, the biosensors are typically based on well-known, already long-time established strategies, where novelty is obtained often only with the implementation of various nanomaterials. In contrast, the following examples describe bioassays based on the dual-functionality of aptamers having the property to hybridize with a complementary DNA string in addition to its specific binding to the target. These strategies could easily be integrated into biosensors. Specifically, Wu *et al.* describe a fast, highly sensitive dual-mode sensor for the detection of *Vibrio parahaemolyticus* using multifunctional nanomaterials. The detection is based on photon upconversion combined with inner filter effect or colorimetric readout. Platinum-plated gold nanorods (AuNR@Pt) are functionalized with a *Vibrio parahaemolyticus* aptamer. Upconverting nanoparticles (UCNP) are conjugated with complementary DNA (cDNA) of the aptamer and both materials are hybridized to form a duplex structure. Inner filter effect within this composite is caused by the overlap of AuNR@Pt absorption with UCNP emission ( $\lambda_{exc} = 980\text{nm}$ ). In the presence of target bacteria the aptamer conjugated to AuNR@Pt forms a stable complex with the bacteria cell and releases the UCNP. After centrifugation the cDNA-UCNPs are left in the supernatant and a higher luminescent signal compared to the absence of bacteria is measured. The peroxidase-like activity of AuNR@Pt is used for a colorimetric detection by resuspending the sediment, containing the AuNR@Pt-Aptamer-*V. parahaemolyticus* complex) and addition of TMB and hydrogenperoxide. The color intensity caused by substrate conversion correlates with bacteria concentration. The photon upconversion mode of the aptasensor enables a fast and sensitive (LOD = 10 CFU/mL) detection [67] (see Fig. 3).

A highly sensitive assay (LOD = 1.5 CFU/mL) with aptameric recognition for *Salmonella typhimurium* uses a fluorescent sensing strategy by combining the dual functionality of phi29 polymerase with isothermal circular strand displacement polymerization (ICSDP) (Fig. 4). The sensing system is composed of five elements. The arched probe for the recognition of the target bacteria *S. typhimurium*, two hairpin probes (HAP1 and HAP2) and two nucleic acid enzymes, phi29 DNA polymerase (phi29) and nicking endonuclease *Nt. AlwI*. HAP1 affords the template of ICSDP and fluorescence-quenched HAP2 act as pre-primer for the ICSDP and as indicator for the emitted fluorescence. The arched probe contains the anti-*S. typhimurium* aptamer hybridized with a trigger oligonucleotide (T). T can anneal with the 5' end of HAP1. HAP1 itself contains a trigger-annealing sequence (T\*), a recognition sequence for *Nt. AlwI* (R\*) and a complementary DNA segment to the loop of HAP2 (S\*). In the presence of *S. typhimurium* specific recognition of the aptamer releases T which binds to the 5' terminus of HAP1. Upon a conformation switch the 3' terminus of HAP1 (S\*) attaches to the loop of HAP2 (S) and functions as a primer to initiate an extension reaction in the presence of phi29 and dNTPs utilizing HAP2 as the template. The unmatched tail of HAP2 (L) is

digested *via* the processive 3' → 5' exonuclease activity of phi29. The fluorophor (FAM) is detached from the quencher (Dabcyl) leading to an enhanced fluorescent signal. The trimmed 3' end of HAP2 can act as a mature primer for initiating the strand displacement polymerization reaction. During the polymerization process T is displaced and a recognition site for *Nt. AlwI* is generated in the DNA duplex. *Nt. AlwI* nicked the side and induces the formation of single-stranded DNA fragments (secondary T, T') that can combine with HAP1 promoting more rounds of the strand displacement polymerization reaction [68]. Even though the assay concept seems rather complicated on a first view the ICSDP can be performed in an one-pot reaction for 90 min at 37 °C by mixing all components (only aptamer and T need to be hybridized beforehand).

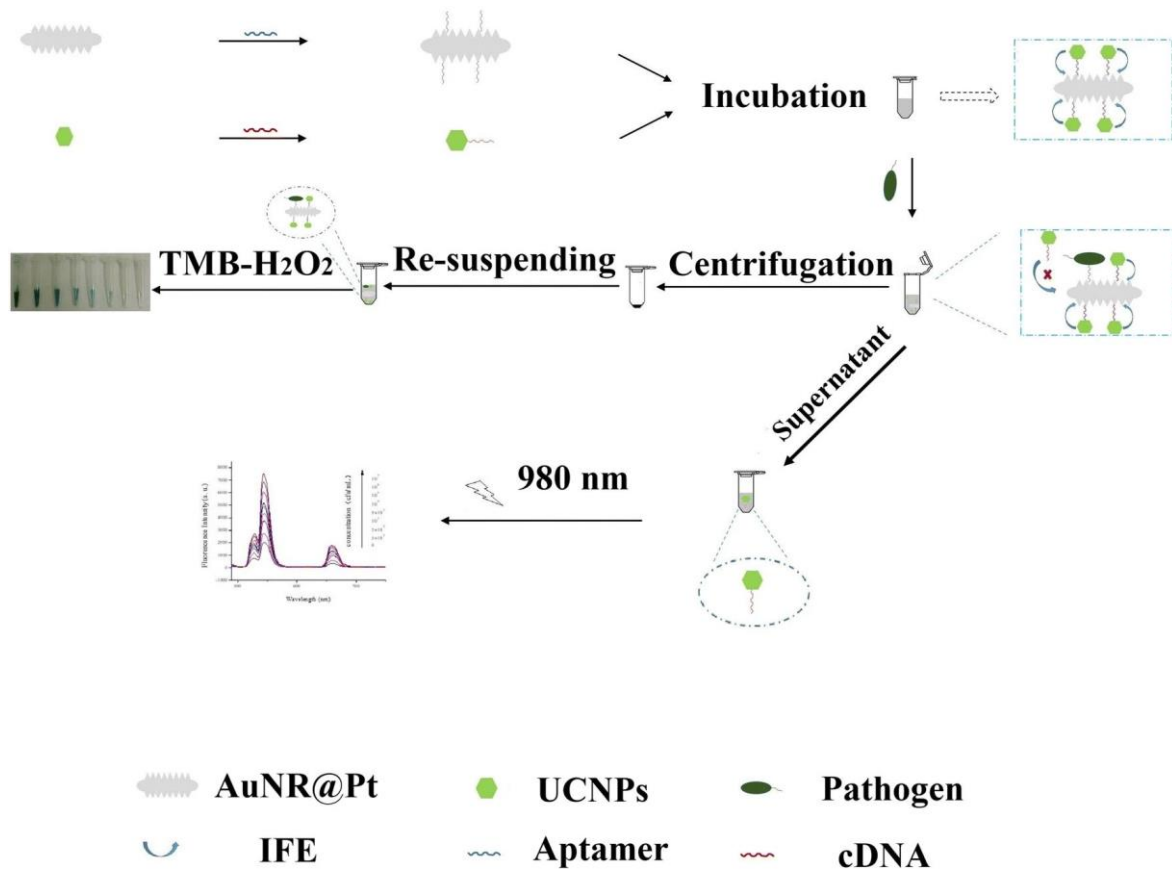


Fig. 3: A dual-mode (Fluorimetric and Colorimetric) Aptasensor for *Vibrio parahaemolyticus* Detection Using Multifunctional Nanoparticles. Reproduced with permission from ref [54]. Copyright 2019 Springer Nature.

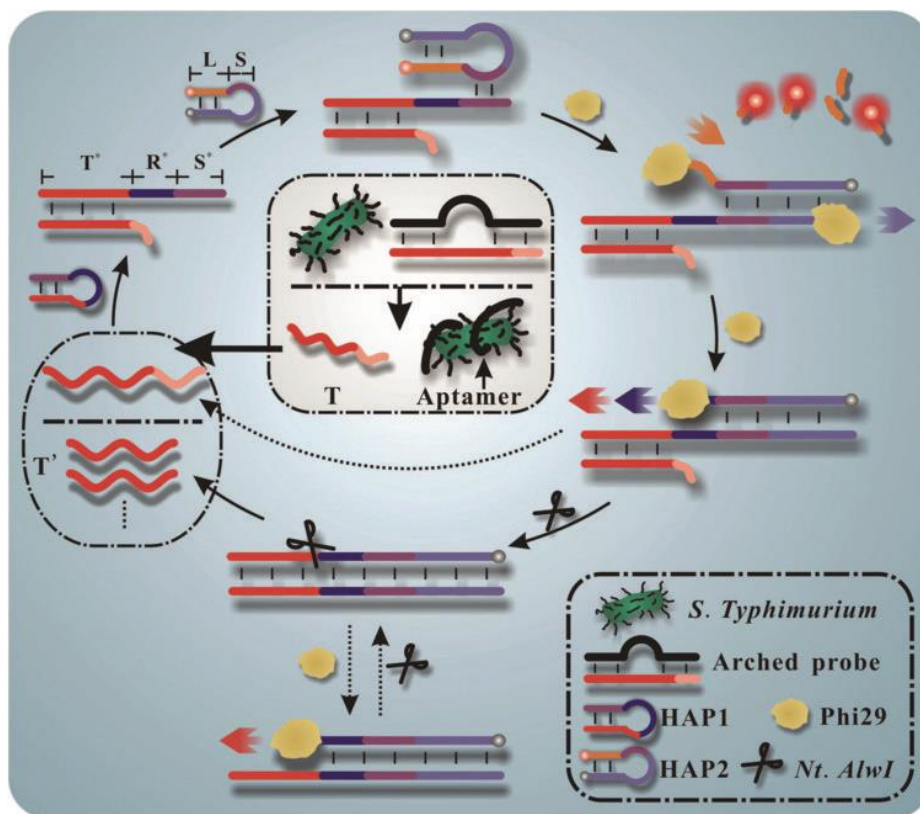


Fig. 4: Schematic illustration of the fluorescence sensing of *S. typhimurium* using dual-functional phi29 DNA-polymerase-mediated ICSDP. Reproduced with permission from ref [68]. Copyright 2019 The Royal Society of Chemistry.

One of the latest trends in the detection of bacterial species is based on the usage of bacteriophages. In principle three different strategies for the detection of bacteria are reported, which are based on the infection of bacteria, the immobilization of bacteriophages to create sensing layers, or the capture and separation of bacteria from the matrix, respectively. Lysis of infected bacteria releases intracellular content which serves as specific detection markers, e.g. indigenous enzymes and their catalytic signal enhancement are used these assays. For *Escherichia coli*  $\beta$ -galactosidase was used as a marker and the color change from the enzymatic substrate chlorophenol Red- $\beta$ -D-galactopyranoside was studied to evaluate the bacteria concentration [69]. Furthermore, through genetically engineering bacteriophages the strategy of enzymatic catalysis was successfully adapted to the expression of alkaline phosphatase [70], NanoLuc luciferase [71] or protease [72] followed by electrochemical [70], bioluminescent [71] or fluorescent [72] detection, respectively.

For the preconcentration of bacteria cells bacteriophages are often coupled to magnetic beads. The preconcentrated bacteria cells can be detected utilizing the enzymatic catalysis of expressed

enzymes [69,70]. A sandwich-type immunoassay after phagomagnetic separation of *Salmonella* is reported by Laube *et al.* [73]. Specific anti-*Salmonella* antibodies with conjugated horseradish peroxidase are added to the pre-concentrated bacteria cells followed by the colorimetric readout of the enzymatic reaction of 3,3',5,5'-tetramethylbenzidine.

Since Bennett *et al.* described a novel biosorbent consisting of a *Salmonella*-specific bacteriophages immobilized to a solid phase of polystyrene in 1997 [74] this concept was applied towards a variety of materials and detection methods. For example, bacterial detections are realized via surface plasmon resonance (SPR) on gold surface (*Escherichia Coli*) [75], surface-enhanced Raman spectroscopy (SERS) on nanosculptured thin films of silver (*Escherichia Coli*) [76] or electrochemical impedance spectroscopy (EIS) on screen-printed graphene electrodes (*Staphylococcus arlettae*) [77].

A detailed review on recent advances in the phage-based detection of bacteria was recently published by Richter *et al* [78].

### 1.3.2 Veterinary Drugs

The researchers focus on the detection of veterinary drugs is dominated by antibiotics (chloramphenicol, sulfadiazine, neomycin, kanamycin) as they are widely used in industrial livestock farming. A highly sensitive bioassay for the detection of chloramphenicol is reported by Sharma *et al.* whose principle can be transferred easily into a biosensor format. [79]. An aptamer for chloramphenicol (thiolated aptamer) is immobilized on a microtiterplate and hybridized with a fluorophore-tagged oligonucleotide (6-carboxyfluorescein). If chloramphenicol is present it binds to the aptamer and the oligonucleotide is detached and further removed by washing. By removing the oligonucleotide the aptaswitch is turned off resulting in a reduced fluorescent signal (Fig. 5).

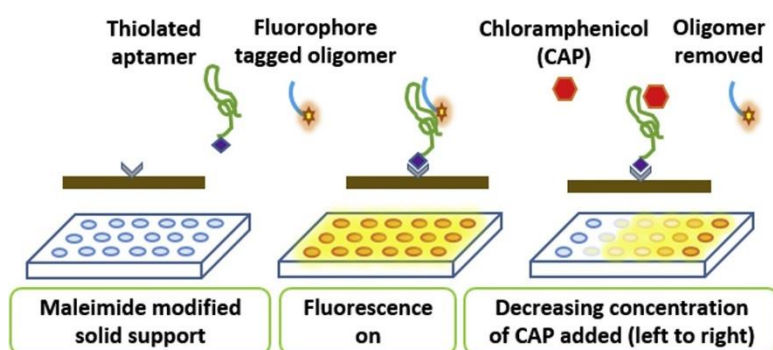


Fig. 5: Schematic of a bioassay for the detection of chloramphenicol (CAP) based on a fluorescent “turn-off” approach. Reproduced with permission from ref [79]. Copyright 2019 Elsevier.

### 1.3.3 Mycotoxins

Mycotoxins are produced by certain molds (fungi) and can be found in foods like nuts, cereals or dried fruits. Adverse health effects for humans or livestock can range from acute poisoning to long-term effects such as cancer or immune deficiency [80]. Mycotoxins (Aflatoxin M<sub>1</sub>, Ochratoxin A) are the only category of food contaminants where aptamers are the preferred biorecognition elements, most likely due to their advantage in the detection of small molecules. Gu *et al.* developed a highly sensitive electrochemical biosensor for the detection of Ochratoxin A (OTA) utilizing an aptamer [50]. OTA aptamer is immobilized on a nanocomposite (AuNP@CuCoPBA) of bimetallic (Cu-Co) Prussian Blue analogs (PBAs) coupled to gold nanoparticles (AuNP). A gold electrode is modified with the nanocomposite and the OTA concentration is directly determined by electrochemical impedance spectroscopy (Fig. 6). The excellent biosensing feature of the aptasensor is caused by the high surface area and porosity, fast electron-transfer kinetics and favorable tuned electronic structure by the combination of transition metals. The biosensor can be easily modified towards other analytes for which aptamers are available.

Somerson and Plaxco developed an inexpensive electrochemical aptamer-based biosensor for the real-time monitoring of ochratoxin A in a food stream. An OTA aptamer, modified with a methylene blue redox reporter, is immobilized on a gold electrode. The aptamer configuration changes upon binding of OTA and the change in methylene blue electron transfer rate can be monitored electrochemically [51].

### 1.3.4 Pesticides

For the detection of organophosphate pesticides (malathion and monocrotophos) and carbamates (carbaryl) new concepts are missing in the latest literature and established principles using acetylcholinesterase as an unspecific biorecognition element are widely applied. Organophosphate pesticides act as inhibitors and thus reduce the enzymatic catalysis. Acetylthiolcholine chloride is usually used as enzymatic substrate and the produced thiolcholine is either detected electrochemically or within bioassays its affinity to bind metal ions such as Cu<sup>2+</sup> [81][82] or Ag<sup>+</sup> [83] is utilized. Both recently published electrochemical biosensors used glassy carbon electrodes and modified them with nanomaterial composites. Bao *et al.* used 3D-graphene-copper oxide-nanoflowers to increase the effective specific surface area that provide a micro-environment for the deposition of an acetylcholine esterase-chitosan film [53]. The electrochemical enzyme-based biosensors enable a faster detection with similar sensitivities compared to aptamer- or antibody-based sensors but due to their nature they are not specific toward single pesticides.



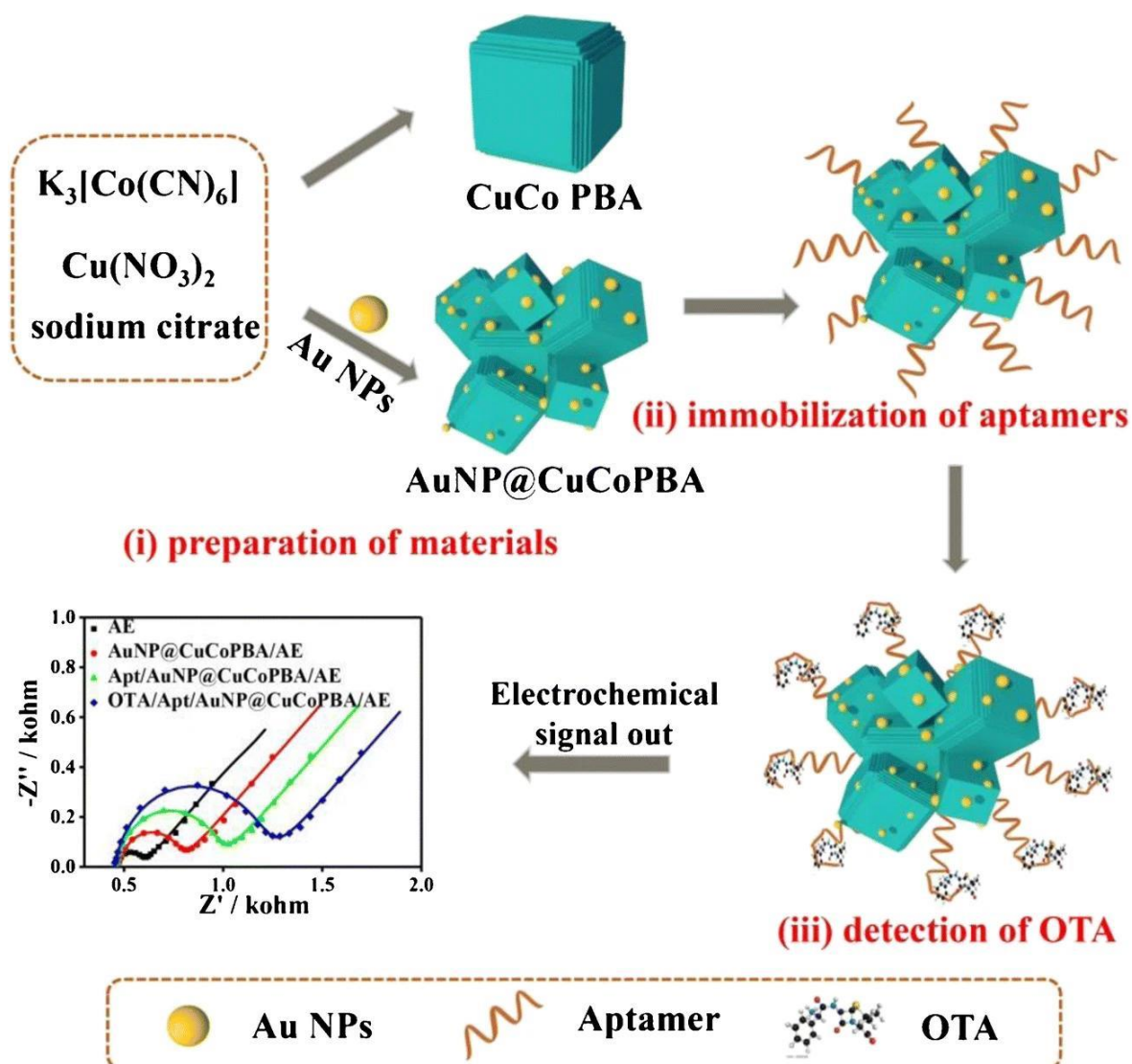


Fig. 6: Schematic diagram of the aptasensor fabrication based on the series of CoCu PBA, including (i) preparation of the CuCo PBA, and AuNP@CuCoPBA, (ii) immobilization of the aptamer strands, and (iii) detection of OTA. Reproduced with permission from ref [50]. Copyright 2019 Springer Nature.

### 1.3.5 Other contaminants

For other contaminants like metals, packaging components and allergens only a small number of publications is found. Melamine detection gained most attention [52, 53], but surprisingly allergenic compounds were not targeted frequently, which again puts most recent research efforts at odds with societal needs. Notable exception is an antibody-based biosensor for the detection of the major shellfish allergen, the protein tropomyosin [64] A biosensor for the detection of bisphenol A was designed using a tyrosinase Au-Pt@SiO<sub>2</sub>/Au-graphene modified glassy carbon



electrode. Au-graphene was used to increase the specific area, while Au-Pt@SiO<sub>2</sub> has a peroxidase- and catalase-like activity. Combined with tyrosinase the direct electrochemical detection of bisphenol A was realized with square wave voltammetry and differential pulse voltammetry [62].

## 1.4 Food Fraud

In contrast to food safety, food fraud is rather seldomly targeted within the development of biosensors as the detection of food fraud mainly focuses on the identification of DNA of plants, meat or fish. As DNA extraction and amplification is required to enable the desired sensitivity, implementation into biosensor concepts remains difficult and expensive. Furthermore, these steps typically require the expertise of a user, negating any advantages of biosensors in contrast to bioassays. DNA amplification is performed with polymerase chain reaction (PCR) using specific primers [84][85] or loop-mediated isothermal amplification (LAMP) [86]. By performing those amplifications of the analyte DNA labels can be introduced into the duplicated DNA via primers and detected using specific antibodies, e.g. anti-biotin antibodies [84] or anti-carboxyfluorescein antibodies [85]. In another strategy, urea is identified as an adulteration compound in milk similar to melamine, feigning a higher protein concentration. One biosensor specific towards urea is based on enzymatic recognition using urease [87]. Another one uses acetylcholinesterase which is capable of detecting urea as well as melamine by its inhibition but is unable to distinguish between those two compounds [88]. For the identification of manuka honey, a honey from New Zealand, the detection of biomarkers is used. Kato *et al.* developed a lateral flow assay for the detection of leptosperin, a glycoside, based on a competitive immunoassay. Anti-leptosperin monoclonal antibodies conjugated with gold nanoparticles are added to the honey sample before the sample is applied to the lateral flow strip. The antibody-leptosperin complex as well as single antibodies migrates towards the test line (leptosperin-conjugated BSA) where solely the single antibodies are captured and are visualized by the reddish-violet color of the gold nanoparticles. The assay standard curve covers a range from 0.014 µmol/L to 10 µmol/L and showed excellent accordance with determinations using high pressure liquid chromatography (HPLC) or ELISA [89]. A recent review article comprises modern analytical methods for the detection of food fraud and adulteration by food category [90].

## 1.5 Biosensors supporting sustainable agriculture

In comparison to food safety matters biosensors supporting sustainable agriculture are published in much lower numbers. Those published between 2015-2019 are summarized in table 3.

Two predominant categories include on the one hand the majority of biosensor developed for the direct detection of pathogens, while a small number is detecting marker molecules that are directly connected to plant health (methyl salicylate and azelaic acid) or indicate if fertilizers are needed (nitrate). This trend will change in the coming years since biosensors can support efforts to enable a sustainable way of agricultural production. This includes the identification of local and transient needs of energy, water and chemicals, and the avoidance of toxins and pesticides above allowable levels. With the high variety of agricultural crops a variety of biosensors for the detection of viruses and fungi are reported. This variety is missing in the detection of pathogenic bacteria or oomycetes. Interestingly, the detection within the reported biosensors is dominated by electrochemistry, which is likely due to the hardware simplicity and inexpensive fabrication costs of electrochemical sensors. Other biosensors are based on the lateral flow assay format. Zhan *et al.* use a DNA hybridization assay for the detection of *Phytophthora infestans* DNA using a gold nanoparticle modified detection probe [96] which enables a visual readout with the bare eye. Other optical lateral flow assay based biosensors use carbon nanoparticles [97] or gold nanoparticles followed by silver enhancement which leads to a 15-fold lower LOD [98].

Biosensors for the detection for markers to identify infected plants are reported for methyl salicylate and azelaic acid. Methyl salicylate is a volatile organic compound (VOC) that's released by plants and was identified as a useful marker for non-destructive identification of pathogenic infections, as infected and healthy plants produce significantly different amounts of VOCs. A bi-enzyme biosensor for methyl salicylate is based on enzymatic recognition by alcohol oxidase. Therefore methyl salicylate needs to be hydrolyzed to methanol which is the substrate for the alcohol oxidase. The hydrogen peroxide formed within the enzymatic reaction is detected electrochemically utilizing its conversion by horseradish peroxidase. The enzymes were immobilized on a glassy carbon rotating disc electrode modified with multiwall carbon nanotubes.

**Table 3** Reviewed biosensors with applications in agriculture sorted by category and analytes with utilized biorecognition element, detection method, detection method, assay time, sample, pretreatment and limit of detection (LOD).

Category	Analyte	Biorecognition element	Detection method	Assay time	Sample	Pretreatment	LOD	ref
Virus	plum pox virus	Antibody	Electronical (Electrolyte Gated Organic Field Effect Transistor)	15 min	-	1a	$180 \times 10^{-9}$ g/L	[100]
	citrus tristeza virus	DNA	Electrochemical	60 min	-	1a	$100 \times 10^{-3}$ mol/L	[101]
	potato leafroll virus	Antibody	Colorimetric	15 min	-	1a	$0.2 \times 10^{-6}$ g/L	[98]
	rice tungro bacilliform virus	Antibody	Electrochemical	≈ 3 h	-	1a	-	[102]
Bacteria	<i>Xanthomonas arboricola</i> pv. <i>pruni</i>	Antibody	Colorimetric	< 15 min	leaf extracts	1b	$10^4$ CFU/mL	[97]
	<i>Xanthomonas arboricola</i>	Antibody	Electrochemical	> 30 min	walnut	2	$1.5 \times 10^2$ CFU/mL	[103]
Fungi	<i>Pseudocercospora fijiensis</i>	Antibody	SPR	10 min	leaf extracts	1b	$11.7 \times 10^{-3}$ g/L	[104]
	<i>Botrytis cinera</i> (DNA)	DNA	SERS	40 min	plant leaves	3, 4	$1.9 \times 10^{-15}$ mol	[105]
Oomycete	<i>Phytophthora infestans</i> (DNA)	DNA	Colorimetric	1.5 h	-	5, 1a	$0.1 \times 10^{-6}$ g/L	[96]
Marker	Methyl salicylate	Enzyme (alcohol oxidase)	Electrochemical	1.05 h	wintergreen oil	-	$0.98 \times 10^{-6}$ mol/L	[106]
	Nitrate	Enzyme (nitrate oxidase)	Electrochemical	≈ 1 min	-	1a	-	[99]

1) Proof of concept a (spiked buffer) b (spiked extracts)

2) Extraction

3) DNA extraction

4) DNA amplification

**Table 4** Reviewed biosensors supporting soil analysis listing here biorecognition element, detection method, assay time, sample, pretreatment and limit of detection (LOD).

Category	Analyte	Biorecognition element	Detection method	Assay time	Sample	Pretreatment	LOD	ref
Heavy metals	Cd(II)	Bacteria	Fluorescence	4 h	water samples	-	$9 \times 10^{-7}$ mol/L	[110]
	Cd(II)	Bacteria	Fluorescence	2 h	water, soil	-	-	[111]
	Pb(II)	Aptamer	Electrochemical	30 min	water soil	1, 3 5, 6, 1, 3	$1.9 \times 10^{-12}$ mol/L	[112]
	Pb(II)	Aptamer	Electrochemical	30 min	soil	5, 3, 7	$0.36 \times 10^{-9}$ mol/L	[113]
	Pb(II)	DNAzyme	Electrochemi-luminescence	60 min	soil	2b	$0.2 \times 10^{-12}$ mol/L	[114]
	Pb(II)	DNA	Electrochemical	30 min	water, soil	1, 8 5, 7, 3	$4.2 \times 10^{-12}$ mol/L	[115]
	Pb(II)	DNAzyme	Electrochemical	5 min	soil	5, 6, 1	$7.4 \times 10^{-12}$ mol/L	[116]
	As(III)	Aptamer	Colorimetric	25 min	soil	9, 1	$1.93 \times 10^7$ mol/L (buffer)	[117]
							$2.63 \times 10^{-5}$ mol/L (soil)	

Category	Analyte	Biorecognition element	Detection method	Assay time	Sample	Pretreatment	LOD	ref
	Cu(II)	DNAzyme	Electrochemical	35 min	water samples soil samples	5, 7, 1, 3	$0.457 \times 10^{-9}$ mol/L	[118]
<b>Explosives</b>	Trinitrotoluene (TNT)	Aptamer	Electrochemical	35 min	soil, water	7, 4	$33 \times 10^{-18}$ mol/L	[119]
	hexahydro-1,3,5-trinitro-1,3,5-triazine (RDX)	Bacteria	Fluorescence	24 h	-	2a	$0.44 \times 10^{-6}$ mol/L	[120]
<b>Pesticides</b>	Ethyl-paraoxon	Bacteria	Colorimetric	3.5 h	Apple, soil	2b	$1 \times 10^{-9}$ mol/L	[108]
	Paraoxon	Enzyme	Electrochemical	1 min	water, soil slurry	1, 3	$3 \times 10^{-9}$ mol/L	[121]
	Acephate	<i>Chlorella sp.</i> algae cells	Electrochemical	10 min	soil	-	$1 \times 10^{-12}$ mol/L	[107]
	1) Filtration							
	2) Proof of concept (a) spiked buffer (b) spiked extracts c (inoculated with whole-cell biosensor)							
	3) pH adjustment							
	4) Standard addition							
	5) Digestion							
	6) Centrifugation							
	7) Dilution							
	8) Boiling							
	9) Extraction							

A biosensor for the detection of the nitrate concentration in plants is developed by the group of Nicolas Plumeré [99]. The developed nitrate biosensor only requires one droplet of plant juice and is designed to be user friendly enabling its use by an untrained user, most likely the farmers themselves. Nitrate is recognized by the enzyme nitrate reductase and the amount of nitrate is quantified electrochemically. The further development of this biosensor towards market maturity is granted by a proof-of-concept project of the European Research Council. For the future, the collection of data from several farmers and their combination with weather and satellite data is planned to predict the plants nitrate needs.

In addition to those biosensors monitoring the agricultural crops' health status and enabling the cautious usage of pesticides and fertilizers, the condition of the soil itself is also key for ensuring sustainable agriculture. The presence of possible food contaminants can be monitored already before cultivation of the field. Soil analysis using biosensors mainly focus on heavy metal, pesticide contamination and the detection of explosive residues (cf. table 4). While the detection of heavy metals is dominated using DNAzymes and aptamers combined with electrochemical detection for the detection of pesticides, the same strategies are applied as used for food samples (cf. table 1). The detection of organophosphorus often is based on enzyme inhibition of acetylcholinesterase. A whole-cell biosensor is reported by Pabbi *et al.* who use the inhibition of alkaline phosphatase on the surface of algal cells for the detection of acephate [107]. A different approach was developed by Khatun *et al.* using engineered bacteria with a colorimetric readout. With utilizing two *E. coli* strains one has the task to hydrolyze the organophosphorus pesticide to p-nitrophenol which induces the production of  $\beta$ -galactosidase [108]. For the potential in-field use the whole cell biosensor showed promising results with a paper-based platform and incubation at mild 28 °C. Other whole-cell biosensors using engineered bacteria for the detection of heavy metals and explosives are also reported. Being considered relatively insensitive with long response times [108] the advantage of whole cell biosensors is their ability to detect only the bioavailable amount of the respective analyte [109].

## 1.6 Biosensors supporting livestock and animal health

In vivo-sensing developed for humans is currently an emerging trend in the (bio)-sensor field. As these will become commercial devices, efforts toward the lowering of costs will go hand-in-hand, which in turn means that ultimately livestock monitoring will benefit through targeting even the individual animal. Recently published biosensors, supporting livestock and animal health are

developed for the detection of pathogens with a focus on bacteria of the genus *Brucella* causing brucellosis. Biosensors focus on either the direct detection of bacteria [122][123], detection of *Brucella* DNA [124][125][126] or the detection of brucellosis antibody in blood serum [127]. In addition pathogenic viruses or the detection of markers are of interest. Like the biosensors supporting sustainable agriculture the biosensors supporting livestock and animal health use predominantly electrochemical detection. A portable, robust inexpensive electrochemical magnetic microbeads-based biosensor for point-of-care serodiagnosis was published by Cortina *et al.* [128]. The potential use of this platform for *in situ* diagnosis is demonstrated for the animal infections bovine brucellosis and foot-mouth disease caused by bacteria and virus, respectively.

Furthermore, online monitoring of physiological markers is of great interest. Carrara *et al.* developed a wireless implantable biosensor suitable for *in-vivo* detection of glucose, lactate, glutamate and ATP based on enzymatic recognition and electrochemical detection [129]. Implantable sensors for monitoring the glucose level of small as well as large animals are already commercial available [130]. An alternative to implantable sensors is the use of wearable sensors monitoring the physiological state of the individual animal by simultaneous monitoring of electrolytes and marker molecules. Today, researcher focus on the use of such sensors for mankind monitoring analytes like glucose or lactate in sweat [131] or saliva as a promising approach adapting towards monitoring livestock health. For readers more interested in this topic reviews on the recent advantages in wearable sensors [132] and biosensors technology [133] for animal health are recommended. These reviews include further information about the application of biosensors in breath analysis, progesterone (detecting ovulation), pathogen detection, salivary detection and the monitoring of animal behavior and movement.

**Table 5** Reviewed biosensors supporting livestock and animal health sorted by analytes with utilized biorecognition element, detection method, assay time, sample, pretreatment and limit of detection (LOD).

Category	Analyte	Biorecognition element	Detection method	Assay time	Sample	Pretreatment	LOD	ref
Bacteria	<i>Brucella melitensis</i>	Aptamer	Piezoelectric	> 30 min	milk	-	$1 \times 10^3$ CFU/mL	[122]
	<i>Brucella</i> spp. (DNA)	Antibody	Colorimetric	≈ 70 min (including DNA amplification)	-	1a	$1 \times 10^{15}$ g	[124]
	<i>Brucella</i> spp. (DNA)	Antibody	Colorimetric	≈ 45 min (including DNA amplification)	whole blood	2, 3	$100 \times 10^{15}$ g	[125]
	<i>Brucella abortus</i> (DNA)	DNA	Electrochemical	≈ 1 h (after DNA amplification)	serum	2, 3	$2.7 \times 10^{20}$ mol/L	[126]
	<i>Brucella abortus</i>	Antibody	Electrochemical	-	milk	4	$1 \times 10^3$ CFU/mL	[123]
	Brucellosis antibody	Protein	Electrochemical	≈ 1 h	serum	-	$0.36 \times 10^{-12}$ g/L	[127]
<i>Streptococcus agalactiae</i>	Antibody	Magnetic detection	4 h	milk	5, 6	100 CFU/mL	[134]	
<i>Streptococcus uberis</i>								



<b>Virus</b>	avian influenza virus H5N1	Aptamer	Piezoelectric	10 min	chicken tracheal swab	1b	$2^{-4}$ HAU/50 $\mu$ L	[135]
	avian influenza virus H5N1	Aptamer	Electrochemical	< 60 min	chicken tracheal swab	1b	0.25 HAU	[136]
	bovine herpes virus-1-specific antibody	Protein	Electrochemical	< 10 min	-	1a	-	[137]
	bovine viral diarrhoea antibody	Virus	Electrochemical	20 min	serum	7	$10 \times 10^{-3}$ g/L	[138]
	foot-and-mouth disease virus	Antibody	Colorimetric	15 min	tissue suspension, swab samples	-	-	[139]
<b>Marker (ovulation)</b>	progesterone	Aptamer	SPR	$\approx$ 20 min	-	1a	$1.575 \times 10^{-6}$ g/L $= 5.01 \times 10^{-9}$ mol/L	[140]
<b>Marker (Physiological)</b>	uric acid	Enzyme (Uricase)	Electrochemical	1 min (Real-time)	artificial and human saliva	-	-	[141]
	1) Proof of concept (a) spiked buffer (b) spiked extract							
	2) DNA extraction							5) Culturing
	3) DNA amplification							6) Milk homogenization (Agitation at 60 °C)
	4) Removing of lipids and proteins							7) Dilution

## **1.7 Conclusion and Future Perspective**

Biosensors to assist in the monitoring of safe food have been a research focus already for decades, as biosensors' key characteristics such as simplicity, sensitivity and low cost match well with the challenging demands that need to be met when ensuring food safety. Considering though that there remain quite many problems which cannot yet be addressed with today's biosensor technologies, it is surprising to see that the trend throughout the latest publications remains on the detection of classical food contaminants, dominated by bacteria, pesticides and mycotoxins, using already well established sensor principles. In fact, truly innovative sensor designs are missing and those new developments published are most often based on established strategies with the implementation of nanomaterials or nanomaterial composites resulting in more sensitive systems. The more complex questions such as integrated sample preparation, direct detection in the food matrix, long-term stability, lowering sensor costs, and further simplification of their use persist. This lack of a major breakthrough in food safety analysis is not only limited to biosensor development but also holds true to food safety analysis in general when observing the last 5 years [11]. On the bright side, novel sensing strategies have been introduced lately in bioassay formats, which clearly have the potential of being integrated into future biosensors. Also, nanomaterials are studied for sample preparation and lowering of detection limits. Yet, nanomaterials are also notoriously associated with increased costs and additional complexity in large-scale production and hence require more in-depth evaluation, especially for their application of food safety and sustainable agriculture. [142] With respect to increased stability and lowered fabrication costs, aptamers as replacement for antibodies are being studied across the bioanalytical field. Their dual functionality for analyte binding and simultaneously nucleic acid hybridization capability offer additional biosensor design strategies. Here, integration of complex food matrices and agricultural matrices would assist in designing those high-affinity aptamers that would then truly address some of the major challenges aforementioned.

It is also surprising that biosensor application toward allergen detection and for food fraud identification were only addressed in smaller numbers over the course of the last five years. Considering that problems associated with food fraud and food adulteration are rising and that these are of high societal, economic and safety concern, the markers identified by food chemists today for food fingerprinting will be a rich target for biosensor development in the future [143]. The same holds true for the identification of allergens in food, as the need and demand for end-product testing increases.

Also reported only in small numbers and hence yet completely underestimated with respect to their potential impact, are biosensors addressing challenges in sustainable agriculture. Where resource spending has to be minimized, and where smart, localized strategies be dynamically adapted to best support agricultural production, biosensors will play a key role in providing required data. For example, continuous monitoring of plant health and the adequate detection of plant pathogens will minimize the amounts of fertilizers and pesticides used. This not only reduces contamination of food but also saves environmental resources. Advanced, but still limited, is the development of biosensors for livestock and animal health focusing on the detection of pathogenic species and therefore the early recognition of diseases. Due to the progress of implantable and wearable sensors in human medical diagnostics, implantable glucose sensors for animals are also commercially available, representing the stepping stone toward further similar (bio)sensors enabling the monitoring of physiological parameters of the individual animal. But even less specific wearable sensors used for real-time monitoring will become of great interest as these can trigger further diagnostics (through portable biosensors) or other actions. These types of (bio)sensors will thus increasingly become a useful tool for livestock monitoring in sustainable agriculture.

With the progressing possibility to store and share large data sets the evolving Internet of Things (IoT) will be a key part to increase food safety and obtain a more sustainable agriculture. With a connected network of devices gathering and sharing information about product irregularities within the food value chain are more likely to be detected early. For the traceability of food, the use of block chain technology is a promising approach to increase food safety and secure food quality. In first pilot projects block chain technology was already tested for this purpose with tracing every single step of mangos in the Americas and pork in China throughout the whole supply chain [144]. This task requires the connectivity of all parties with access to all data, and requires regular testing at many points, at all stages from field-to-fork. The IoT combined with block chain technology means that data from real-time monitoring and from point-to-point determinations are combined. This will be a powerful tool to ensure food safety and avoid food fraud within global food chains. Here, advantageous combination of biosensors with already established sensors and detection methods will be key. In the end, the slowly starting change in customer thinking, i.e. becoming more aware of food quality, animal welfare and the environmental consequences of today's agricultural practices can be taken as a start signal, and push towards sustainable developments. In this case, the possibly increased costs of (bio)sensors supporting the sustainability in agriculture and additional testing of food may either be negligible or simply accepted.

## 1.8 References

- [1] Food safety, (2019). <https://www.who.int/news-room/fact-sheets/detail/food-safety> (accessed December 17, 2019).
- [2] WHO, WHO estimates of the global burden of foodborne diseases: foodborne disease burden epidemiology reference group 2007-2015., (2015). [https://www.who.int/foodsafety/publications/foodborne\\_disease/fergreport/en/](https://www.who.int/foodsafety/publications/foodborne_disease/fergreport/en/) (accessed December 17, 2019).
- [3] Food Recalls Are Getting More Common. Here's Why | Time, (2019). <https://time.com/5504355/food-recalls-more-common/> (accessed December 17, 2019).
- [4] Gefährlicher Genuss: Warum die Zahl der Lebensmittelrückrufe steigt - Wirtschaft - Tagesspiegel, (2019). <https://www.tagesspiegel.de/wirtschaft/gefaehrlicher-genuss-warum-die-zahl-der-lebensmittelrueckrufe-steigt/24188026.html> (accessed December 17, 2019).
- [5] Scientific topic: Climate change and food safety | European Food, <https://www.efsa.europa.eu/en/topics/topic/climate-change-and-food-safety> (accessed December 17, 2019).
- [6] S. Online, Ehec-Epidemie 2011: Die Infektionsquelle wurde nie gefunden - SPIEGEL ONLINE, (2013). <https://www.spiegel.de/wirtschaft/service/ehec-epidemie-2011-die-infektionsquelle-wurde-nie-gefunden-a-923249.html> (accessed December 17, 2019).
- [7] Food Safety Testing Market Size, Share, and Growth - Forecast to 2023, <https://www.marketsandmarkets.com/Market-Reports/food-safety-365.html> (accessed December 17, 2019).
- [8] Food Safety Testing Market « Global Market Insights, Inc., <https://gminsights.wordpress.com/tag/food-safety-testing-market/> (accessed April 13, 2020).
- [9] J.F.C.A. Commission, General Standard for Contaminants and Toxins in Food and Feed, Codex Alimentarius CXS 193-1995;, World Health Organization; Food and Agriculture Organization of the United States, 1995.
- [10] M.L.K. Tang, R.J. Mullins, Food allergy: is prevalence increasing?, Intern. Med. J. 47 (2017) 256–261. <https://doi.org/10.1111/imj.13362>.
- [11] C.A. Hermann, A. Duerkop, A.J. Baeumner, Food Safety Analysis Enabled through Biological and Synthetic Materials: A Critical Review of Current Trends, Anal. Chem. 91 (2019) 569–587. <https://doi.org/10.1021/acs.analchem.8b04598>.
- [12] Food Safety Testing Market Size, Share and Growth Forecast - 2025, <https://www.alliedmarketresearch.com/food-safety-testing-market> (accessed December 17, 2019).
- [13] J.C. Moore, J. Spink, M. Lipp, Development and Application of a Database of Food Ingredient Fraud and Economically Motivated Adulteration from 1980 to 2010, J. Food Sci. 77 (2012) R118–R126. <https://doi.org/10.1111/j.1750-3841.2012.02657.x>.
- [14] Sustainable Agriculture | National Institute of Food and Agriculture, <https://nifa.usda.gov/topic/sustainable-agriculture> (accessed December 17, 2019).
- [15] Sustainable agriculture | Sustainable Development Goals | Food and Agriculture Organization of the United Nations, <http://www.fao.org/sustainable-development-goals/overview/fao-and-the-post-2015-development-agenda/sustainable-agriculture/en/> (accessed December 17, 2019).

- [16] What is sustainable agriculture | Agricultural Sustainability Institute, <https://asi.ucdavis.edu/programs/ucsarep/about/what-is-sustainable-agriculture> (accessed December 17, 2019).
- [17] C. by A.D.M. and A. Wilkinson., IUPAC Compendium of Chemical Terminology, 2nd ed. (the "GoldBook"), Blackwell Scientific Publications, Oxford, 1997. <https://doi.org/10.1351/goldbook>.
- [18] Y. Wu, I. Belmonte, K.S. Sykes, Y. Xiao, R.J. White, A Perspective on the Future Role of Aptamers in Analytical Chemistry, *Anal. Chem.* (2019) [acs.analchem.9b03853](https://doi.org/10.1021/acs.analchem.9b03853). <https://doi.org/10.1021/acs.analchem.9b03853>.
- [19] SIRA Technologies Food Sentinel System – Barcode Equipment and Labeling Solution, (n.d.). <https://www.adazonusa.com/blog/barcode-industry/sira-technologies-food-sentinel-system> (accessed April 13, 2020).
- [20] Toxin Alert! | The Engineer The Engineer, <https://www.theengineer.co.uk/toxin-alert/> (accessed April 13, 2020).
- [21] K.B. Biji, C.N. Ravishankar, C.O. Mohan, T.K. Srinivasa Gopal, Smart packaging systems for food applications: a review, *J. Food Sci. Technol.* 52 (2015) 6125–6135. <https://doi.org/10.1007/s13197-015-1766-7>.
- [22] TTI Label › Vitsab International AB, (n.d.). <http://vitsab.com/en/tti-label/> (accessed April 10, 2020).
- [23] FIS - Companies & Products - Cryolog Offers Intelligent Traceability Solutions, <https://www.fis.com/fis/techno/newtechno.asp?id=36695&l=e&ndb=1> (accessed April 10, 2020).
- [24] Y.W. Park, S.M. Kim, J.Y. Lee, W. Jang, Application of biosensors in smart packaging, *Mol. Cell. Toxicol.* 11 (2015) 277–285. <https://doi.org/10.1007/s13273-015-0027-1>.
- [25] H. Yousefi, M.M. Ali, H.M. Su, C.D.M. Filipe, T.F. Didar, Sentinel Wraps: Real-Time Monitoring of Food Contamination by Printing DNAzyme Probes on Food Packaging, *ACS Nano.* 12 (2018) 3287–3294. <https://doi.org/10.1021/acsnano.7b08010>.
- [26] T. Dodevska, Y. Lazarova, I. Shterev, Amperometric biosensors for glucose and lactate with applications in food analysis: A brief review, *Acta Chim. Slov.* 66 (2019) 762–776. <https://doi.org/10.17344/acsi.2019.5261>.
- [27] H. Okuma, W. Okazaki, R. Usami, K. Horikoshi, Development of the enzyme reactor system with an amperometric detection and application to estimation of the incipient stage of spoilage of chicken, *Anal. Chim. Acta.* 411 (2000) 37–43. [https://doi.org/10.1016/S0003-2670\(00\)00739-X](https://doi.org/10.1016/S0003-2670(00)00739-X).
- [28] K. Punakivi, M. Smolander, M.L. Niku-Paavola, J. Mattinen, J. Buchert, Enzymatic determination of biogenic amines with transglutaminase, *Talanta.* 68 (2006) 1040–1045. <https://doi.org/10.1016/j.talanta.2005.06.009>.
- [29] P. Müller, M. Schmid, Intelligent packaging in the food sector: A brief overview, *Foods.* 8 (2019). <https://doi.org/10.3390/foods8010016>.
- [30] H. Yousefi, H.M. Su, S.M. Imani, K. Alkhalidi, C.D. Filipe, T.F. Didar, Intelligent Food Packaging: A Review of Smart Sensing Technologies for Monitoring Food Quality, *ACS Sensors.* 4 (2019) 808–821. <https://doi.org/10.1021/acssensors.9b00440>.
- [31] S. Díaz-Amaya, L.-K. Lin, A.J. Deering, L.A. Stanciu, Aptamer-based SERS biosensor for whole cell analytical detection of *E. coli* O157:H7, *Anal. Chim. Acta.* 1081 (2019) 146–156. <https://doi.org/10.1016/j.aca.2019.07.028>.

- [32] S. Díaz-Amaya, M. Zhao, L. Lin, C. Ostos, J.P. Allebach, G.T. -C. Chiu, A.J. Deering, L.A. Stanciu, Inkjet Printed Nanopatterned Aptamer-Based Sensors for Improved Optical Detection of Foodborne Pathogens, *Small*. 15 (2019) 1805342. <https://doi.org/10.1002/smll.201805342>.
- [33] Y. Li, H. Ma, L. Gan, A. Gong, H. Zhang, D. Liu, Q. Sun, Selective and sensitive Escherichia coli detection based on a T4 bacteriophage-immobilized multimode microfiber, *J. Biophotonics*. 11 (2018) e201800012. <https://doi.org/10.1002/jbio.201800012>.
- [34] F. Zheng, P. Wang, Q. Du, Y. Chen, N. Liu, Simultaneous and Ultrasensitive Detection of Foodborne Bacteria by Gold Nanoparticles-Amplified Microcantilever Array Biosensor, *Front. Chem.* 7 (2019) 232. <https://doi.org/10.3389/fchem.2019.00232>.
- [35] Q. Pei, X. Song, S. Liu, J. Wang, X. Leng, X. Cui, J. Yu, Y. Wang, J. Huang, A facile signal-on electrochemical DNA sensing platform for ultrasensitive detection of pathogenic bacteria based on Exo III-assisted autonomous multiple-cycle amplification, *Analyst*. 144 (2019) 3023–3029. <https://doi.org/10.1039/c9an00036d>.
- [36] J.A. Capobianco, J. Lee, C.M. Armstrong, A.G. Gehring, Rapid detection of Salmonella enterica serotype Typhimurium in large volume samples using porous electrodes in a flow-through, enzyme-amplified immunoelectrochemical sensor, *Anal. Bioanal. Chem.* (2019). <https://doi.org/10.1007/s00216-019-01901-3>.
- [37] S. Wang, L. Zheng, G. Cai, N. Liu, M. Liao, Y. Li, X. Zhang, J. Lin, A microfluidic biosensor for online and sensitive detection of Salmonella typhimurium using fluorescence labeling and smartphone video processing, *Biosens. Bioelectron.* 140 (2019). <https://doi.org/10.1016/j.bios.2019.111333>.
- [38] Y. Xu, Y. Wei, N. Cheng, K. Huang, W. Wang, L. Zhang, W. Xu, Y. Luo, Nucleic Acid Biosensor Synthesis of an All-in-One Universal Blocking Linker Recombinase Polymerase Amplification with a Peptide Nucleic Acid-Based Lateral Flow Device for Ultrasensitive Detection of Food Pathogens, *Anal. Chem.* 90 (2018) 708–715. <https://doi.org/10.1021/acs.analchem.7b01912>.
- [39] D.L. Alexandre, A.M.A. Melo, R.F. Furtado, M.F. Borges, E.A.T. Figueiredo, A. Biswas, H.N. Cheng, C.R. Alves, A Rapid and Specific Biosensor for Salmonella Typhimurium Detection in Milk, *Food Bioprocess Technol.* 11 (2018) 748–756. <https://doi.org/10.1007/s11947-017-2051-8>.
- [40] Z. Wang, X. Yao, R. Wang, Y. Ji, T. Yue, J. Sun, T. Li, J. Wang, D. Zhang, Label-free strip sensor based on surface positively charged nitrogen-rich carbon nanoparticles for rapid detection of Salmonella enteritidis, *Biosens. Bioelectron.* 132 (2019) 360–367. <https://doi.org/10.1016/j.bios.2019.02.061>.
- [41] T. Bu, Q. Huang, L. Yan, W. Zhang, L. Dou, L. Huang, Q. Yang, B. Zhao, B. Yang, T. Li, J. Wang, D. Zhang, Applicability of biological dye tracer in strip biosensor for ultrasensitive detection of pathogenic bacteria, *Food Chem.* 274 (2019) 816–821. <https://doi.org/10.1016/j.foodchem.2018.09.066>.
- [42] A. Fulgione, M. Cimafonte, B. Della Ventura, M. Iannaccone, C. Ambrosino, F. Capuano, Y.T.R. Proroga, R. Velotta, R. Capparelli, QCM-based immunosensor for rapid detection of Salmonella Typhimurium in food, *Sci. Rep.* 8 (2018). <https://doi.org/10.1038/s41598-018-34285-y>.
- [43] J. Chen, B. Park, Label-free screening of foodborne Salmonella using surface plasmon resonance imaging, *Anal. Bioanal. Chem.* 410 (2018) 5455–5464. <https://doi.org/10.1007/s00216-017-0810-z>.
- [44] Z. Wu, Simultaneous Detection of Listeria monocytogenes and Salmonella typhimurium by a SERS-Based Lateral Flow Immunochromatographic Assay, *Food Anal. Methods*. 12 (2019) 1086–1091. <https://doi.org/10.1007/s12161-019-01444-4>.

- [45] M. Chiriaco, I. Parlangei, F. Sirsi, P. Poltronieri, E. Primiceri, Impedance Sensing Platform for Detection of the Food Pathogen *Listeria monocytogenes*, *Electronics*. 7 (2018) 347. <https://doi.org/10.3390/electronics7120347>.
- [46] D. Ren, C. Sun, Z. Huang, Z. Luo, C. Zhou, Y. Li, A novel FRET biosensor based on four-way branch migration HCR for *Vibrio parahaemolyticus* detection, *Sensors Actuators, B Chem.* 296 (2019). <https://doi.org/10.1016/j.snb.2019.05.054>.
- [47] F. Yang, T.L. Chang, T. Liu, D. Wu, H. Du, J. Liang, F. Tian, Label-free detection of *Staphylococcus aureus* bacteria using long-period fiber gratings with functional polyelectrolyte coatings, *Biosens. Bioelectron.* 133 (2019) 147–153. <https://doi.org/10.1016/j.bios.2019.03.024>.
- [48] B.D. Abera, A. Falco, P. Ibba, G. Cantarella, L. Petti, P. Lugli, Development of Flexible Dispense-Printed Electrochemical Immunosensor for Aflatoxin M1 Detection in Milk, *Sensors*. 19 (2019) 3912. <https://doi.org/10.3390/s19183912>.
- [49] X. Guo, F. Wen, Q. Qiao, N. Zheng, M. Saive, M.-L. Fauconnier, J. Wang, A Novel Graphene Oxide-Based Aptasensor for Amplified Fluorescent Detection of Aflatoxin M1 in Milk Powder, *Sensors*. 19 (2019) 3840. <https://doi.org/10.3390/s19183840>.
- [50] C. Gu, L. Yang, M. Wang, N. Zhou, L. He, Z. Zhang, M. Du, A bimetallic (Cu-Co) Prussian Blue analogue loaded with gold nanoparticles for impedimetric aptasensing of ochratoxin a, *Microchim. Acta*. 186 (2019). <https://doi.org/10.1007/s00604-019-3479-5>.
- [51] J. Somerson, K. Plaxco, Electrochemical Aptamer-Based Sensors for Rapid Point-of-Use Monitoring of the Mycotoxin Ochratoxin A Directly in a Food Stream, *Molecules*. 23 (2018) 912. <https://doi.org/10.3390/molecules23040912>.
- [52] G. Xu, J. Hou, Y. Zhao, J. Bao, M. Yang, H. Fa, Y. Yang, L. Li, D. Huo, C. Hou, Dual-signal aptamer sensor based on polydopamine-gold nanoparticles and exonuclease I for ultrasensitive malathion detection, *Sensors Actuators, B Chem.* (2019) 428–436. <https://doi.org/10.1016/j.snb.2019.01.113>.
- [53] J. Bao, T. Huang, Z. Wang, H. Yang, X. Geng, G. Xu, M. Samalo, M. Sakinati, D. Huo, C. Hou, 3D graphene/copper oxide nano-flowers based acetylcholinesterase biosensor for sensitive detection of organophosphate pesticides, *Sensors Actuators, B Chem.* 279 (2019) 95–101. <https://doi.org/10.1016/j.snb.2018.09.118>.
- [54] B. Zou, Y. Chu, J. Xia, Monocrotophos detection with a bienzyme biosensor based on ionic-liquid-modified carbon nanotubes, *Anal. Bioanal. Chem.* 411 (2019) 2905–2914. <https://doi.org/10.1007/s00216-019-01743-z>.
- [55] Z. Bin, C. Yanhong, X. Jiaojiao, Y. Jing, Acetylcholinesterase biosensor based on functionalized surface of carbon nanotubes for monocrotophos detection, *Anal. Biochem.* 560 (2018) 12–18. <https://doi.org/10.1016/j.ab.2018.08.024>.
- [56] M.K.L. da Silva, H.C. Vanzela, L.M. Defavari, I. Cesarino, Determination of carbamate pesticide in food using a biosensor based on reduced graphene oxide and acetylcholinesterase enzyme, *Sensors Actuators, B Chem.* 277 (2018) 555–561. <https://doi.org/10.1016/j.snb.2018.09.051>.
- [57] L. Cervera-Chiner, M. Juan-Borrás, C. March, A. Arnau, I. Escriche, Á. Montoya, Y. Jiménez, High Fundamental Frequency Quartz Crystal Microbalance (HFF-QCM) immunosensor for pesticide detection in honey, *Food Control*. 92 (2018) 1–6. <https://doi.org/10.1016/j.foodcont.2018.04.026>.
- [58] Q. Li, X. Dou, L. Zhang, X. Zhao, J. Luo, M. Yang, Oriented assembly of surface plasmon resonance biosensor through staphylococcal protein A for the chlorpyrifos detection, *Anal. Bioanal. Chem.* 411 (2019) 6057–6066. <https://doi.org/10.1007/s00216-019-01990-0>.

- [59] R. Nie, X. Xu, Y. Chen, L. Yang, Optical Fiber-Mediated Immunosensor with a Tunable Detection Range for Multiplexed Analysis of Veterinary Drug Residues, *ACS Sensors*. 4 (2019) 1864–1872. <https://doi.org/10.1021/acssensors.9b00653>.
- [60] T. Ye, Y. Peng, M. Yuan, H. Cao, J. Yu, Y. Li, F. Xu, A “turn-on” fluorometric assay for kanamycin detection by using silver nanoclusters and surface plasmon enhanced energy transfer, *Microchim. Acta*. 186 (2019). <https://doi.org/10.1007/s00604-018-3161-3>.
- [61] J. Wu, Y. Lu, N. Ren, M. Jia, R. Wang, J. Zhang, DNAzyme-Functionalized R-Phycoerythrin as a Cost-Effective and Environment-Friendly Fluorescent Biosensor for Aqueous Pb<sup>2+</sup> Detection, *Sensors*. 19 (2019) 2732. <https://doi.org/10.3390/s19122732>.
- [62] L. Wu, H. Yan, J. Wang, G. Liu, W. Xie, Tyrosinase Incorporated with Au-Pt@SiO<sub>2</sub> Nanospheres for Electrochemical Detection of Bisphenol A, *J. Electrochem. Soc.* 166 (2019) B562–B568. <https://doi.org/10.1149/2.0141908jes>.
- [63] X. Peng, L. Kang, F. Pang, H. Li, R. Luo, X. Luo, F. Sun, A signal-enhanced lateral flow strip biosensor for ultrasensitive and on-site detection of bisphenol A, *Food Agric. Immunol.* 29 (2018) 216–227. <https://doi.org/10.1080/09540105.2017.1365822>.
- [64] Y. Wang, Z. Rao, J. Zhou, L. Zheng, L. Fu, A chiral assembly of gold nanoparticle trimer-based biosensors for ultrasensitive detection of the major allergen tropomyosin in shellfish, *Biosens. Bioelectron.* 132 (2019) 84–89. <https://doi.org/10.1016/j.bios.2019.02.038>.
- [65] Y. Xia, P. Zhang, H. Yuan, R. Su, R. Huang, W. Qi, Z. He, Sequential sandwich immunoassay for simultaneous detection in trace samples using single-channel surface plasmon resonance, *Analyst*. 144 (2019) 5700–5705. <https://doi.org/10.1039/c9an01183h>.
- [66] Y. Gu, J. Wang, M. Pan, S. Li, G. Fang, S. Wang, Label-free impedimetric immunosensor based on one-step co-electrodeposited poly-(pyrrole-co-pyrrole-1-propionic acid) and reduced graphene oxide polymer modified layer for the determination of melamine, *Sensors Actuators, B Chem.* 283 (2019) 571–578. <https://doi.org/10.1016/j.snb.2018.12.046>.
- [67] Z. Wu, A Dual-Mode (Fluorometric and Colorimetric) Aptasensor for *Vibrio parahaemolyticus* Detection Using Multifunctional Nanoparticles, *Food Anal. Methods*. (2019). <https://doi.org/10.1007/s12161-019-01483-x>.
- [68] S. Li, S. Liu, Y. Xu, R. Zhang, Y. Zhao, X. Qu, Y. Wang, J. Huang, J. Yu, Robust and highly specific fluorescence sensing of *Salmonella typhimurium* based on dual-functional phi29 DNA polymerase-mediated isothermal circular strand displacement polymerization, *Analyst*. 144 (2019) 4795–4802. <https://doi.org/10.1039/c9an00843h>.
- [69] J. Chen, S.D. Alcaine, Z. Jiang, V.M. Rotello, S.R. Nugen, Detection of *Escherichia coli* in Drinking Water Using T7 Bacteriophage-Conjugated Magnetic Probe, *Anal. Chem.* 87 (2015) 8977–8984. <https://doi.org/10.1021/acs.analchem.5b02175>.
- [70] D. Wang, T. Hinkley, J. Chen, J.N. Talbert, S.R. Nugen, Phage based electrochemical detection of: *Escherichia coli* in drinking water using affinity reporter probes, *Analyst*. 144 (2019) 1345–1352. <https://doi.org/10.1039/c8an01850b>.
- [71] D. Zhang, C.P. Coronel-Aguilera, P.L. Romero, L. Perry, U. Minocha, C. Rosenfield, A.G. Gehring, G.C. Paoli, A.K. Bhunia, B. Applegate, The Use of a Novel NanoLuc-Based Reporter Phage for the Detection of *Escherichia coli* O157:H7, *Sci. Rep.* 6 (2016). <https://doi.org/10.1038/srep33235>.
- [72] S.D. Alcaine, L. Tilton, M.A.C. Serrano, M. Wang, R.W. Vachet, S.R. Nugen, Phage-protease-peptide: a novel trifecta enabling multiplex detection of viable bacterial pathogens, *Appl. Microbiol. Biotechnol.* 99 (2015) 8177–8185. <https://doi.org/10.1007/s00253-015-6867-8>.



- [73] T. Laube, P. Cortés, M. Llagostera, S. Alegret, M.I. Pividori, Phagomagnetic immunoassay for the rapid detection of Salmonella, *Appl. Microbiol. Biotechnol.* 98 (2014) 1795–1805. <https://doi.org/10.1007/s00253-013-5434-4>.
- [74] A.R. Bennett, F.G.C. Davids, S. Vlahodimou, J.G. Banks, R.P. Betts, The use of bacteriophage-based systems for the separation and concentration of Salmonella, *J. Appl. Microbiol.* 83 (1997) 259–265. <https://doi.org/10.1046/j.1365-2672.1997.00257.x>.
- [75] S.K. Arya, A. Singh, R. Naidoo, P. Wu, M.T. McDermott, S. Evoy, Chemically immobilized T4-bacteriophage for specific Escherichia coli detection using surface plasmon resonance, *Analyst.* 136 (2011) 486–492. <https://doi.org/10.1039/c0an00697a>.
- [76] S.K. Srivastava, H. Ben Hamo, A. Kushmaro, R.S. Marks, C. Grüner, B. Rauschenbach, I. Abdulhalim, Highly sensitive and specific detection of E. coli by a SERS nanobiosensor chip utilizing metallic nanosculptured thin films, *Analyst.* 140 (2015) 3201–3209. <https://doi.org/10.1039/c5an00209e>.
- [77] N. Bhardwaj, S.K. Bhardwaj, J. Mehta, G.C. Mohanta, A. Deep, Bacteriophage immobilized graphene electrodes for impedimetric sensing of bacteria (*Staphylococcus arlettae*), *Anal. Biochem.* 505 (2016) 18–25. <https://doi.org/10.1016/j.ab.2016.04.008>.
- [78] Ł. Richter, M. Janczuk-Richter, J. Niedziółka-Jönsson, J. Paczesny, R. Hołyst, Recent advances in bacteriophage-based methods for bacteria detection, *Drug Discov. Today.* 23 (2018) 448–455. <https://doi.org/10.1016/j.drudis.2017.11.007>.
- [79] R. Sharma, U.S. Akshath, P. Bhatt, K.S.M.S. Raghavarao, Fluorescent aptaswitch for chloramphenicol detection – Quantification enabled by immobilization of aptamer, *Sensors Actuators, B Chem.* (2019) 110–117. <https://doi.org/10.1016/j.snb.2019.03.093>.
- [80] Mycotoxins,. <https://www.who.int/news-room/fact-sheets/detail/mycotoxins> (accessed December 17, 2019).
- [81] N. Huang, Y. Qin, M. Li, T. Chen, M. Lu, J. Zhao, A sensitive fluorescence assay of organophosphorus pesticides using acetylcholinesterase and copper-catalyzed click chemistry, *Analyst.* 144 (2019) 3436–3441. <https://doi.org/10.1039/c9an00260j>.
- [82] Reshma, B. Gupta, R. Sharma, K.K. Ghosh, Facile and visual detection of acetylcholinesterase inhibitors by carbon quantum dots, *New J. Chem.* 43 (2019) 9924–9933. <https://doi.org/10.1039/c9nj02347j>.
- [83] R. Jin, D. Kong, X. Yan, X. Zhao, H. Li, F. Liu, P. Sun, Y. Lin, G. Lu, Integrating Target-Responsive Hydrogels with Smartphone for On-Site ppb-Level Quantitation of Organophosphate Pesticides, *ACS Appl. Mater. Interfaces.* 11 (2019) 27605–27614. <https://doi.org/10.1021/acsami.9b09849>.
- [84] W. Wang, Y. Zhu, Y. Chen, X. Xu, G. Zhou, Rapid visual detection of eight meat species using optical thin-film biosensor chips, *J. AOAC Int.* 98 (2015) 410–414. <https://doi.org/10.5740/jaoacint.14-230>.
- [85] L. Taboada, A. Sánchez, R.I. Pérez-Martín, C.G. Sotelo, A new method for the rapid detection of Atlantic cod (*Gadus morhua*), Pacific cod (*Gadus macrocephalus*), Alaska pollock (*Gadus chalcogrammus*) and ling (*Molva molva*) using a lateral flow dipstick assay, *Food Chem.* 233 (2017) 182–189. <https://doi.org/10.1016/j.foodchem.2017.04.087>.
- [86] Y. Xu, W. Xiang, Q. Wang, N. Cheng, L. Zhang, K. Huang, W. Xu, A smart sealed nucleic acid biosensor based on endogenous reference gene detection to screen and identify mammals on site, *Sci. Rep.* 7 (2017). <https://doi.org/10.1038/srep43453>.
- [87] R. Ramesh, P. Puhazhendi, J. Kumar, M.K. Gowthaman, S.F. D'Souza, N.R. Kamini, Potentiometric biosensor for determination of urea in milk using immobilized *Arthrobacter*

creatinolytic urease, *Mater. Sci. Eng. C.* 49 (2015) 786–792. <https://doi.org/10.1016/j.msec.2015.01.048>.

[88] M. Ezhilan, M.B. Gumpu, B.L. Ramachandra, N. Nesakumar, K.J. Babu, U.M. Krishnan, J.B.B. Rayappan, Design and development of electrochemical biosensor for the simultaneous detection of melamine and urea in adulterated milk samples, *Sensors Actuators, B Chem.* 238 (2017) 1283–1292. <https://doi.org/10.1016/j.snb.2016.09.100>.

[89] Y. Kato, Y. Araki, M. Juri, A. Ishisaka, Y. Nitta, T. Niwa, N. Kitamoto, Y. Takimoto, Competitive immunochromatographic assay for leptosperin as a plausible authentication marker of manuka honey, *Food Chem.* 194 (2016) 362–365. <https://doi.org/10.1016/j.foodchem.2015.08.040>.

[90] E. Hong, S.Y. Lee, J.Y. Jeong, J.M. Park, B.H. Kim, K. Kwon, H.S. Chun, Modern analytical methods for the detection of food fraud and adulteration by food category, *J. Sci. Food Agric.* 97 (2017) 3877–3896. <https://doi.org/10.1002/jsfa.8364>.

[91] S. Barrias, J.R. Fernandes, J.E. Eiras-Dias, J. Brazão, P. Martins-Lopes, Label free DNA-based optical biosensor as a potential system for wine authenticity, *Food Chem.* 270 (2019) 299–304. <https://doi.org/10.1016/j.foodchem.2018.07.058>.

[92] J. Mandli, I. EL Fatimi, N. Seddaoui, A. Amine, Enzyme immunoassay (ELISA/immunosensor) for a sensitive detection of pork adulteration in meat, *Food Chem.* 255 (2018) 380–389. <https://doi.org/10.1016/j.foodchem.2018.01.184>.

[93] Z. He, H. Yang, Colourimetric detection of swine-specific DNA for halal authentication using gold nanoparticles, *Food Control.* 88 (2018) 9–14. <https://doi.org/10.1016/j.foodcont.2018.01.001>.

[94] F.L. Migliorini, R.C. Sanfelice, L.A. Mercante, R.S. Andre, L.H.C. Mattoso, D.S. Correa, Urea impedimetric biosensing using electrospun nanofibers modified with zinc oxide nanoparticles, *Appl. Surf. Sci.* 443 (2018) 18–23. <https://doi.org/10.1016/j.apsusc.2018.02.168>.

[95] M. Berto, C. Diacci, L. Theuer, M. Di Lauro, D.T. Simon, M. Berggren, F. Biscarini, V. Beni, C.A. Bortolotti, Label free urea biosensor based on organic electrochemical transistors, *Flex. Print. Electron.* 3 (2018). <https://doi.org/10.1088/2058-8585/aac8a8>.

[96] F. Zhan, T. Wang, L. Iradukunda, J. Zhan, A gold nanoparticle-based lateral flow biosensor for sensitive visual detection of the potato late blight pathogen, *Phytophthora infestans*, *Anal. Chim. Acta.* 1036 (2018) 153–161. <https://doi.org/10.1016/j.aca.2018.06.083>.

[97] P. López-Soriano, P. Noguera, M.T. Gorris, R. Puchades, Á. Maquieira, E. Marco-Noales, M.M. López, Lateral flow immunoassay for on-site detection of *Xanthomonas arboricola* pv. *pruni* in symptomatic field samples, *PLoS One.* 12 (2017) e0176201. <https://doi.org/10.1371/journal.pone.0176201>.

[98] V.G. Panferov, I. V. Safenkova, N.A. Byzova, Y.A. Varitsev, A. V. Zherdev, B.B. Dzantiev, Silver-enhanced lateral flow immunoassay for highly-sensitive detection of potato leafroll virus, *Food Agric. Immunol.* 29 (2018) 445–457. <https://doi.org/10.1080/09540105.2017.1401044>.

[99] M. Drießen, Düngen oder nicht düngen - keine Frage, RUBIN, Wissenschaftsmagazin Der Ruhr-Universität Bochum. (2018) 18–21. [https://news.rub.de/sites/default/files/rubin\\_01\\_2018.pdf](https://news.rub.de/sites/default/files/rubin_01_2018.pdf).

[100] M. Berto, E. Vecchi, L. Baiamonte, C. Condò, M. Sensi, M. Di Lauro, M. Sola, A. De Stradis, F. Biscarini, A. Minafra, C.A. Bortolotti, Label free detection of plant viruses with organic transistor biosensors, *Sensors Actuators, B Chem.* 281 (2019) 150–156. <https://doi.org/10.1016/j.snb.2018.10.080>.

- [101] M. Khater, A. de la Escosura-Muñiz, D. Quesada-González, A. Merkoçi, Electrochemical detection of plant virus using gold nanoparticle-modified electrodes, *Anal. Chim. Acta.* 1046 (2019) 123–131. <https://doi.org/10.1016/j.aca.2018.09.031>.
- [102] M.N.A. Uda, C.M. Hasfalina, A.A. Samsuzana, U. Hashim, S.A.B. Ariffin, I. Zamri, W. Nur Sabrina, B.B. Siti Noraini, S. Faridah, M. Mazidah, S.C.B. Gopinath, Immunosensor development for rice tungro bacilliform virus (RTBV) detection using antibody nano-gold conjugate, in: *AIP Conf. Proc.*, American Institute of Physics Inc., 2017. <https://doi.org/10.1063/1.4975291>.
- [103] M. Regiart, M. Rinaldi-Tosi, P.R. Aranda, F.A. Bertolino, J. Villarreal-Rocha, K. Sapag, G.A. Messina, J. Raba, M.A. Fernández-Baldo, Development of a nanostructured immunosensor for early and in situ detection of *Xanthomonas arboricola* in agricultural food production, *Talanta.* 175 (2017) 535–541. <https://doi.org/10.1016/j.talanta.2017.07.086>.
- [104] D. Luna-Moreno, A. Sánchez-Álvarez, I. Islas-Flores, B. Canto-Canche, M. Carrillo-Pech, J. Villarreal-Chiu, M. Rodríguez-Delgado, Early Detection of the Fungal Banana Black Sigatoka Pathogen *Pseudocercospora fijiensis* by an SPR Immunosensor Method, *Sensors.* 19 (2019) 465. <https://doi.org/10.3390/s19030465>.
- [105] H.Y. Lau, Y. Wang, E.J.H. Wee, J.R. Botella, M. Trau, Field Demonstration of a Multiplexed Point-of-Care Diagnostic Platform for Plant Pathogens, *Anal. Chem.* 88 (2016) 8074–8081. <https://doi.org/10.1021/acs.analchem.6b01551>.
- [106] Y. Fang, Y. Umasankar, R.P. Ramasamy, A novel bi-enzyme electrochemical biosensor for selective and sensitive determination of methyl salicylate, *Biosens. Bioelectron.* 81 (2016) 39–45. <https://doi.org/10.1016/j.bios.2016.01.095>.
- [107] M. Pabbi, S.K. Mittal, An electrochemical algal biosensor based on silica coated ZnO quantum dots for selective determination of acephate, *Anal. Methods.* 9 (2017) 1672–1680. <https://doi.org/10.1039/c7ay00111h>.
- [108] M.A. Khatun, M.A. Hoque, Y. Zhang, T. Lu, L. Cui, N.Y. Zhou, Y. Feng, Bacterial Consortium-Based Sensing System for Detecting Organophosphorus Pesticides, *Anal. Chem.* 90 (2018) 10577–10584. <https://doi.org/10.1021/acs.analchem.8b02709>.
- [109] R. Francisco, R. Branco, S. Schwab, I. Baldani, P. V. Morais, Two plant-hosted whole-cell bacterial biosensors for detection of bioavailable Cr(VI), *World J. Microbiol. Biotechnol.* 35 (2019) 1–15. <https://doi.org/10.1007/s11274-019-2703-0>.
- [110] L. Bereza-Malcolm, S. Aracic, R. Kannan, G. Mann, A.E. Franks, Functional characterization of Gram-negative bacteria from different genera as multiplex cadmium biosensors, *Biosens. Bioelectron.* 94 (2017) 380–387. <https://doi.org/10.1016/j.bios.2017.03.029>.
- [111] H. Kim, W. Lee, Y. Yoon, Heavy metal(loid) biosensor based on split-enhanced green fluorescent protein: development and characterization, *Appl. Microbiol. Biotechnol.* 103 (2019) 6345–6352. <https://doi.org/10.1007/s00253-019-09908-7>.
- [112] H. Wang, Y. Liu, G. Liu, Reusable resistive aptasensor for Pb(II) based on the Pb(II)-induced despiralization of a DNA duplex and formation of a G-quadruplex, *Microchim. Acta.* 185 (2018) 1–8. <https://doi.org/10.1007/s00604-018-2682-0>.
- [113] J. Ding, Y. liu, D. Zhang, M. Yu, X. Zhan, D. Zhang, P. Zhou, An electrochemical aptasensor based on gold@polypyrrole composites for detection of lead ions, *Microchim. Acta.* 185 (2018) 1–7. <https://doi.org/10.1007/s00604-018-3068-z>.
- [114] J. Ni, H. Zhang, Y. Chen, F. Luo, J. Wang, L. Guo, B. Qiu, Z. Lin, DNAzyme-based Y-shaped label-free electrochemiluminescent biosensor for lead using electrically heated indium-tin-oxide electrode for in situ temperature control, *Sensors Actuators, B Chem.* 289 (2019) 78–84. <https://doi.org/10.1016/j.snb.2019.03.076>.

- [115] S. Xu, X. Chen, G. Peng, L. Jiang, H. Huang, An electrochemical biosensor for the detection of Pb<sup>2+</sup> based on G-quadruplex DNA and gold nanoparticles, *Anal. Bioanal. Chem.* 410 (2018) 5879–5887. <https://doi.org/10.1007/s00216-018-1204-6>.
- [116] H. Wang, Y. Yin, L. Gang, Single-gap Microelectrode Functionalized with Single-walled Carbon Nanotubes and Pbzyme for the Determination of Pb<sup>2+</sup>, *Electroanalysis*. 31 (2019) 1174–1181. <https://doi.org/10.1002/elan.201900016>.
- [117] M.F. Siddiqui, Z.A. Khan, H. Jeon, S. Park, SPE based soil processing and aptasensor integrated detection system for rapid on site screening of arsenic contamination in soil, *Ecotoxicol. Environ. Saf.* 196 (2020) 110559. <https://doi.org/10.1016/j.ecoenv.2020.110559>.
- [118] S. Xu, B. Dai, J. Xu, L. Jiang, H. Huang, An Electrochemical Sensor for the Detection of Cu<sup>2+</sup> Based on Gold Nanoflowers-modified Electrode and DNAzyme Functionalized Au@MIL-101 (Fe), *Electroanalysis*. 31 (2019) 2330–2338. <https://doi.org/10.1002/elan.201900343>.
- [119] M. Roushani, F. Shahdost-fard, A glassy carbon electrode with electrodeposited silver nanoparticles for aptamer based voltammetric determination of trinitrotoluene using riboflavin as a redox probe, *Microchim. Acta.* 185 (2018) 1–8. <https://doi.org/10.1007/s00604-018-3098-6>.
- [120] J.O. Eberly, M.L. Mayo, M.R. Carr, F.H. Crocker, K.J. Indest, Detection of hexahydro-1,3,5-trinitro-1,3,5-triazine (RDX) with a microbial sensor, *J. Gen. Appl. Microbiol.* 65 (2019) 145–150. <https://doi.org/10.2323/jgam.2018.08.001>.
- [121] J.A. Hondred, J.C. Breger, N.J. Alves, S.A. Trammell, S.A. Walper, I.L. Medintz, J.C. Claussen, Printed Graphene Electrochemical Biosensors Fabricated by Inkjet Maskless Lithography for Rapid and Sensitive Detection of Organophosphates, *ACS Appl. Mater. Interfaces*. 10 (2018) 11125–11134. <https://doi.org/10.1021/acsami.7b19763>.
- [122] G. Bayramoglu, V.C. Ozalp, M. Oztekin, M.Y. Arica, Rapid and label-free detection of *Brucella melitensis* in milk and milk products using an aptasensor, *Talanta*. 200 (2019) 263–271. <https://doi.org/10.1016/j.talanta.2019.03.048>.
- [123] S. Khan, Z.A. Ansari, H.K. Seo, S.G. Ansari, Synthesis and Application of Cu-Doped Nickel and Zirconium Oxide Nanoparticles as *Brucella abortus* Electrochemical Device Development, *Sens. Lett.* 16 (2018) 267–276. <https://doi.org/10.1166/sl.2018.3949>.
- [124] S. Li, Y. Liu, Y. Wang, M. Wang, C. Liu, Y. Wang, Rapid Detection of *Brucella* spp. and Elimination of Carryover Using Multiple Cross Displacement Amplification Coupled With Nanoparticles-Based Lateral Flow Biosensor, *Front. Cell. Infect. Microbiol.* 9 (2019). <https://doi.org/10.3389/fcimb.2019.00078>.
- [125] S. Li, Y. Liu, Y. Wang, H. Chen, C. Liu, Y. Wang, Lateral flow biosensor combined with loop-mediated isothermal amplification for simple, rapid, sensitive, and reliable detection of *Brucella* spp, *Infect. Drug Resist.* 12 (2019) 2343–2353. <https://doi.org/10.2147/IDR.S211644>.
- [126] A. Rahi, N. Sattarahmady, H. Heli, An ultrasensitive electrochemical genosensor for *Brucella* based on palladium nanoparticles, *Anal. Biochem.* 510 (2016) 11–17. <https://doi.org/10.1016/j.ab.2016.07.012>.
- [127] S. Lv, J. Sheng, S. Zhao, M. Liu, L. Chen, The detection of brucellosis antibody in whole serum based on the low-fouling electrochemical immunosensor fabricated with magnetic Fe<sub>3</sub>O<sub>4</sub>@Au@PEG@HA nanoparticles, *Biosens. Bioelectron.* 117 (2018) 138–144. <https://doi.org/10.1016/j.bios.2018.06.010>.
- [128] M.E. Cortina, L.J. Melli, M. Roberti, M. Mass, G. Longinotti, S. Tropea, P. Lloret, D.A.R. Serantes, F. Salomón, M. Lloret, A.J. Caillava, S. Restuccia, J. Altcheh, C.A. Buscaglia, L. Malatto, J.E. Ugalde, L. Fraigi, C. Moina, G. Ybarra, A.E. Ciochini, D.J. Comerçi, Electrochemical magnetic

microbeads-based biosensor for point-of-care serodiagnosis of infectious diseases, *Biosens. Bioelectron.* 80 (2016) 24–33. <https://doi.org/10.1016/j.bios.2016.01.021>.

[129] S. Carrara, L. Bolomey, C. Boero, A. Cavallini, E. Meurville, G. De Micheli, T.R. Jost, M. Proietti, F. Grassi, Remote system for monitoring animal models with single-metabolite bio-nanosensors, *IEEE Sens. J.* 13 (2013) 1018–1024. <https://doi.org/10.1109/JSEN.2012.2231670>.

[130] Implantable Glucose Telemetry, (n.d.). <https://www.datasci.com/glucose/home> (accessed December 17, 2019).

[131] W. Gao, S. Emaminejad, H.Y.Y. Nyein, S. Challa, K. Chen, A. Peck, H.M. Fahad, H. Ota, H. Shiraki, D. Kiriya, D.H. Lien, G.A. Brooks, R.W. Davis, A. Javey, Fully integrated wearable sensor arrays for multiplexed in situ perspiration analysis, *Nature.* 529 (2016) 509–514. <https://doi.org/10.1038/nature16521>.

[132] S. Neethirajan, Recent advances in wearable sensors for animal health management, *Sens. Bio-Sensing Res.* 12 (2017) 15–29. <https://doi.org/10.1016/j.sbsr.2016.11.004>.

[133] S. Neethirajan, S.K. Tuteja, S.T. Huang, D. Kelton, Recent advancement in biosensors technology for animal and livestock health management, *Biosens. Bioelectron.* 98 (2017) 398–407. <https://doi.org/10.1016/j.bios.2017.07.015>.

[134] C. Duarte, T. Costa, C. Carneiro, R. Soares, A. Jitariu, S. Cardoso, M. Piedade, R. Bexiga, P. Freitas, Semi-Quantitative Method for Streptococci Magnetic Detection in Raw Milk, *Biosensors.* 6 (2016) 19. <https://doi.org/10.3390/bios6020019>.

[135] R. Wang, L. Wang, Z.T. Callaway, H. Lu, T.J. Huang, Y. Li, A nanowell-based QCM aptasensor for rapid and sensitive detection of avian influenza virus, *Sensors Actuators, B Chem.* 240 (2017) 934–940. <https://doi.org/10.1016/j.snb.2016.09.067>.

[136] S. Karash, R. Wang, L. Kelso, H. Lu, T.J. Huang, Y. Li, Rapid detection of avian influenza virus H5N1 in chicken tracheal samples using an impedance aptasensor with gold nanoparticles for signal amplification, *J. Virol. Methods.* 236 (2016) 147–156. <https://doi.org/10.1016/j.jviromet.2016.07.018>.

[137] A. Tarasov, D.W. Gray, M.Y. Tsai, N. Shields, A. Montrose, N. Creedon, P. Lovera, A. O’Riordan, M.H. Mooney, E.M. Vogel, A potentiometric biosensor for rapid on-site disease diagnostics, *Biosens. Bioelectron.* 79 (2016) 669–678. <https://doi.org/10.1016/j.bios.2015.12.086>.

[138] A.M. Niamh, C. Ryona Sayers, S.B. Alan O’riordan, Novel Single Gold Nanowire-based Electrochemical Immunosensor for Rapid Detection of Bovine Viral Diarrhoea Antibodies in Serum, *J. Biosens. Bioelectron.* 06 (2015). <https://doi.org/10.4172/2155-6210.1000174>.

[139] M. Yang, N.R. Caterer, W. Xu, M. Goolia, Development of a multiplex lateral flow strip test for foot-and-mouth disease virus detection using monoclonal antibodies, *J. Virol. Methods.* 221 (2015) 119–126. <https://doi.org/10.1016/j.jviromet.2015.05.001>.

[140] E. Zeidan, R. Shivaji, V.C. Henrich, M.G. Sandros, Nano-SPRi Aptasensor for the Detection of Progesterone in Buffer, *Sci. Rep.* 6 (2016). <https://doi.org/10.1038/srep26714>.

[141] J. Kim, S. Imani, W.R. de Araujo, J. Warchall, G. Valdés-Ramírez, T.R.L.C. Paixão, P.P. Mercier, J. Wang, Wearable salivary uric acid mouthguard biosensor with integrated wireless electronics, *Biosens. Bioelectron.* 74 (2015) 1061–1068. <https://doi.org/10.1016/j.bios.2015.07.039>.

[142] A matter of scale, *Nat. Nanotechnol.* 11 (2016) 733. <https://doi.org/10.1038/nnano.2016.180>.

[143] S. Medina, J.A. Pereira, P. Silva, R. Perestrelo, J.S. Câmara, Food fingerprints – A valuable tool to monitor food authenticity and safety, *Food Chem.* 278 (2019) 144–162. <https://doi.org/10.1016/j.foodchem.2018.11.046>.

[144] R. Kamath, Food Traceability on Blockchain: Walmart's Pork and Mango Pilots with IBM, J. Br. Blockchain Assoc. 1 (2018) 47–53. [https://doi.org/10.31585/jbba-1-1-\(10\)2018](https://doi.org/10.31585/jbba-1-1-(10)2018).

## 2 Electrochemical Lab-on-a-Chip Systems

### 2.1 Definition

LOC is a device which is capable to scale down laboratory functions to a chip-format up to a range of only a few square centimeters [1]. A LOC platform integrates and automates different laboratory functions. For analytical LOC systems, as here reviewed electrochemical LOC, the term miniaturized or micro total-analysis-system ( $\mu$ TAS) often is used as a synonym. Manz *et al.* defined  $\mu$ TAS as a total analysis system performing all sample handling steps extremely close to the place of measurement [2].

### 2.2 Design of lab-on-a-chip systems

As LOC systems enable the complete analysis of a sample the components of each system are chosen according to the analysis. Usually LOC systems contain microfluidic channels for the transportation of the sample. In addition to the microfluidic system several functionalities are combined on a LOC system according to the analytical problem. The most important features integrated into analytical LOC systems are sample preparation, separation and a detection system.

#### 2.2.1 Materials and fabrication

Fabrications of LOC systems from a variety of materials are reported (Figure 1 and Table 1). The first microfluidic devices were fabricated with inorganic substrates such as silicon or glass. With ongoing research and increasing popularity in the field of microfluidics polymers became the most common substrate for the fabrication of LOC systems. More recently, LOC systems based on paper have been described. Three main factors have to be taken into account when designing the microfluidic system: required function, degree of integration and application [3]. A brief overview of LOC materials with respect to their characteristics and fabrication techniques is given in Table 1. Each material for fabrications of LOC systems has its pros and cons (shown in Table 2) that have to be taken into consideration for proper applications. Excellent comprehensive reviews about the fabrication of microfluidic chips have been published recently [3–7].

---

**This chapter is published as chapter 2 in a review article.**

Nongnoot Wongkaew, Marcel Simsek, Christian Griesche, and Antje J. Baeumner, *Chem. Rev.* **2019**, 119, 1, 120–194, DOI: <https://doi.org/10.1021/acs.chemrev.8b00172>

**Author Contributions:** NW and AJB developed the idea of the manuscript. CG wrote the manuscript of this chapter. NW, MS and AJB revised the manuscript. AJB is corresponding author.

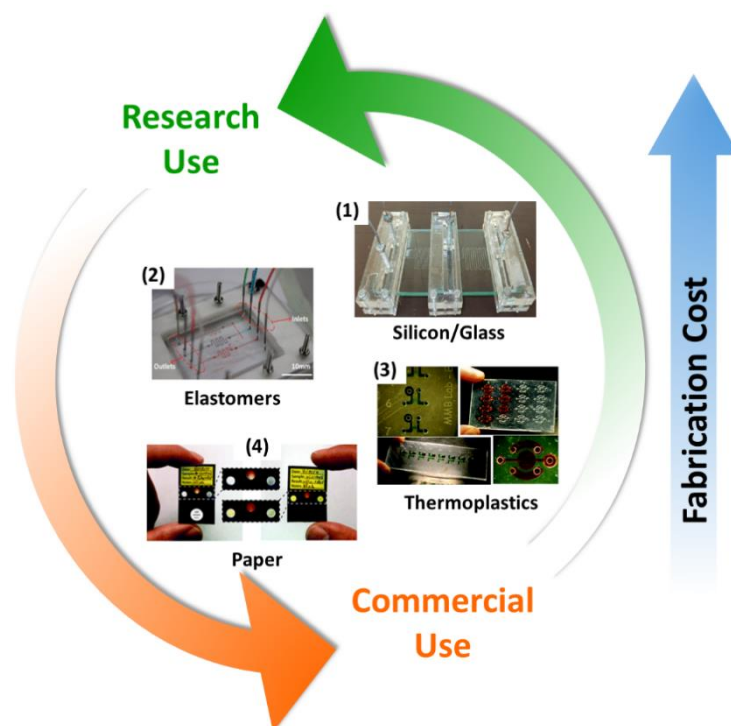


Figure 1 Schematic presentation of the relationship between fabrication costs of LOC devices using common materials and the fields of application. (1) Reproduced from [8]. Copyright 2017 American Chemical Society. (2) Reproduced from [9] Copyright 2017 American Chemical Society. (3) Reproduced from [10]. Copyright 2011 American Chemical Society. (4) Reproduced from [11]. Copyright 2012 American Chemical Society.

## 2.2.2 Integration of Sample Preparation

When handling real samples a variety of the sample characteristics can disturb the detection. Typically interfering species, complex matrix effects or non-specific binding affect the detection signal in a negative manner up to a disabled analysis. One strategy to reduce matrix effects and unspecific binding is the coating and blocking of the microfluidic structures. When coating and blocking is not sufficient for the required sensitivity two pathways are possible to obtain the same sample preparation as available during the bench-top approach. Micro-techniques can copy macro-techniques or micro-phenomena can be exploited [26]. Reviews with more detailed microfluidic sample preparation were published recently [26–29].



Table 1 Comparison of typical materials used for the fabrication of LOC systems.

Material	Characteristics	Material costs	Fabrication techniques	References
<b>Silicon</b>	Rigid, High temperature resistance, Ease of surface modifications (silanol), Biocompatible, Low unspecific binding, Not gas-permeable, An active fluidic system requires a polymer hybrid device	~2 \$/kg	photolithography, dry etching, wet etching, deep reactive ion etching, chemical vapor deposition	[6,12,13]
<b>Ceramics</b>	Rigid, Good mechanical, thermal and electrical properties		mechanical milling or using a laser mean followed by firing of the organic binder	[14,15]
<b>Glass</b>	Rigid, transparent, Ease of surface modification	1 ~ 13 \$/kg	photolithography, wet etching, dry etching,	[6,16,17]
<b>Poly(methyl methacrylate) (PMMA)</b>	Rigid, Transparent, Low water absorption	2 ~ 4 \$/kg	injection molding, hot embossing, laser photoablation, X-ray lithography	[17–21]
<b>Cyclic olefin copolymer (COC)</b>	Rigid, Transparent, Low water absorption	20 ~ 25 \$/kg	injection molding, hot embossing	[17,19–22]
<b>Polystyrene (PS)</b>	Rigid, Transparent	< 3 \$/kg	injection molding, hot embossing, laser photoablation	[17–19,21]
<b>Polycarbonate (PC)</b>	Rigid, Transparent, Highly heat resistant	< 3 \$/kg	injection molding, hot embossing, laser photoablation	[17–21]
<b>Polydimethylsiloxane (PDMS)</b>	Flexible, Transparent, Biocompatible, Chemically inert, Highly gas permeable	~ 150 \$/Kit (1 kg)	soft-lithography, direct laser plotting, casting	[17–19,23,24]
<b>Whatman chromatography paper</b>	Rigid, Pure cellulose, Homogenous, Reproducible, Biocompatible	~ 6 \$/m <sup>2</sup>	photolithography, plotting, plasma treatment, inkjet printing, wax printing, screen printing	[25]

Table 2 Evaluation of practicability of LOC materials for use in biosensor-related applications [6].

applications	silicon/glass	elastomers	thermoplastics	paper
<b>electrochemical detection</b>	good	limited	moderate	moderate
<b>cost of production</b>	high	medium	low	low
<b>reusability</b>	yes	no	yes	no
<b>disposable device use</b>	expensive	good	good	good
<b>online-monitoring</b>	yes	yes	yes	no

For several miniaturized preparation techniques as filtration, extraction, purification and enrichment significant progress is reported [3]. Yang *et al.* developed microfilter membranes based on paper for the separation of plasma from whole blood with comparable results to conventional centrifugation methods [30]. Solid-phase extraction (SPE) is used for purification and enrichment of samples. Together with other processes such as separation and detection SPE can be integrated into LOC systems [31]. Reversed-phase, using silica columns, and affinity SPE are the most common ones used in LOC systems. Monolithic structures for reversed phase SPE can be directly formed on the chip by UV polymerization of butyl-, lauryl-, octadecyl-, or 2-hydroxyethyl methacrylates [3]. Acrylate polymers also are reported for their application in on-chip SPE [27].

Immunoaffinity monolith is integrated in microchip electrophoresis for extraction and separation of preterm birth biomarkers directly from a human serum matrix [32]. The use of magnetic bead-based preconcentration is widely applied as an immune affinity interaction preconcentration method. Clean-up of the sample as well as preconcentration is achieved when the magnetic beads exhibit high affinity to the analyte [27]. The immobilization of analyte molecules and the following cleanup enable full control about solvent specific parameters as conductivity, pH and ionic strength.

Other preconcentration techniques applied to LOC systems utilize analyte characteristics like charge, affinity, mobility and size. Electrocapture can be used for preconcentration and cleanup of the sample by applying an electric field on a conductive membrane [27]. Other preparation and separation techniques based on electrophoresis are widely applied to LOC systems.[3] Porous membranes and a variety of nanomaterials can be used for a size-dependent sample preconcentration.

The lysis of cells in LOC systems can be performed with the same lysis efficiency as in the macro system using a miniaturized magnetically actuated bead-beating system [33].

For the cell separation and concentration various techniques exploiting micro-phenomena that leads to comparable results with bench-top approaches are reported. Cell separation was performed using the Zweifach-Fung bifurcation effect, inertial force-based cell separation, pinched flow fractionation, hydrodynamic filtration or diffusion-based separation using H-filters as well as electrokinetic or acoustic strategies [26].

### 2.2.3 On-chip electrochemistry

Electrochemistry is a promising detection strategy combined with LOC systems as it offers high sensitivity, low costs, low power requirement, independency of optical pathways and a distinctive compatibility with microfabrication and micromachining technologies [34]. The WE is the heart of the electrochemical detection. It is the place where the detection reaction occurs. The WE has to be selected regarding the redox behavior of the target analyte and the background current over the region of interest. The most common WE materials in LOC devices are carbon, gold and platinum. Different forms of carbon electrodes are integrated into LOC systems, e.g. carbon paste, carbon ink or glassy carbon [35]. In the following, the most successful strategies of how to integrate electrochemical detection with LOC are described. Some refer back to older publications so that a good overview of possible solutions can be provided. The most recent publications were selected as they portray the range of new strategies that help in overcoming the inherent challenges of electrode integration.

Electrodes in microfluidic systems can be produced with thin-film or thick-film techniques, respectively. Thick-film technology, with screen printing as its most established technique, in general is significantly cheaper than thin-film technology of noble metals and highly compatible with the fabrication of carbon electrodes. Screen printing of carbon electrodes can be performed on various substrates, e.g. alumina ceramic plate, [36] PDMS, [37] thermoplastics, [38][39][40] and can successfully be integrated in to microfluidic systems. Also, the technique is popular to provide Ag/AgCl REs (Figure 2) [41][42]. In fact, for the integration of electrodes into paper-based LOC platforms screen printing of the electrodes is the most common technique.

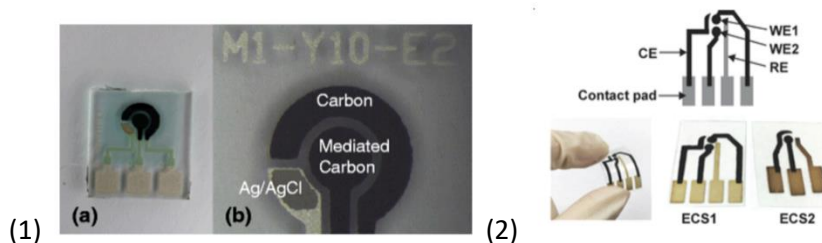


Figure 2 Screen-printed electrode. **(1)** Co-Phthalocyanine mediated SPE (a) and the electrode region (b). Reproduced with permission from Ref. [41]. Copyright 2014 Springer. **(2)** Electrochemical sensor (ECS) modules, ECS1 and ECS2. Reproduced with permission from Ref. [42]. Copyright 2017 Wiley-VCH Verlag GmbH & Co.

Additionally, inkjet printing has been employed as an efficient technique to pattern electrodes on flexible substrates. For example, inkjet printing of silver electrodes on PDMS is reported by Wu *et al.* [43] (Figure 3-1). Inkjet-printed gold electrodes on paper are reported as well [44]. Common electrode materials for the WE and CE are carbon, copper, gold or aluminum ink while the RE is usually fabricated with Ag/AgCl inks [25]. In 2009 Dungchai *et al.* demonstrated the electrochemical detection of glucose, lactate and uric acid (UA) on a paper-based LOC system [45]. Ko *et al.* report an electrical paper device with inkjet printed carbon nanotube electrodes (Figure 3-2) [46].

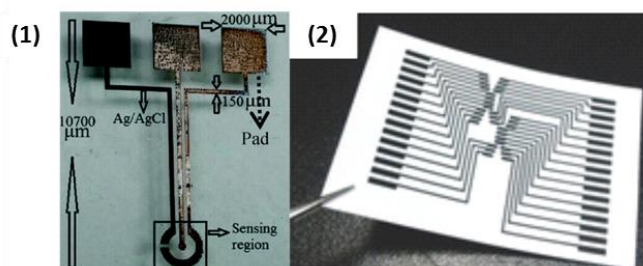


Figure 3 (1) Optical image of a three-electrode electrochemical sensor on PDMS after AgCl (black) formation. Reproduced with permission from Ref. [43]. Copyright 2015 The Royal Society of Chemistry. (2) Photograph of the printed-paper chip. Reproduced with permission from Ref. [46]. Copyright 2014 Wiley-VCH Verlag GmbH & Co.

Thin-film technology requires sophisticated instruments to create an electrode film (tens to a few hundreds of nanometers film thickness), especially for metals such as gold and platinum on rigid substrates such as glass and silicon wafers. For example, Ginet *et al.* fabricated gold microwires on a glass wafer by thermal evaporation (Figure 4-1) [47].

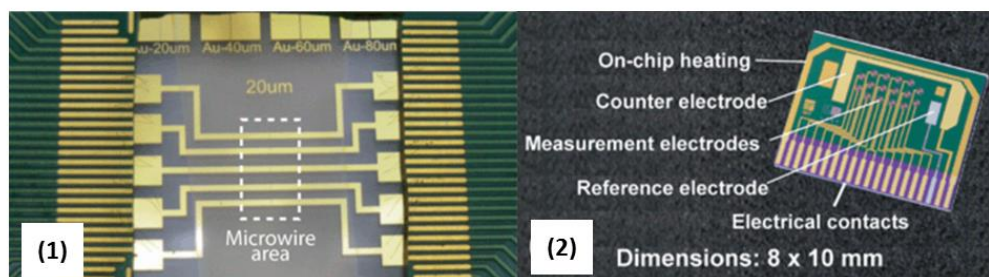


Figure 4 (1) Image of a device consisting of five gold electrodes deposited on a glass substrate. Microwires are patterned in the central part of the electrodes as indicated by the white rectangle. Reproduced with permission from Ref. [47]. Copyright 2011 The Royal Society of Chemistry. (2) Electrical biochip for single electrode redox cycling. Reproduced with permission from Ref. [48]. Copyright 2012 The Royal Society of Chemistry.

Deposition of gold electrodes by sputtering is also widely used [49]. In addition, Hilmi *et al.* reported electroless deposition of thin film gold electrodes to a glass substrate, which can be simply and routinely performed in any wet-chemistry laboratory [50]. Thin-film fabrication-based techniques typically requires added adhesive layer, e.g. Ti and Cr, in order to support the bonding between metal film and substrates [47][48][50][51]. Patterning electrodes can be performed using depositing thin film through a mask,[52] laser ablation, or using standard lithography followed by a lift-off process with higher resolution [53]. Furthermore, electrodeposition performed on base conductive electrodes has been employed to form thin-film bismuth electrodes on patterned gold electrodes [54,55].

The REs can be integrated using Ag/AgCl pastes, [39] screen printing,[42][56] using an Ag/AgCl wire as RE [40] or using sputtered Ag REs [57]. The integration of Ag/AgCl REs into microfluidic systems often is challenging. One major problem is the difficulty in transferring an internal electrolyte solution to miniaturized systems to construct the Ag/AgCl RE configuration similar to the stable macro RE. Thus, most miniaturized Ag/AgCl REs simply rely on “quasi-REs” or “pseudo-REs” where the Ag/AgCl is in direct contact with test solutions. Although the RE system has been successfully implemented to LOCs-based voltammetric sensors degradation of AgCl limits the longevity of pseudo-Ag/AgCl REs.[58] Moreover, the unstable ionic strength restricts the application of pseudo-REs in potentiometric measurement. As a result, a variety of strategies are proposed to overcome those problems [59]. A widely used strategy is the generation of salt bridges between the electrode and the channel [60–62]. A similar approach without the need of a solid salt bridge is reported by Wongkaew *et al.* A Ag RE is implemented into a side channel, containing KCl solution, that is pushed uninterrupted into the main channel [63]. The strategy is highly suitable for application in

miniaturized potentiometric sensors in which a stable potential regardless of ionic strengths of test solutions is required.

Alternatively, also pseudo-REs made of other metallic materials were integrated into microfluidic systems. For example, Odijk *et al.* used sputtered palladium as quasi-RE [64] while Noh *et al.* used a RE of nanoporous platinum [65]. Schumacher *et al.* reported the use of a sputtered iridium/iridiumoxide RE on a silicon wafer (Figure 4-2) [48].

## 2.3 References

- [1] S. Gupta, K. Ramesh, S. Ahmed, V. Kakkar, Lab-on-Chip Technology: A Review on Design Trends and Future Scope in Biomedical Applications, *Int. J. Bio-Science Bio-Technology*. 8 (2016) 311–322. <https://doi.org/10.14257/ijbsbt.2016.8.5.28>.
- [2] A. Manz, H.M. Widmers, N. Graber, Miniaturized total chemical analysis systems: A novel concept for chemical sensing, *Sensors Actuators B Chem.* 1 (1990) 244–248. [https://doi.org/10.1016/0925-4005\(90\)80209-I](https://doi.org/10.1016/0925-4005(90)80209-I).
- [3] P.N. Nge, C.I. Rogers, A.T. Woolley, Advances in microfluidic materials, functions, integration, and applications, *Chem. Rev.* 113 (2013) 2550–2583. <https://doi.org/10.1021/cr300337x>.
- [4] E. Verpoorte, N.F. De Rooij, Microfluidics meets MEMS, *Proc. IEEE*. 91 (2003) 930–953. <https://doi.org/10.1109/JPROC.2003.813570>.
- [5] P. Abgrall, A.M. Gué, Lab-on-chip technologies: Making a microfluidic network and coupling it into a complete microsystem - A review, *J. Micromechanics Microengineering*. 17 (2007) R15. <https://doi.org/10.1088/0960-1317/17/5/R01>.
- [6] K. Ren, J. Zhou, H. Wu, Materials for microfluidic chip fabrication, *Acc. Chem. Res.* 46 (2013) 2396–2406. <https://doi.org/10.1021/ar300314s>.
- [7] Y. Temiz, R.D. Lovchik, G. V. Kaigala, E. Delamarche, Lab-on-a-chip devices: How to close and plug the lab?, *Microelectron. Eng.* 132 (2015) 156–175. <https://doi.org/10.1016/j.mee.2014.10.013>.
- [8] S. Zeibi Shirejini, A. Mohammadi, Halogen-Lithium Exchange Reaction Using an Integrated Glass Microfluidic Device: An Optimized Synthetic Approach, *Org. Process Res. Dev.* 21 (2017) 292–303. <https://doi.org/10.1021/acs.oprd.6b00307>.
- [9] J. Qiu, Q. Gao, H. Zhao, J. Fu, Y. He, Rapid Customization of 3D Integrated Microfluidic Chips via Modular Structure-Based Design, *ACS Biomater. Sci. Eng.* 3 (2017) 2606–2616. <https://doi.org/10.1021/acsbiomaterials.7b00401>.
- [10] E.W.K. Young, E. Berthier, D.J. Guckenberger, E. Sackmann, C. Lamers, I. Meyvantsson, A. Huttenlocher, D.J. Beebe, Rapid prototyping of arrayed microfluidic systems in polystyrene for cell-based assays, *Anal. Chem.* 83 (2011) 1408–1417. <https://doi.org/10.1021/ac102897h>.
- [11] K.M. Schilling, A.L. Lepore, J.A. Kurian, A.W. Martinez, Fully enclosed microfluidic paper-based analytical devices, *Anal. Chem.* 84 (2012) 1579–1585. <https://doi.org/10.1021/ac202837s>.
- [12] C. Iliescu, H. Taylor, M. Avram, J. Miao, S. Franssila, A practical guide for the fabrication of microfluidic devices using glass and silicon, *Biomicrofluidics*. 6 (2012). <https://doi.org/10.1063/1.3689939>.
- [13] Silicon prices, <https://www.statista.com/statistics/301564/us-silicon-price-by-type/> (accessed March 14, 2018).
- [14] E.S. Fakunle, I. Fritsch, Low-temperature co-fired ceramic microchannels with individually addressable screen-printed gold electrodes on four walls for self-contained electrochemical immunoassays, *Anal. Bioanal. Chem.* 398 (2010) 2605–2615. <https://doi.org/10.1007/s00216-010-4098-5>.
- [15] C.S. Henry, M. Zhong, S.M. Lunte, M. Kim, H. Bau, J.J. Santiago, Ceramic microchips for capillary electrophoresis-electrochemistry, *Anal. Commun.* 36 (1999) 305307. <https://doi.org/10.1039/a904807c>.

- [16] Toughened borosilicate sight glass sheet, [https://www.alibaba.com/product-detail/Toughened-borosilicate-sight-glass-sheet-price\\_60690210760.html?spm=a2700.7724857.main07.10.782bd91dN00jLc&s=p](https://www.alibaba.com/product-detail/Toughened-borosilicate-sight-glass-sheet-price_60690210760.html?spm=a2700.7724857.main07.10.782bd91dN00jLc&s=p) (accessed March 14, 2018).
- [17] R.O. Rodrigues, R. Lima, H.T. Gomes, A.M.T. Silva, Polymer microfluidic devices: an overview of fabrication methods, *U.Porto J. Eng.* 1 (2017) 67–79. [https://doi.org/10.24840/2183-6493\\_001.001\\_0007](https://doi.org/10.24840/2183-6493_001.001_0007).
- [18] H. Becker, L.E. Locascio, Polymer microfluidic devices, *Talanta*. 56 (2002) 267–287. [https://doi.org/10.1016/S0039-9140\(01\)00594-X](https://doi.org/10.1016/S0039-9140(01)00594-X).
- [19] C.W. Tsao, Polymer microfluidics: Simple, low-cost fabrication process bridging academic lab research to commercialized production, *Micromachines*. 7 (2016) 1–11. <https://doi.org/10.3390/mi7120225>.
- [20] U.M. Attia, S. Marson, J.R. Alcock, Micro-injection moulding of polymer microfluidic devices, *Microfluid. Nanofluidics*. 7 (2009) 1–28. <https://doi.org/10.1007/s10404-009-0421-x>.
- [21] S. Li, Z. Xu, A. Mazzeo, D. Burns, G. Fu, M. Dirckx, V. Shilpiekandula, X. Chen, N. Nayak, E. Wong, S. Fatt Yoon, Z. Fang, Review of production of microfluidic devices: Material, manufacturing and metrology, *Proc. SPIE - Int. Soc. Opt. Eng.* 6993 (2008) 1–12. <https://doi.org/10.1117/12.781942>.
- [22] G. Khanarian, Optical properties of cyclic olefin copolymers, *Opt. Eng.* 40 (2001) 1024–1029. <https://doi.org/10.1117/1.1369411>.
- [23] H. Becker, C. Gärtner, Polymer microfabrication methods for microfluidic analytical applications, *Electrophoresis*. 21 (2000) 12–26. [https://doi.org/10.1002/\(SICI\)1522-2683\(20000101\)21:1<12::AID-ELPS12>3.0.CO;2-7](https://doi.org/10.1002/(SICI)1522-2683(20000101)21:1<12::AID-ELPS12>3.0.CO;2-7).
- [24] J.C. McDonald, D.C. Duffy, J.R. Anderson, D.T. Chiu, H. Wu, O.J. Schueller, G.M. Whitesides, Fabrication of Microfluidic Systems in Poly(dimethylsiloxane)., *Electrophoresis*. 21 (2000) 27–40. [https://doi.org/10.1002/\(SICI\)1522-2683\(20000101\)21:1<27::AID-ELPS27>3.0.CO;2-C](https://doi.org/10.1002/(SICI)1522-2683(20000101)21:1<27::AID-ELPS27>3.0.CO;2-C).
- [25] Y. Xu, M. Liu, N. Kong, J. Liu, Lab-on-paper micro- and nano-analytical devices: Fabrication, modification, detection and emerging applications, *Microchim. Acta*. 183 (2016) 1521–1542. <https://doi.org/10.1007/s00604-016-1841-4>.
- [26] N. Bunyakul, A.J. Baeumner, Combining electrochemical sensors with miniaturized sample preparation for rapid detection in clinical samples, *Sensors (Switzerland)*. 15 (2015) 547–564. <https://doi.org/10.3390/s150100547>.
- [27] X. Chen, D.F. Cui, Microfluidic devices for sample pretreatment and applications, *Microsyst. Technol.* 15 (2009) 667–676. <https://doi.org/10.1007/s00542-009-0783-8>.
- [28] B.C. Giordano, D.S. Burgi, S.J. Hart, A. Terray, On-line sample pre-concentration in microfluidic devices: A review, *Anal. Chim. Acta*. 718 (2012) 11–24. <https://doi.org/10.1016/j.aca.2011.12.050>.
- [29] M. Ritzi-Lehnert, Development of chip-compatible sample preparation for diagnosis of infectious diseases, *Expert Rev. Mol. Diagn.* 12 (2012) 189–206. <https://doi.org/10.1586/erm.11.98>.
- [30] X. Yang, O. Forouzan, T.P. Brown, S.S. Shevkopyas, Integrated separation of blood plasma from whole blood for microfluidic paper-based analytical devices, *Lab Chip*. 12 (2012) 274–280. <https://doi.org/10.1039/c1lc20803a>.
- [31] C.R. Reedy, K.A. Hagan, B.C. Strachan, J.J. Higginson, J.M. Bienvenue, S.A. Greenspoon, J.P. Ferrance, J.P. Landers, Dual-domain microchip-based process for volume reduction solid phase



extraction of nucleic acids from dilute, large volume biological samples, *Anal. Chem.* 82 (2010) 5669–5678. <https://doi.org/10.1021/ac100649b>.

[32] M. Sonker, E.K. Parker, A. V. Nielsen, V. Sahore, A.T. Woolley, Electrokinetically operated microfluidic devices for integrated immunoaffinity monolith extraction and electrophoretic separation of preterm birth biomarkers, *Analyst.* 143 (2018) 224–231. <https://doi.org/10.1039/c7an01357d>.

[33] A. Berasaluce, L. Matthys, J. Mujika, M. Antoñana-Díez, A. Valero, M. Agirregabiria, Bead beating-based continuous flow cell lysis in a microfluidic device, *RSC Adv.* 5 (2015) 22350–22355. <https://doi.org/10.1039/c5ra01251a>.

[34] J. Wang, Portable electrochemical systems, *TrAC - Trends Anal. Chem.* 21 (2002) 226–232. [https://doi.org/10.1016/S0165-9936\(02\)00402-8](https://doi.org/10.1016/S0165-9936(02)00402-8).

[35] J. Wang, Electrochemical detection for microscale analytical systems: A review, *Talanta.* 56 (2002) 223–231. [https://doi.org/10.1016/S0039-9140\(01\)00592-6](https://doi.org/10.1016/S0039-9140(01)00592-6).

[36] J. Wang, B. Tian, E. Sahlin, Micromachined electrophoresis chips with thick-film electrochemical detectors, *Anal. Chem.* 71 (1999) 5436–5440. <https://doi.org/10.1021/ac990807d>.

[37] R.S. Martin, A.J. Gawron, B.A. Fogarty, F.B. Regan, E. Dempsey, S.M. Lunte, Carbon paste-based electrochemical detectors for microchip capillary electrophoresis/electrochemistry, *Analyst.* 126 (2001) 277–280. <https://doi.org/10.1039/B009827M>.

[38] J.S. Bossier, M.A. Roberts, R. Ferrigno, H.H. Girault, Electrochemical detection in polymer microchannels, *Anal. Chem.* 71 (1999) 4294–4299. <https://doi.org/10.1021/ac981382i>.

[39] A. Chałupniak, A. Merkoçi, Graphene Oxide–Poly(dimethylsiloxane)-Based Lab-on-a-Chip Platform for Heavy-Metals Preconcentration and Electrochemical Detection, *ACS Appl. Mater. Interfaces.* 9 (2017) 44766–44775. <https://doi.org/10.1021/acsami.7b12368>.

[40] J. Wang, M. Pumera, M.P. Chatrathi, A. Escarpa, R. Konrad, A. Griebel, W. Dörner, H. Löwe, Towards disposable lab-on-a-chip: Poly(methylmethacrylate) microchip electrophoresis device with electrochemical detection, *Electrophoresis.* 23 (2002) 596–601. [https://doi.org/10.1002/1522-2683\(200202\)23:4<596::AID-ELPS596>3.0.CO;2-C](https://doi.org/10.1002/1522-2683(200202)23:4<596::AID-ELPS596>3.0.CO;2-C).

[41] H.Y. Tan, W.K. Loke, N.T. Nguyen, S.N. Tan, N.B. Tay, W. Wang, S.H. Ng, Lab-on-a-chip for rapid electrochemical detection of nerve agent Sarin, *Biomed. Microdevices.* 16 (2014) 269–275. <https://doi.org/10.1007/s10544-013-9830-4>.

[42] N. Ruecha, J. Lee, H. Chae, H. Cheong, V. Soum, P. Preechakasedkit, O. Chailapakul, G. Tanev, J. Madsen, N. Rodthongkum, O.-S. Kwon, K. Shin, Paper-Based Digital Microfluidic Chip for Multiple Electrochemical Assay Operated by a Wireless Portable Control System, *Adv. Mater. Technol.* 2 (2017) 1600267. <https://doi.org/10.1002/admt.201600267>.

[43] J. Wu, R. Wang, H. Yu, G. Li, K. Xu, N.C. Tien, R.C. Roberts, D. Li, Inkjet-printed microelectrodes on PDMS as biosensors for functionalized microfluidic systems, *Lab Chip.* 15 (2015) 690–695. <https://doi.org/10.1039/C4LC01121J>.

[44] P. Sjöberg, A. Määttänen, U. Vanamo, M. Novell, P. Ihalainen, F.J. Andrade, J. Bobacka, J. Peltonen, Paper-based potentiometric ion sensors constructed on ink-jet printed gold electrodes, *Sensors Actuators, B Chem.* 224 (2016) 325–332. <https://doi.org/10.1016/j.snb.2015.10.051>.

[45] W. Dungchai, O. Chailapakul, C.S. Henry, Electrochemical detection for paper-based microfluidics, *Anal. Chem.* 81 (2009) 5821–5826. <https://doi.org/10.1021/ac9007573>.

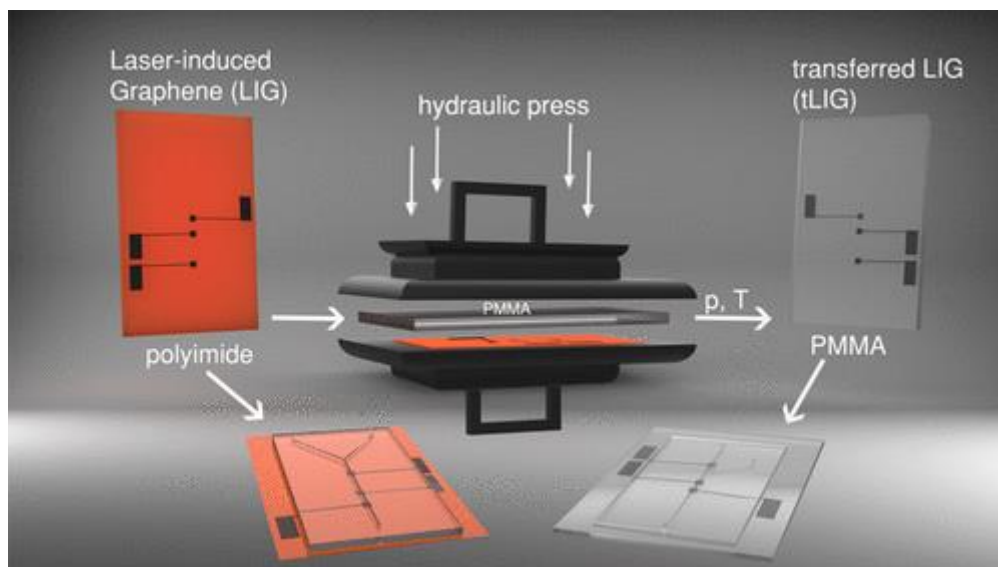
[46] H. Ko, J. Lee, Y. Kim, B. Lee, C.H. Jung, J.H. Choi, O.S. Kwon, K. Shin, Active digital microfluidic paper chips with inkjet-printed patterned electrodes, *Adv. Mater.* 26 (2014) 2335–2340. <https://doi.org/10.1002/adma.201305014>.

- [47] P. Ginet, K. Montagne, S. Akiyama, A. Rajabpour, A. Taniguchi, T. Fujii, Y. Sakai, B. Kim, D. Fourmy, S. Volz, Towards single cell heat shock response by accurate control on thermal confinement with an on-chip microwire electrode, *Lab Chip*. 11 (2011) 1513–1520. <https://doi.org/10.1039/c0lc00701c>.
- [48] S. Schumacher, J. Nestler, T. Otto, M. Wegener, E. Ehrentreich-Forster, D. Michel, K. Wunderlich, S. Palzer, K. Sohn, A. Weber, M. Burgard, A. Grzesiak, A. Teichert, A. Brandenburg, B. Koger, J. Albers, E. Nebling, F.F. Bier, Highly-integrated lab-on-chip system for point-of-care multiparameter analysis, *Lab Chip*. 12 (2012) 464–473. <https://doi.org/10.1039/C1LC20693A>.
- [49] J. Wang, B. Tian, E. Sahlin, Integrated electrophoresis chips/ampereometric detection with sputtered gold working electrodes, *Anal. Chem.* 71 (1999) 3901–3904. <https://doi.org/10.1021/ac9904720>.
- [50] A. Hilml, J.H.T. Luong, Electrochemical detectors prepared by electroless deposition for microfabricated electrophoresis chips, *Anal. Chem.* 72 (2000) 4677–4682. <https://doi.org/10.1021/ac000524h>.
- [51] A.T. Woolley, K. Lao, A.N. Glazer, R.A. Mathies, Capillary Electrophoresis Chips with Integrated Electrochemical Detection, *Anal. Chem.* 70 (1998) 684–688. <https://doi.org/10.1021/ac971135z>.
- [52] S. Saem, Y. Zhu, H. Luu, J. Moran-Mirabal, Bench-top fabrication of an all-PDMS microfluidic electrochemical cell sensor integrating micro/nanostructured electrodes, *Sensors (Switzerland)*. 17 (2017). <https://doi.org/10.3390/s17040732>.
- [53] J. Min, A.J. Baeumner, Characterization and Optimization of Interdigitated Ultramicroelectrode Arrays as Electrochemical Biosensor Transducers, *Electroanalysis*. 16 (2004) 724–729. <https://doi.org/10.1002/elan.200302872>.
- [54] Z. Zou, A. Jang, E. MacKnight, P.M. Wu, J. Do, P.L. Bishop, C.H. Ahn, Environmentally friendly disposable sensors with microfabricated on-chip planar bismuth electrode for in situ heavy metal ions measurement, *Sensors Actuators, B Chem.* 134 (2008) 18–24. <https://doi.org/10.1016/j.snb.2008.04.005>.
- [55] P. Jothimuthu, R.A. Wilson, J. Herren, E.N. Haynes, W.R. Heineman, I. Papautsky, Lab-on-a-chip sensor for detection of highly electronegative heavy metals by anodic stripping voltammetry, *Biomed. Microdevices*. 13 (2011) 695–703. <https://doi.org/10.1007/s10544-011-9539-1>.
- [56] D. Desmond, B. Lane, J.C. Alderman, J.D. Glennon, D. Diamond, D.W.M. Arrigan, Evaluation of miniaturised solid state reference electrodes on a silicon based component, *Sensors Actuators, B Chem.* 44 (1997) 389–396. [https://doi.org/10.1016/S0925-4005\(97\)00231-1](https://doi.org/10.1016/S0925-4005(97)00231-1).
- [57] A. Wisitsoraat, P. Sritongkham, C. Karuwan, D. Phokharatkul, T. Maturos, A. Tuantranont, Fast cholesterol detection using flow injection microfluidic device with functionalized carbon nanotubes based electrochemical sensor, *Biosens. Bioelectron.* 26 (2010) 1514–1520. <https://doi.org/10.1016/j.bios.2010.07.101>.
- [58] C.C. Shih, C.M. Shih, K.Y. Chou, S.J. Lin, Y.Y. Su, R.A. Gerhardt, Mechanism of degradation of AgCl coating on biopotential sensors, *J. Biomed. Mater. Res. - Part A*. 82 (2007) 872–883. <https://doi.org/10.1002/jbm.a.31140>.
- [59] R. Mamińska, A. Dybko, W. Wróblewski, All-solid-state miniaturised planar reference electrodes based on ionic liquids, *Sensors Actuators, B Chem.* 115 (2006) 552–557. <https://doi.org/10.1016/j.snb.2005.10.018>.
- [60] S.K. Kim, H. Lim, T.D. Chung, H.C. Kim, A miniaturized electrochemical system with a novel polyelectrolyte reference electrode and its application to thin layer electroanalysis, *Sensors Actuators, B Chem.* 115 (2006) 212–219. <https://doi.org/10.1016/j.snb.2005.09.005>.

- [61] M. Ciobanu, J.P. Wilburn, N.I. Buss, P. Ditavong, D. Lowy, Miniaturized Reference Electrodes Based on Ag/Ag<sub>2</sub>X Internal Reference Elements. I. Manufacturing and Performance, *Electroanalysis*. 14 (2002) 989–997. [https://doi.org/10.1002/1521-4109\(200208\)14:14<989::AID-ELAN989>3.0.CO;2-6](https://doi.org/10.1002/1521-4109(200208)14:14<989::AID-ELAN989>3.0.CO;2-6).
- [62] M. Ciobanu, J.P. Wilburn, D.A. Lowy, Miniaturized reference electrodes. II. Use in corrosive, biological, and organic media, *Electroanalysis*. 16 (2004) 1351–1358. <https://doi.org/10.1002/elan.200302960>.
- [63] N. Wongkaew, S.E.K. Kirschbaum, W. Surareungchai, R.A. Durst, A.J. Baeumner, A Novel Three-Electrode System Fabricated on Polymethyl Methacrylate for On-Chip Electrochemical Detection, *Electroanalysis*. 24 (2012) 1903–1908. <https://doi.org/10.1002/elan.201200336>.
- [64] M. Odijk, A. Baumann, W. Lohmann, F.T.G. Van Den Brink, W. Olthuis, U. Karst, A. Van Den Berg, A microfluidic chip for electrochemical conversions in drug metabolism studies, *Lab Chip*. 9 (2009) 1687–1693. <https://doi.org/10.1039/b822962g>.
- [65] J. Noh, S. Park, H. Boo, H.C. Kim, T.D. Chung, Nanoporous platinum solid-state reference electrode with layer-by-layer polyelectrolyte junction for pH sensing chip, *Lab Chip*. 11 (2011) 664–671. <https://doi.org/10.1039/c0lc00293c>.

### 3 Substrate-Independent Laser-Induced Graphene Electrodes for Microfluidic Electroanalytical Systems

#### Graphical Abstract



---

**This chapter has been published.**

Christian Griesche, Kilian Hoecherl, and Antje J. Baeumner, *ACS Appl. Nano. Mater.*, **2021**, 4, 3114 – 3121. DOI: <https://doi.org/10.1021/acsnm.1c00299>

**Author contributions:** CG and AJB planned the experiments. CG did most of the experiments and wrote the initial draft of the manuscript. KH performed initial microfluidic experiments. AJB is corresponding author.

### Abstract

Laser-induced graphene's (LIG) inherent graphene-like and highly porous characteristics and its simple, scalable, and inexpensive fabrication render it a desirable electrode material for bio- and chemosensors. The best LIG electrodes are made in polyimide foils using a CO<sub>2</sub> laser scribe, which unfortunately limits their integration into more sophisticated analytical devices due to polyimide's inertness. The transfer of LIG electrodes onto standard polymer substrates used in microfluidic systems and their use in microfluidic assays were therefore studied and the resulting electrodes characterized morphologically, chemically, and electroanalytically. It was found that a direct pressure-driven transfer produces highly functional transfer-LIG (tLIG) electrodes. tLIG differed from LIG electrodes with respect to a much smoother surface and hence a lower active surface area, a loss of the graphene characteristic Raman 2D peak, and a slight decrease in electron transfer rates. biosensors, food safety, food fraud, sustainable agriculture, livestock monitoring, wearable sensors.

However, their performance in amperometric detection strategies were comparable also when used in adhesive-tape enabled microfluidic channels for the detection of p-aminophenol. tLIG outperformed LIG electrodes in their ability to be integrated into more advanced microfluidic channel systems made of an all-polymethyl methacrylate (PMMA) substrate for the biosensing detection of alkaline phosphatase, commonly used as a biomarker and as a biosensor amplification system. LIG and tLIG have hence the potential to change electroanalytical sensing in diagnostic systems as their fabrication requires minimal resources, is highly scalable, and allows their integration into simple and, as tLIG, also sophisticated analytical systems.

### Keywords

Laser-induced graphene, functional composite, microfluidics, electrochemical detection, biosensor, lab-on-a-chip

### 3.1 Introduction

Since 2010 the laser reduction of graphene oxide (GO) was reported [1–3]. In 2012, the group of Kaner reported then on a cheap method for the reduction of GO using a DVD optical drive unit. The hereby formed graphene material was named laser-scribed graphene (LSG) [4]. LIG derived from the direct formation of polyimide using a CO<sub>2</sub>-laser was discovered by the group of James M. Tour

in 2014 [5]. Since then, in several publications the term laser-scribed graphene is used as an equivalent to laser-induced graphene.

Kapton HN is a commercially available polyimide with high chemical resistance toward known organic solvents and high thermal stability until 400 °C. These properties enable the direct scribing of laser-induced graphene but also cause limitations for other applications. These limitations influence possible applications of LIG as integration into existing platforms, microfluidic systems, and sensors is difficult. This can be overcome by the transfer of LIG to other substrates as well as the generation of LIG from other materials. In early studies polymers with similar structure to PI, such as polyetherimide or polysulfone-class polymers, were reported to be suitable for LIG synthesis [5,6]. Later, LIG was generated from phenolic resins [7] as well as other materials like wood, cloth, paper, food, and cross-linked polystyrene [8,9]. However, for vinyl polymers and polymers with low melting points that are desirable for microfluidic device fabrication, depolymerization and ablation are reported instead of LIG formation [9]. This puts emphasis on finding strategies to transfer LIG electrodes after their synthesis onto other substrates. Such transfer strategies include the infiltration of the porous LIG with a viscous compound which enables transfer of LIG after peeling off of the solidified/hardened compound. Latex paint, Portland cement, wax, epoxy, alkaline activated geopolymer, polydimethylsiloxane (PDMS), and PMMA have been reported to work with this strategy [10]. The quality of LIG to function as electrode after such treatment, however, remains uninvestigated and questionable. Physical methods are more promising, such as through adhesive tapes [11,12], the hot pressing into melted thermoplastic materials like polyethylene (PE), polypropylene (PP), and polystyrene (PS) [10] or via a lamination process [13]. The multifunctional surfaces of LIG composites have been shown to be a promising material for several applications in electronic or joule heating devices, microsupercapacitors, resistive memory devices, or salinity sensors; however, also here its characterization for electroanalytical detection has not been described [10,14,15].

The inherent inertness of the polyimide substrate slowed down studies focusing on the integration of LIG electrodes into microfluidic systems. So far, one PDMS channel strategy was reported by Karakurt *et al.*, [16] and an adhesive tape transfer into 15 mm wide channels consisting of two PMMA sidewalls was reported by Khan *et al.* [11] Hence, much work needs to be done in order to prepare LIG electrode integrated with microfluidic systems in order to render electroanalytical miniaturized sensing platforms. We therefore report here on two such strategies, i.e., a novel solvent bonding protocol for the integration of LIG using hot-embossed PMMA microfluidic channels, and a pressure-driven transfer method of LIG electrodes to thermoplastic polymers. They are compared to an adhesive tape transfer and the infiltration approach. The electrodes are

electrochemically characterized, and their performance inside the microfluidic chips was studied with respect to the influence of channel height and flow rate on amperometric detection of bioanalytical enzyme reactions.

### 3.2 Experimental Section

#### 3.2.1 Reagents

Phosphate buffered saline (PBS), pH 7.4, contained 137 mmol L<sup>-1</sup> NaCl (Carl Roth GmbH, Germany), 2.7 mmol L<sup>-1</sup> KCl (neoFroxx GmbH, Germany), 2 mmol L<sup>-1</sup> KH<sub>2</sub>PO<sub>4</sub> (Merck, Germany), and 10 mmol L<sup>-1</sup> Na<sub>2</sub>HPO<sub>4</sub>·2 H<sub>2</sub>O (Merck, Germany). K<sub>4</sub>Fe(CN)<sub>6</sub>·3 H<sub>2</sub>O, Ru(NH<sub>3</sub>)<sub>6</sub>Cl<sub>3</sub>, Ru(NH<sub>3</sub>)<sub>6</sub>Cl<sub>2</sub>, *p*-aminophenol, *p*-aminophenyl phosphate, ZnCl<sub>2</sub>, MgCl<sub>2</sub>·6 H<sub>2</sub>O, and alkaline phosphatase from bovine intestinal mucosa were obtained from Sigma (Germany). TRIS was obtained from Affymetrix (USA). All chemicals were obtained in analytical grade and used without further purification.

#### 3.2.2 Laser-Induced Graphene (LIG)

Laser-induced graphene was generated from Kapton HN polyimide film (thickness 125 μm) using a VLS 2.30 laser cutting platform (Universal Laser Systems, USA) with a wavelength of 10.6 μm. The electrodes were scribed under ambient conditions with a 2 in. lens. The polyimide foil was placed in the focus of the laser beam, and LIG was scribed in raster mode with laser power of 1 % corresponding to 0.3 W, speed of 10 % corresponding to 12.7 cm s<sup>-1</sup>, and image density 7 under ambient conditions.

##### 3.2.2.1 Infiltration Transfer of Laser-Induced Graphene to PDMS

PDMS is made from Dowsil Sylgard 184 silicone elastomer kit. Sylgard 184 elastomer kit base is mixed with the Sylgard 184 elastomer kit curing agent at a ratio of 10:1 and degassed under vacuum for 30 min. PDMS is poured on top of LIG in a mold and cured at room temperature for 24 h. The transfer is finalized by peeling of the polyimide film and removing the mold.

##### 3.2.2.2 Pressure-Driven Transfer of Laser-Induced Graphene to PMMA (tLIG)

PMMA was used as template for the transfer of laser-scribed graphene from its original polyimide substrate using a hot-pressing process. PMMA and polyimide film containing LIG are stacked in a press equipped with heated platens, ATLAS manual 15Ton hydraulic press (Specac Ltd., Great Britain), and heated from RT to 105 °C (30 °C min<sup>-1</sup>). The optimized pressure of 370 kg cm<sup>-2</sup> was evaluated by performing experiments with pressures of 370 kg cm<sup>-2</sup>, 185 kg cm<sup>-2</sup>, and 37 kg cm<sup>-2</sup>, respectively. The pressure is applied for 15 min at 105 °C followed by cooling of the substrates to RT (1.3 °C min<sup>-1</sup>). The transfer is finalized by peeling of the polyimide film.

### **3.2.3 Microfluidic Setup**

All measurements are performed using an in-house designed chip-holder. Fluidic transport outside the microfluidic setup is carried out through Teflon tubing with inner diameter of 0.25 mm and an outer diameter of 1.59 mm (Techlab GmbH, Germany). Inlets and outlets of the microfluidic chips are sealed using flexible PDMS seals, while the electrodes are contacted with spring-loaded gold-copper contacts. For the injection of probes Legato 180 syringe pumps (KD Scientific, USA) equipped with BD syringes or Hamilton glass syringes are used.

#### **3.2.3.1 Fabrication of Microfluidic Channels with Indirect Bonding using Adhesive Tape**

Prototypes of microfluidic chips are fabricated using a VLS 2.30 laser cutting platform. Double-sided adhesive tape (3M 9088FL, 210  $\mu\text{m}$  thickness) is taped on top of a 1.5 mm thick PMMA slide (Plexiglas XT, Kunststoff Acryl Design GmbH, Germany). The microfluidic channel is cut out of the adhesive tape (100 % power, 75 % speed, 200 PPI). To create channels of different height, the desired amount of PMMA is removed by engraving the PMMA base (45 % power, 90 % speed, 500 PPI). Inlets and outlets are cut using the laser cutting platform (100 % power, 6.7 % speed, 1000 PPI) followed by gluing the channel on the substrate containing the electrodes. The dimensions of the microfluidic chips are 60 mm  $\times$  45 mm with thicknesses of approximately 1.8 mm (polyimide substrate) or 3.2 mm (PMMA substrate), respectively. Contact pads of the electrodes are protected using conductive adhesive copper tape. Thicker adhesive tape could substitute for the here described method.

#### **3.2.3.2 Fabrication of Microfluidic Channels with Solvent Bonding of Polyimide to PMMA Microfluidic Channels**

PMMA microfluidic channels are fabricated via hot embossing using an ATLAS manual 15Ton hydraulic press. PMMA is placed on a brazen mold and heated to 120  $^{\circ}\text{C}$  (30  $^{\circ}\text{C min}^{-1}$ ). The brass template was fabricated using a Kern Evo micromilling machine. The temperature is hold for 10 min before applying a pressure of 5 kg  $\text{cm}^2$  for 30 s followed by cooling to RT (1.3  $^{\circ}\text{C min}^{-1}$ ). The channel width is 500  $\mu\text{m}$  and channel height 250 or 1000  $\mu\text{m}$ . For solvent bonding the PMMA channel and the polyimide containing LIG are clamped together and an amount of 60  $\mu\text{L}$  of toluene is injected between the polymers. Bonding is completed by applying UV/ozone (Jelight UVO cleaner 144 AX-220) for 5 min (oxygen flow rate 0.5 L  $\text{min}^{-1}$ ). Contact pads of the electrodes are protected using conductive adhesive copper tape.



### **3.2.4 LIG Characterization**

#### **3.2.4.1 Sheet Resistance**

The sheet resistance of LIG and tLIG was measured with the four-point probe method ( $I = 10 \mu\text{A}$ ).

#### **3.2.4.2 Contact Angle**

Contact angles were measured with a sessile drop method using optical contact angle system OCA 25 (DataPhysics Instruments GmbH, Germany) with software-guided (SCA 20) droplet shape detection.

#### **3.2.4.3 Electrode Morphology**

SEM (Zeiss/LEO 1530, Germany) was used to image LIG and tLIG morphology and thickness.

#### **3.2.4.4 Raman Spectroscopy**

Raman spectra were performed using a DXR Raman microscope (Thermo Fisher Scientific GmbH, Germany) at 532 nm laser excitation (8 mW), 50  $\mu\text{m}$  slit width with 100 times magnification (Mplan N objective 100 $\times$ /0.90 BD, Olympus SE Co. KG, Hamburg, Germany). Spectra were acquired for 0.2 s and averaged over 40 spectra.

### **3.2.5 Electrochemical Measurements**

Electrochemical measurements were performed using a potentiostat (PalmSens4, Palmsens BV, Houten, The Netherlands). Data evaluation was performed with PSTrace 5.7 software (Palmsens BV, Houten, The Netherlands). All analytes are dissolved in phosphate buffered saline buffer (pH 7.4). Electrochemical measurements outside the microfluidic channel were performed using LSG or tLIG (4 mm diameter, as working electrode (WE) and a Pt wire (0.5 mm diameter) as counter electrode (CE). All measurements were performed versus an Ag/AgCl (3 M KCl) reference electrode (RE). tLIG transferred with 370 kg  $\text{cm}^{-1}$  was used in all experiments. Electrochemical measurements in the microfluidic chip were performed using a LIG or tLIG WE. CE and RE were painted with conductive silver paint (Silber-Leitlack, Busch GmbH & Co. KG, Germany).

#### **3.2.5.1 Cyclic Voltammetry**

Cyclic voltammetry of 5 mmol  $\text{L}^{-1}$   $\text{K}_4\text{Fe}(\text{CN})_6$  in PBS was performed with 5 s equilibration time from  $-0.2$  to  $0.7$  V with varying scan rates (25  $\text{mV s}^{-1}$ , 50  $\text{mV s}^{-1}$ , 100  $\text{mV s}^{-1}$ , and 200  $\text{mV s}^{-1}$ ). Cyclic voltammetry of 5 mmol  $\text{L}^{-1}$   $\text{Ru}(\text{NH}_3)_6\text{Cl}_2$  in PBS was performed with 5 s equilibration time from  $-0.6$  to  $0.3$  V with varying scan rates (25  $\text{mV s}^{-1}$ , 50  $\text{mV s}^{-1}$ , 100  $\text{mV s}^{-1}$ , and 200  $\text{mV s}^{-1}$ ).  $k^0$  values were determined using a modified Nicholson method.  $k^0$  was evaluated by the slope of plotting the

dimensionless parameter  $\Psi$  versus  $[\pi DnF/(RT)]^{-1/2}v^{-1/2}$  [17]. Diffusion coefficients for the calculations were  $6.50 \times 10^{-6} \text{ cm}^2 \text{ s}^{-1}$  for  $\text{Fe}(\text{CN})_6^{4-}$  and  $5.48 \times 10^{-6} \text{ cm}^2 \text{ s}^{-1}$  for  $\text{Ru}(\text{NH}_3)_6^{3+}$  [18,19].

### 3.2.5.2 Square Wave Voltammetry

Square wave voltammetry for  $\text{Ru}(\text{NH}_3)_6\text{Cl}_2$  in PBS was measured from  $-0.6$  to  $0.2$  V with  $E_{\text{step}} = 5$  mV, an amplitude of 50 mV, and frequency of 10 Hz. Peak currents are determined after subtraction of a nonlinear baseline created with PSTrace5.7 software (nonlinear baseline with markers at  $-0.52$  V,  $-0.48$  V, and  $0.07$  V). Square wave voltammetry for  $\text{K}_4\text{Fe}(\text{CN})_6$  in PBS was from  $-0.4$  to  $0.8$  V with  $E_{\text{step}} = 5$  mV, an amplitude of 50 mV, and frequency of 10 Hz. Peak heights are determined after subtraction of a nonlinear baseline created with PSTrace5.7 software (nonlinear baseline with markers at  $0.0$  V,  $0.08$  V, and  $0.40$  V).

### 3.2.5.3 Amperometry

Amperometric measurements were performed at constant potentials for the oxidation of  $\text{Fe}(\text{CN})_6^{4-}$  ( $0.34$  V), the reduction of  $\text{Ru}(\text{NH}_3)_6^{3+}$  ( $-0.10$  V), and the oxidation of *p*-aminophenol ( $0.08$  V). Within the data evaluation the measured current after 60 s was plotted versus the analyte concentration.

### 3.2.5.4 Detection of Alkaline Phosphatase

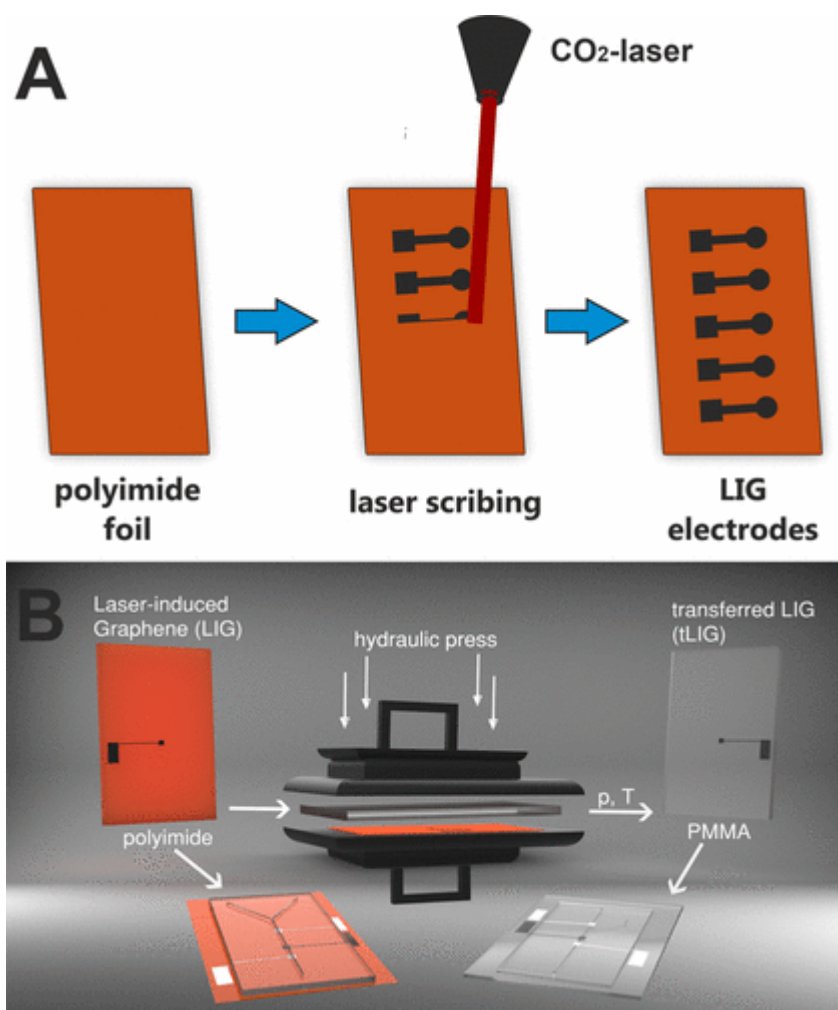
Alkaline phosphatase was diluted in  $100 \text{ mmol L}^{-1}$  Tris-HCl buffer, pH 7.5, containing  $100 \text{ mmol L}^{-1}$  KCl,  $1 \text{ mmol L}^{-1}$   $\text{ZnCl}_2$ , and  $1 \text{ mmol L}^{-1}$   $\text{MgCl}_2$ , to a total volume of  $25 \mu\text{L}$ . An amount of  $25 \mu\text{L}$  of  $10 \text{ mmol L}^{-1}$  *p*-aminophenyl phosphate was added, and the mixture was incubated for 30 min at  $37^\circ\text{C}$  under shaking (400 rpm, Eppendorf Thermomixer comfort). The complete sample volume was injected into the microfluidic chip via a side channel. The enzymatically generated *p*-aminophenol was detected at  $0.08$  V using a flow rate of  $5 \mu\text{L min}^{-1}$ .

## 3.3 Results and Discussion

The transfer of LIG onto other polymeric substrates and the resulting electrochemical performance were investigated using an infiltration method through PDMS, adhesive tape delamination, and a novel transfer strategy using high pressure in combination with heating of the polymeric substrate (Scheme 1) just to its glass transition temperature (Figure S1). In all scenarios, the LIG is flipped upon transfer which leads to a less porous surface (Figure 1A–C and Figure S2). Compared to adhesive tape delamination the here presented transfer and the infiltration method were found to be more reproducible and also allow transfer to multiple substrates [10]. In fact, the here reported method can be applied to various thermoplastic polymers by solely adjusting the transfer

## Substrate-Independent Laser-Induced Graphene Electrodes for Microfluidic Electroanalytical Systems

temperature toward the substrates glass transition temperature. Besides the transfer to PMMA the transfer to PET, PS, and PVC was achieved (Figure S3). The infiltration methods can be adapted toward a wider range of materials which only require the ability of getting solidified during the transfer process. Further experiments were performed with PMMA as a widely accepted and used polymer substrate for microfluidic devices. Especially for further integration into microfluidic chips the transfer to a thermoplastic material like PMMA is advantageous. By bonding of the polymer to itself, chips consisting of a single material can be generated that have advantageous uniform properties [20].



Scheme 1. (A) Illustration of the Direct Fabrication of Laser-Induced Graphene (LIG) from Polyimide Using a CO<sub>2</sub> Laser and (B) Schematic of the Pressure-Driven Transfer of LIG to a PMMA Substrate and the Fabricated Electrochemical Microfluidic Chips.

It was found that the transfer using high pressure only minimally influences the thickness with a decrease from  $39 \pm 1 \mu\text{m}$  to  $37 \pm 1 \mu\text{m}$  (Figure 1D,E). Furthermore, the cross-sectional laminar structure is as well maintained in the pressure-assisted transfer as in the infiltration transfer as

additionally indicated by the comparable Raman spectra (Figure 1H,I) and sheet resistance values (Figure 2). Interestingly though, the characteristic 2D peak at approximately  $2700\text{ cm}^{-1}$  is not observed any more upon transfer independently of the transfer technique.

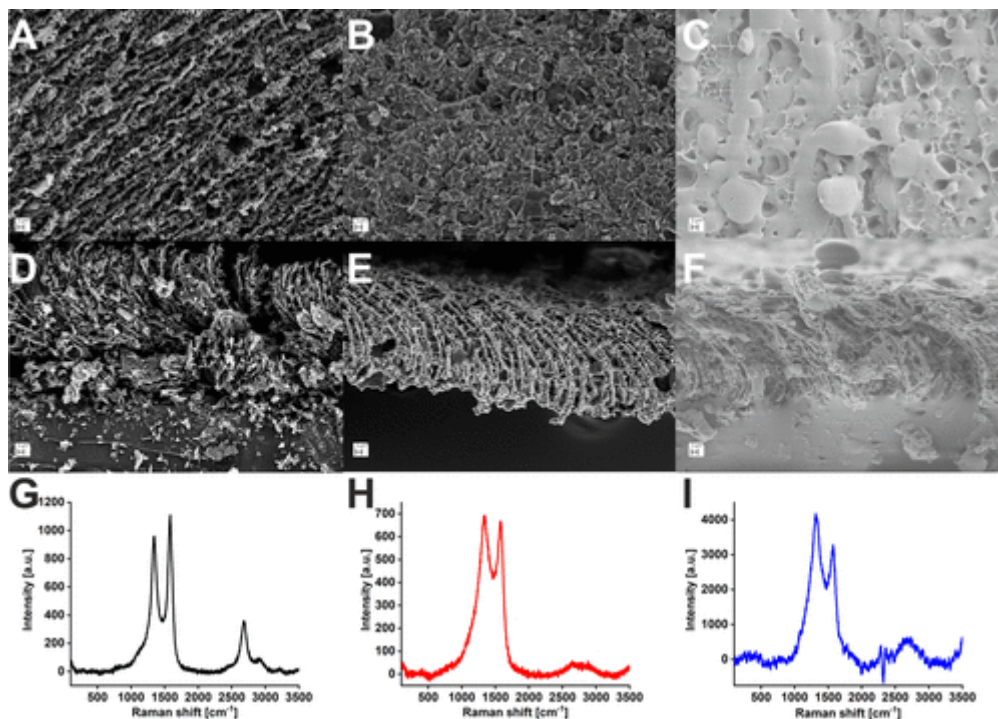


Figure 1. SEM pictures of LIG (left), tLIG (middle), and infiltration-transferred LIG (right): (A) top view on LIG, (B) top view on tLIG, (C) top view on infiltration-transferred LIG, (D) side view to LIG, (E) side view to tLIG, and (F) side view on infiltration-transferred LIG. All scale bars represent  $2\ \mu\text{m}$ . Raman spectra of (G) LIG, (H) tLIG, and (I) infiltration-transferred LIG are shown.

Hence the originally observed peak is presumably caused by the turbostratic nature of the LIG prior to transfer. With respect to the hydrophilicity of the materials, it is not surprising that in the case of LIG its porous surface leads to complete spreading of the surface, whereas the change in its surface microstructure after transfer results in a hydrophobic surface. For pressure derived tLIG a contact angle of  $68^\circ \pm 4^\circ$  shows it to be significantly more hydrophilic than infiltration-derived tLIG with  $127^\circ \pm 2^\circ$  (Figure S4). This latter value compares well to those reported by others with infiltration materials of PDMS, PE, PP, PS, or wax resulting in contact angles above  $150^\circ$  [10].

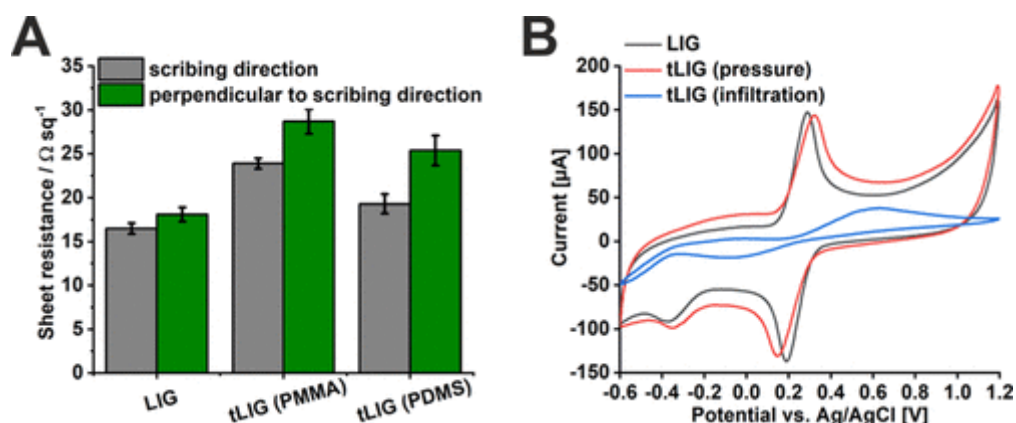


Figure 2. (A) Sheet resistance of LIG, tLIG, and tLIG measured in scribing direction and perpendicular to scribing direction ( $n = 3$ ). (B) Cyclic voltammograms of LIG (black), tLIG (red), and infiltration-transferred LIG (blue) of  $5 \text{ mmol L}^{-1} \text{ K}_4[\text{Fe}(\text{CN})_6]$  in PBS with  $v = 50 \text{ mV s}^{-1}$ .

Besides all similarities in the morphological characterization of the obtained tLIG composites, the electrochemical performance for the redox-marker  $\text{K}_4[\text{Fe}(\text{CN})_6]$  shows substantial differences in their suitability as electrode materials. In cyclic voltammetry the infiltration-transferred LIG shows a much lower sensitivity toward the analyte and higher peak separation of the redox couple while the pressure-transferred LIG only shows slight differences compared to LIG and maintains the electrochemical performance (Figure 2B). Since this transfer method utilizes relatively high pressures but low heating temperatures (i.e., just to PMMA's glass temperature of  $105 \text{ }^\circ\text{C}$ ), the electrode structure is reliably maintained in its original shape during the transfer [20]. This is in contrast to the hot pressing transfer reported by Luong et al., using higher temperatures but low pressure, making it more similar to the infiltration method as the melted polymer is more prone to fill the porous LIG [10].

When comparing the sheet resistance of the three different LIG variations, the lowest values are obtained for LIG which are in good accordance with literature values [5,21] and not surprisingly slightly increased values for the two tLIGs. Also, due to different overlap of the laser beam during the fabrication process higher sheet resistances are measured perpendicular to the scribing direction for LIG and tLIG, respectively (Figure 2 A). With increasing pressures during the transfer, a more stable tLIG/PMMA composite is obtained while observing a slightly increasing sheet resistance toward higher pressures (Figure S5). Further electrochemical characterization of LIG and tLIG electrodes was performed with the inner-sphere redox-marker potassium ferrocyanide (Figure S6) and outer-sphere redox-marker ruthenium hexamine using cyclic voltammetry (Figure S7). The heterogeneous electron transfer rates ( $k^0$ ) of LIG and tLIG in PBS containing  $5 \text{ mmol L}^{-1} \text{ K}_4[\text{Fe}(\text{CN})_6]$  or  $5 \text{ mmol L}^{-1} \text{ Ru}(\text{NH}_3)_6\text{Cl}_2$  were calculated with an extended method of the Nicholson treatment

(Figure S8) [17]. Regardless of all structural changes resulting from the transfer of LIG, the electron transfer rate  $k^0$  for both investigated redox-markers differs only slightly. The fabricated electrodes exhibit high electron transfer rates with  $k^0$  values being higher compared to reported electrodes, fabricated with the same technique [22]. Interestingly, when compared to other carbon-based materials the electron transfer rates obtained for LIG and tLIG are very favorable, especially when considering the ease of their fabrication (Table S1). In some instances, they are better (e.g., for the inner redox-marker  $[\text{Fe}(\text{CN})_6]^{4-}$  compared to highly ordered pyrolytic graphite electrodes (basal- and edge-plane pyrolytic graphite)) [23] or comparable (e.g., for  $[\text{Ru}(\text{NH}_3)_6]^{3+}$  in comparison to BPPG and EPPG) [24]. In some instances they are slower, especially when compared to electrodes with more complex fabrication processes, such as for CVD graphene on copper [25] or laser-scribed graphene from graphene oxide [23]. Thus, among all of these carbon materials tLIG appears as a promising candidate to further expand the diverse field of carbon-based electrode materials.

While the heterogeneous electron transfer rate is barely affected by the transfer, the active surface area decreases significantly upon transfer. The active surface areas of LIG and tLIG composites respectively were calculated from cyclic voltammetry with varying scan rates for  $[\text{Fe}(\text{CN})_6]^{4-}$  (Figure S6) and  $[\text{Ru}(\text{NH}_3)_6]^{3+}$  (Figure S7) using the Randles–Sevcik equation. As to be expected, all transfer methods resulted in a reduced electroactive surface area, with the most drastic effect observed for the infiltration method using PDMS. Pressure-driven transfer and adhesive tape delamination resulted in surface areas close to the actual geometrical electrode area (Table 1). Considering the obtained electroactive surface area and the reproducibility, the pressure-driven transfer performed best.

## Substrate-Independent Laser-Induced Graphene Electrodes for Microfluidic Electroanalytical Systems

Table 1. Electrochemical Active Surface Areas and Geometrical Electrode Areas Determined with the Randles–Sevcik Equation<sup>a</sup>

	geometrical surface area (mm <sup>2</sup> )	active surface area [Fe(CN) <sub>6</sub> ] <sup>4-</sup> (mm <sup>2</sup> )	active surface area [Ru(NH <sub>3</sub> ) <sub>6</sub> ] <sup>3+</sup> (mm <sup>2</sup> )
LIG	12.6	19.6 ± 1.6	27.6 ± 0.5
tLIG (pressure-driven transfer)	12.6	14.7 ± 0.6	14.4 ± 1.6
tLIG (infiltration transfer)	12.6	4.0 ± 0.6	8.9 ± 1.7
tLIG (adhesive tape delamination)	12.6	11.9 ± 0.5	13.0 ± 0.3

<sup>a</sup> Resolution of the laser scribe is 0.1 mm.

The electrochemical performance of LIG and tLIG was evaluated with the detection of [Fe(CN)<sub>6</sub>]<sup>4-</sup> and [Ru(NH<sub>3</sub>)<sub>6</sub>]<sup>2+</sup> using amperometry and square wave voltammetry (Figure 3). Interestingly, in the amperometric strategy both electrodes behave similar to both analytes, in contrast to analyses with CV (Figure S6) and SWV (Figure 3, Table S2). We assume that the different electrode behavior is most likely influenced by differences in the material porosity rather than other material variations. The porous nature of LIG effectively increases the reaction rate in SWV and CV which consequently results in its enhanced performance. This influence of electrode morphology on the electrochemical behavior is not often considered in electroanalytical investigations when comparing different electrode materials, even though already in 1997 Zu *et al.* reported theoretical calculations stating a change of peak separation in cyclic voltammograms and a dependency of peak current and potential scan rate in linear scan voltammetry are caused by electrode roughness [26]. More detailed theoretical and experimental works on cyclic voltammetry were done by the group of Compton. They investigated a high influence of electrode porosity on the peak current and peak separation [27]. While only extremely high values of electrode roughness have a significant

effect on these parameters [28]. The morphology-related electrocatalytic effect was approved by Punckt *et al.*'s experimental findings using porous electrodes. They found that increasing porosity of their porous functionalized graphene electrodes leads to more falsified kinetics for reversible and irreversible reactions, respectively [29]. Additionally, different edge densities of the electrode materials contribute to the different behavior. For a linear-diffusion based system the theoretical wave current density for a planar electrode at a scan rate of  $10 \text{ mV s}^{-1}$  is  $3.54 \times 10^{-4} \text{ A cm}^{-2}$ , calculated with the Randles–Sevcik equation. The measured wave current density for tLIG ( $3.54 \times 10^{-4} \text{ A cm}^{-2}$ ) is in excellent agreement with the planar electrode, while the original LIG electrodes show a higher edge density with a measured wave current density of  $4.14 \times 10^{-4} \text{ A cm}^{-2}$  (Figure S9). As a drawback of this electrocatalytic effect of porous LIG the linear detection range tends to be more limited which is indicated by the correlation coefficients of the linear fit (Figure 3).

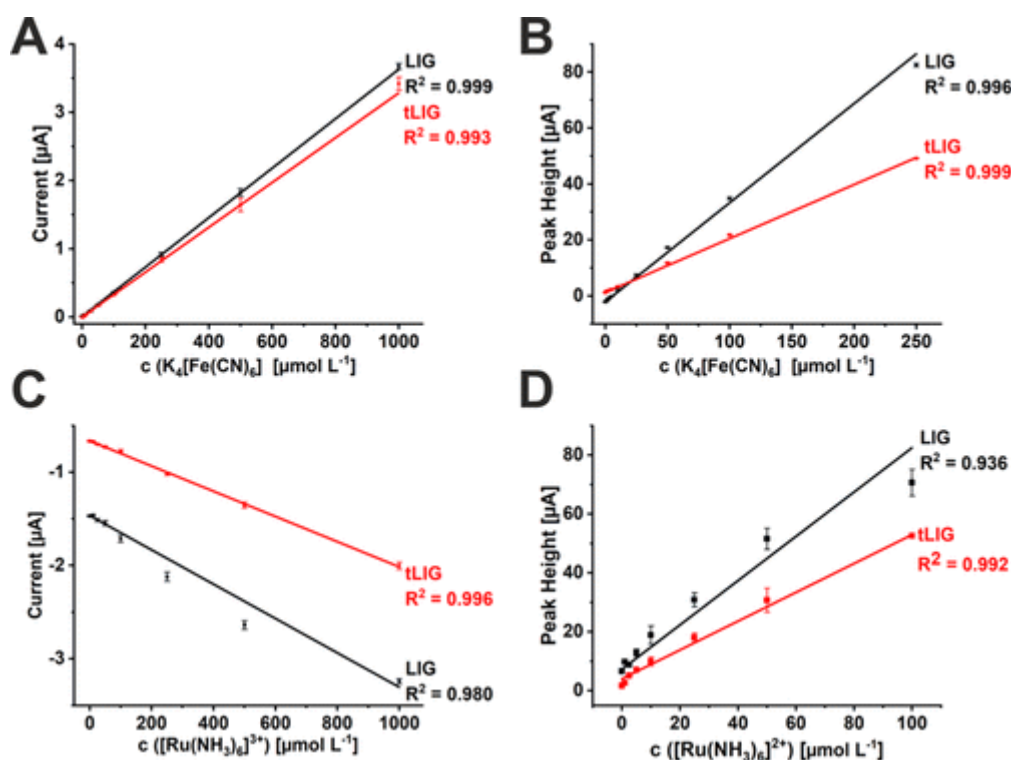


Figure 3. Detection of  $\text{K}_4[\text{Fe}(\text{CN})_6]$  using amperometry (A) and square wave voltammetry (B). Detection of  $[\text{Ru}(\text{NH}_3)_6]\text{Cl}_3$  using amperometry (C) and detection of  $[\text{Ru}(\text{NH}_3)_6]\text{Cl}_2$  using square wave voltammetry (D). All determinations are performed with LIG (red) and tLIG (black) ( $n = 3$ ).

### 3.3.1 Laser-Induced Graphene Electrodes in Microfluidics

Amperometric detection using pump driven electrochemical microfluidic setups enables two detection strategies, i.e., stopped flow or in-flow measurements. LIG and tLIG were studied in



adhesive tape and in PMMA-based microfluidic channels, studying furthermore the influence of the channel height on the electrode performance (0.2, 0.5, and 1 mm) (Figure 4A). The tape-based microfluidic systems were easily assembled but suffer from the fact that the walls are made of the tape rather than a defined polymer substrate (Figure 5A). Here, it was quickly determined that the electrode material itself had minimal influence on the analytical performance, whereas low channel heights led to lower sensitivities and higher LOQs (Figure 4A and B, Table S3). Higher channels behaved similar to bulk measurements in all criteria (Figure 4D, Table S3), in contrast to the low channel heights used. Since measurements are done under stop-flow conditions, it can be assumed that not enough bulk concentration solution is available above the diffusion layer to maintain its stable formation.

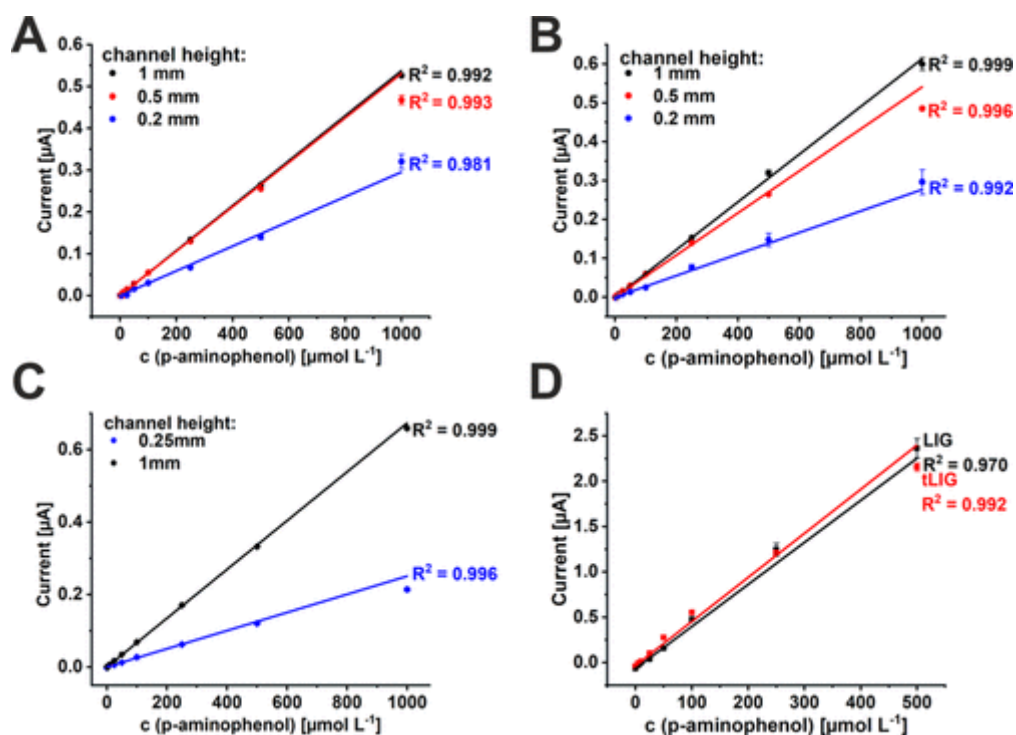


Figure 4. Calibration curves of *p*-aminophenol in microfluidic channels using indirect bonding with adhesive tape of different heights, 0.2 mm (blue), 0.5 mm (red), and 1 mm (black) using (A) LIG and (B) tLIG and (C) microfluidic channels incorporating LIG with toluene bonding. (D) Calibration curve for *p*-aminophenol measured outside a microfluidic channel ( $n \geq 3$ ).

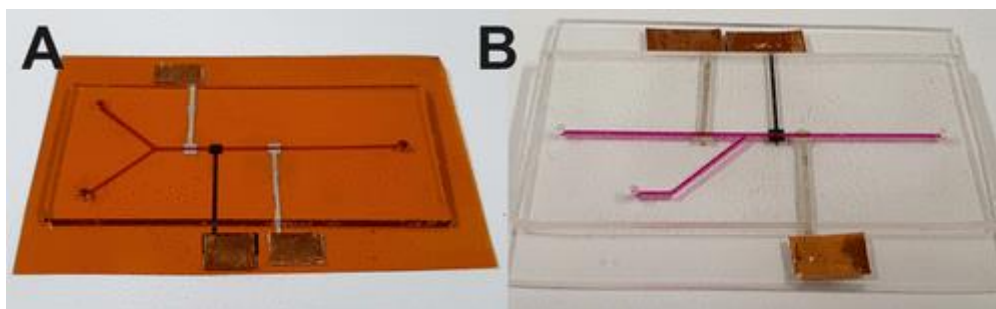


Figure 5. (A) Picture of a microfluidic chip containing a LIG working electrode on polyimide substrate, fabricated by solvent bonding with a hot-embossed PMMA microfluidic channel. (B) Picture of a microfluidic chip containing a tLIG working electrode on PMMA substrate, fabricated with indirect bonding using adhesive tape and a PMMA cover.

More interesting is the approach in which polyimide was bonded to PMMA microfluidic channels, generating a mere 2-polymer system (Figure 5B). In our strategy, microfluidic channels incorporating LIG were achieved by using toluene in a novel UV/ozone assisted solvent bonding technique with PMMA hot embossed channels. In order to compare findings to the tape-based method, two channel heights (0.25 mm and 1.0 mm) were studied and found to give very comparable results (Figure 4C). The bonding of polyimide to other polymers is rarely reported because of its inertness to organic solvents and high thermal stability. In the literature several bonding protocols for the bonding to PDMS via oxygen plasma treatment of PDMS, a thiol-epoxy based click reaction, or using epoxy adhesive are described [16,30,31]. While PDMS has the advantage of being flexible leading to flexible microfluidic devices when combined with thin polyimide films, it does not lend itself well for large scale manufacturing, hence limiting its commercial use [32].

The electrochemical detection of different concentrations of *p*-aminophenol in flow measurements was performed using both electrode materials in adhesive tape-based channels of different heights (0.2, 0.5, 1.0 mm) with varying flow rates (0–100  $\mu\text{L min}^{-1}$ ) (Figure S10). Corresponding to earlier observations solely, the channel height is causing different electrochemical responses independent of the respective electrode material. Overall, the amount of sample passing the electrode is influenced by the channel dimensions and the flow rate. Therefore, increasing signals are expected with higher flow rates and/or smaller channels, which was confirmed for high flow rates leading to highest currents for the 0.2 mm channels. However, studies at low flow rates gave a contrary image. At low flow rates the higher channels lead to higher currents and better resolution. It is assumed that the developing analyte concentration gradient directly above the surface cannot be replenished well in small channels at slow flow rates. With little difference between the two higher

channel types, the 0.5 mm high channel was chosen for further investigations as it required less sample and provided higher currents. Two flow rates (5 and 25  $\mu\text{L min}^{-1}$ ) were studied, and it was found that a higher sensitivity (factor 1.5 for LIG and 1.4 for tLIG) was achieved at faster flow with the cost of a 5 times higher sample volume (Figure 6, Table S4). For both flow rates the limit of quantification (LOQ = blank value +  $10\sigma$ ), represented by the lowest value of the linear range, was increased compared to measurements under the previously described stopped flow conditions. In future applications, depending on the respective analytical question, the channel height and flow rates of microfluidic chips using LIG/tLIG can therefore be adjusted toward the individual requirements such as available sample volumes or required detection range.

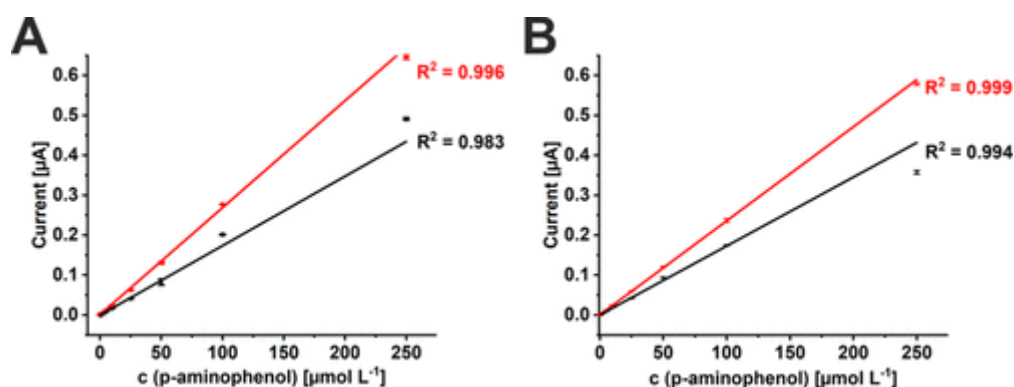


Figure 6. Determination of *p*-aminophenol in a 0.5 mm high microfluidic channel using flow rates of 5  $\mu\text{L min}^{-1}$  (black) and 25  $\mu\text{L min}^{-1}$  (red) with (A) LIG WE and (B) tLIG WE ( $n = 4$ ).

### 3.3.2 Detection of Alkaline Phosphatase

Finally, the optimized system was applied toward the detection of enzymatically generated *p*-aminophenol to determine alkaline phosphatase (ALP) concentrations. Enzyme product was injected through a side channel for on-chip detection. (Figure 7A). It can be observed that the signals increase over time, which is likely due to the continuing enzymatic reaction. A linear correlation of the measured current and the concentration of alkaline phosphatase was obtained (Figure 7B). The limit of detection (blank value +  $3\sigma$ ) of the microfluidic chip is 0.3  $\text{U L}^{-1}$ . ALP itself is often used for the diagnostics and monitoring of several diseases. Besides its direct detection, ALP is frequently used as label in bioassay formats. Researchers have published a variety of electrochemical sensors for both applications [33]. Lately published electrochemical sensors for the direct detection of ALP reach limits of detection of 0.03  $\text{U L}^{-1}$ , 0.25  $\text{U L}^{-1}$ , and 2  $\text{U L}^{-1}$ , [34–36] matching commercial available optical alkaline phosphatase kits with LOD of

0.02 U L<sup>-1</sup> (fluorescence) and 2 U L<sup>-1</sup> (absorbance) [37,38]. As a proof-of-concept, the tLIG microfluidic chip has shown its ability to serve as platform for future (bio)sensor developments.

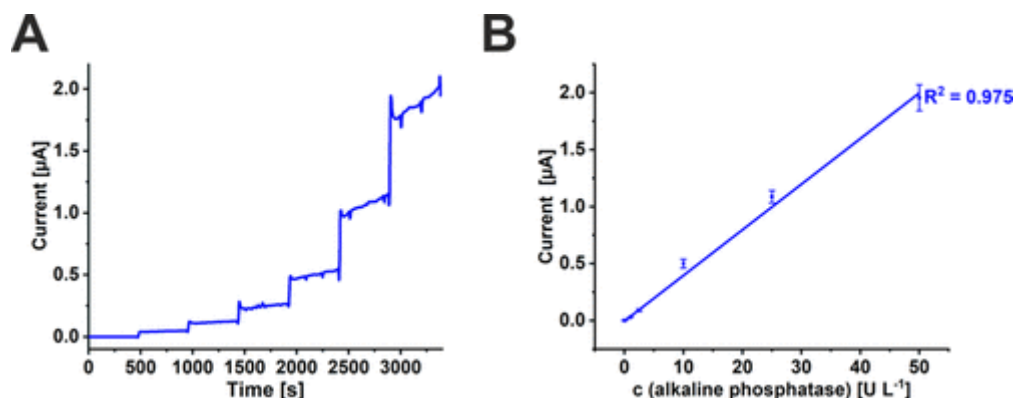


Figure 7. (A) Chronoamperogram of the electrochemical detection of enzymatically generated pAP at 0.08 V using increasing amounts of ALP (0 U L<sup>-1</sup>, 1 U L<sup>-1</sup>, 2.5 U L<sup>-1</sup>, 5 U L<sup>-1</sup>, 10 U L<sup>-1</sup>, 25 U L<sup>-1</sup>, and 50 U L<sup>-1</sup>). (B) Dose–response curve for the detection of alkaline phosphatase ( $n = 3$ ).

### 3.4 Conclusions

In summary, we have presented a simple method for the transfer of LIG to thermoplastic polymers exemplary for PMMA as well as a method for solvent bonding of polyimide to PMMA. Especially the reliable transfer to thermoplastic polymeric materials, like PMMA, enables the manifold integration of LIG in the form of tLIG into microfluidic devices using several well-known direct bonding techniques, like solvent vapor bonding, thermal bonding or solvent bonding [39,40]. A microfluidic chip consisting of a single material offers several advantages due to its uniform thermal, chemical, and electrical properties [20]. While tLIG behaves very similarly to the original LIG, the most remarkable change is its reduced porosity which reduces the electrocatalytic effect and thereby reduces the sensitivity in electrochemical detection methods like SWV and CV. Interestingly, this effect is less distinctive if nonexistent within amperometric detections applying a constant potential. Thus, when studying the amperometric detection of *p*-aminophenol, tLIG and LIG perform the same in microfluidic channels. As to be expected, the channel height significantly influences amperometric detections as these are dependent on the diffusion gradient. Thus, careful selection of channel height and flow rates can be used to quickly optimize the electrochemical on-chip detection. Considering LIG and tLIG future applications, research studies on surface modifications for signal enhancement [41,42] and biofunctionalization [22] point toward a rapid adaptation toward highly functional point-of-care sensing in the future.

### 3.5 References

- [1] D.A. Sokolov, K.R. Shepperd, T.M. Orlando, Formation of graphene features from direct laser-induced reduction of graphite oxide, *J. Phys. Chem. Lett.* 1 (2010) 2633–2636. <https://doi.org/10.1021/jz100790y>.
- [2] V. Abdelsayed, S. Moussa, H.M. Hassan, H.S. Aluri, M.M. Collinson, M.S. El-Shall, Photothermal deoxygenation of graphite oxide with laser excitation in solution and graphene-aided increase in water temperature, *J. Phys. Chem. Lett.* 1 (2010) 2804–2809. <https://doi.org/10.1021/jz1011143>.
- [3] Y. Zhang, L. Guo, S. Wei, Y. He, H. Xia, Q. Chen, H.B. Sun, F.S. Xiao, Direct imprinting of microcircuits on graphene oxides film by femtosecond laser reduction, *Nano Today*. 5 (2010) 15–20. <https://doi.org/10.1016/j.nantod.2009.12.009>.
- [4] V. Strong, S. Dubin, M.F. El-Kady, A. Lech, Y. Wang, B.H. Weiller, R.B. Kaner, Patterning and electronic tuning of laser scribed graphene for flexible all-carbon devices, *ACS Nano*. 6 (2012) 1395–1403. <https://doi.org/10.1021/nn204200w>.
- [5] J. Lin, Z. Peng, Y. Liu, F. Ruiz-Zepeda, R. Ye, E.L.G. Samuel, M.J. Yacaman, B.I. Yakobson, J.M. Tour, Laser-induced porous graphene films from commercial polymers, *Nat. Commun.* 5 (2014) 1–8. <https://doi.org/10.1038/ncomms6714>.
- [6] S.P. Singh, Y. Li, J. Zhang, J.M. Tour, C.J. Arnsch, Sulfur-Doped Laser-Induced Porous Graphene Derived from Polysulfone-Class Polymers and Membranes, *ACS Nano*. 12 (2018) 289–297. <https://doi.org/10.1021/acsnano.7b06263>.
- [7] Z. Zhang, M. Song, J. Hao, K. Wu, C. Li, C. Hu, Visible light laser-induced graphene from phenolic resin: A new approach for directly writing graphene-based electrochemical devices on various substrates, *Carbon N. Y.* 127 (2018) 287–296. <https://doi.org/10.1016/j.carbon.2017.11.014>.
- [8] R. Ye, Y. Chyan, J. Zhang, Y. Li, X. Han, C. Kittrell, J.M. Tour, Laser-Induced Graphene Formation on Wood, *Adv. Mater.* 29 (2017). <https://doi.org/10.1002/adma.201702211>.
- [9] Y. Chyan, R. Ye, Y. Li, S.P. Singh, C.J. Arnsch, J.M. Tour, Laser-Induced Graphene by Multiple Lasing: Toward Electronics on Cloth, Paper, and Food, *ACS Nano*. 12 (2018) 2176–2183. <https://doi.org/10.1021/acsnano.7b08539>.
- [10] D.X. Luong, K. Yang, J. Yoon, S.P. Singh, T. Wang, C.J. Arnsch, J.M. Tour, Laser-Induced Graphene Composites as Multifunctional Surfaces, *ACS Nano*. (2019) acsnano.8b09626. <https://doi.org/10.1021/acsnano.8b09626>.
- [11] M.A. Khan, I.R. Hristovski, G. Marinaro, J. Kosel, Magnetic Composite Hydrodynamic Pump with Laser-Induced Graphene Electrodes, *IEEE Trans. Magn.* 53 (2017). <https://doi.org/10.1109/TMAG.2017.2707598>.
- [12] A. Nag, S. Mukhopadhyay, J. Kosel, Development of printed sensors for taste sensing, in: 2017 IEEE Life Sci. Conf. LSC 2017, Institute of Electrical and Electronics Engineers Inc., 2018: pp. 1–4. <https://doi.org/10.1109/LSC.2017.8268129>.
- [13] J.T. Li, M.G. Stanford, W. Chen, S.E. Presutti, J.M. Tour, Laminated Laser-Induced Graphene Composites, *ACS Nano*. (2020). <https://doi.org/10.1021/acsnano.0c02835>.
- [14] W. Song, J. Zhu, B. Gan, S. Zhao, H. Wang, C. Li, J. Wang, Flexible, Stretchable, and Transparent Planar Microsupercapacitors Based on 3D Porous Laser-Induced Graphene, *Small*. 14 (2018) 1702249. <https://doi.org/10.1002/smll.201702249>.

- [15] A. Nag, S.C. Mukhopadhyay, J. Kosel, Sensing system for salinity testing using laser-induced graphene sensors, *Sensors Actuators, A Phys.* 264 (2017) 107–116. <https://doi.org/10.1016/j.sna.2017.08.008>.
- [16] L. Karakurt, Ilbey; Elwood, Jaqueline; Li, Xiaoqiaun; Beker, Levant; Sweet, Eric; Cai, Weihua; Lin, Membraneless microfluidic redox battery for wearable electronics application, in: 19th Int. Conf. Solid-State Sensors, Actuators Microsystems, IEEE, Piscataway, NJ, USA, 2017: pp. 1820–1823.
- [17] I. Lavagnini, R. Antiochia, F. Magno, An extended method for the practical evaluation of the standard rate constant from cyclic voltammetric data, *Electroanalysis*. 16 (2004) 505–506. <https://doi.org/10.1002/elan.200302851>.
- [18] M. von Stackelberg, M. Pilgram, V. Toome, Bestimmung von Diffusionskoeffizienten einiger Ionen in wäßriger Lösung in Gegenwart von Fremdelektrolyten - I, *Zeitschrift Für Elektrochemie*. 57 (1953) 342–350. <https://doi.org/10.1002/bbpc.195300073>.
- [19] J.E. Baur, R.M. Wightman, Diffusion coefficients determined with microelectrodes, *J. Electroanal. Chem.* 305 (1991) 73–81. [https://doi.org/10.1016/0022-0728\(91\)85203-2](https://doi.org/10.1016/0022-0728(91)85203-2).
- [20] H. Klank, J.P. Kutter, O. Geschke, CO<sub>2</sub>-laser micromachining and back-end processing for rapid production of PMMA-based microfluidic systems, *Lab Chip*. 2 (2002) 242–246. <https://doi.org/10.1039/b206409j>.
- [21] L. Jiao, Z. Chua, S. Moon, J. Song, G. Bi, H. Zheng, B. Lee, J. Koo, Laser-Induced Graphene on Additive Manufacturing Parts, *Nanomaterials*. 9 (2019) 90. <https://doi.org/10.3390/nano9010090>.
- [22] C. Fenzl, P. Nayak, T. Hirsch, O.S. Wolfbeis, H.N. Alshareef, A.J. Baeumner, Laser-Scribed Graphene Electrodes for Aptamer-Based Biosensing, *ACS Sensors*. 2 (2017) 616–620. <https://doi.org/10.1021/acssensors.7b00066>.
- [23] K. Griffiths, C. Dale, J. Hedley, M.D. Kowal, R.B. Kaner, N. Keegan, Laser-scribed graphene presents an opportunity to print a new generation of disposable electrochemical sensors, *Nanoscale*. 6 (2014) 13613–13622. <https://doi.org/10.1039/c4nr04221b>.
- [24] D.A.C. Brownson, S.A. Varey, F. Hussain, S.J. Haigh, C.E. Banks, Electrochemical properties of CVD grown pristine graphene: Monolayer- vs. quasi-graphene, *Nanoscale*. 6 (2014) 1607–1621. <https://doi.org/10.1039/c3nr05643k>.
- [25] C. Bosch-Navarro, Z.P.L. Laker, J.P. Rourke, N.R. Wilson, Reproducible, stable and fast electrochemical activity from easy to make graphene on copper electrodes, *Phys. Chem. Chem. Phys.* 17 (2015) 29628–29636. <https://doi.org/10.1039/c5cp04070a>.
- [26] X. Zuo, C. Xu, H. Xin, Simulation of voltammogram on rough electrode, *Electrochim. Acta*. 42 (1997) 2555–2558. [https://doi.org/10.1016/S0013-4686\(96\)00448-3](https://doi.org/10.1016/S0013-4686(96)00448-3).
- [27] D. Menshykau, R.G. Compton, The Influence of Electrode Porosity on Diffusional Cyclic Voltammetry, *Electroanalysis*. 20 (2008) 2387–2394. <https://doi.org/10.1002/elan.200804334>.
- [28] D. Menshykau, I. Streeter, R.G. Compton, Influence of electrode roughness on cyclic voltammetry, *J. Phys. Chem. C*. 112 (2008) 14428–14438. <https://doi.org/10.1021/jp8047423>.
- [29] C. Punckt, M.A. Pope, I.A. Aksay, On the electrochemical response of porous functionalized graphene electrodes, *J. Phys. Chem. C*. 117 (2013) 16076–16086. <https://doi.org/10.1021/jp405142k>.
- [30] M. V. Hoang, H.J. Chung, A.L. Elias, Irreversible bonding of polyimide and polydimethylsiloxane (PDMS) based on a thiol-epoxy click reaction, *J. Micromechanics Microengineering*. 26 (2016) 105019. <https://doi.org/10.1088/0960-1317/26/10/105019>.

- [31] S. Wang, S. Yu, M. Lu, L. Zuo, Microfabrication of plastic-PDMS microfluidic devices using polyimide release layer and selective adhesive bonding, *J. Micromechanics Microengineering*. 27 (2017) 055015. <https://doi.org/10.1088/1361-6439/aa66ed>.
- [32] N. Wongkaew, M. Simsek, C. Griesche, A.J. Baeumner, Functional Nanomaterials and Nanostructures Enhancing Electrochemical Biosensors and Lab-on-a-Chip Performances: Recent Progress, Applications, and Future Perspective, *Chem. Rev.* 119 (2019) 120–194. <https://doi.org/10.1021/acs.chemrev.8b00172>.
- [33] A. Nsabimana, Y. Lan, F. Du, C. Wang, W. Zhang, G. Xu, Alkaline phosphatase-based electrochemical sensors for health applications, *Anal. Methods*. 11 (2019) 1996–2006. <https://doi.org/10.1039/c8ay02793e>.
- [34] Y. Liu, E. Xiong, X. Li, J. Li, X. Zhang, J. Chen, Sensitive electrochemical assay of alkaline phosphatase activity based on TdT-mediated hemin/G-quadruplex DNAzyme nanowires for signal amplification, *Biosens. Bioelectron.* 87 (2017) 970–975. <https://doi.org/10.1016/j.bios.2016.09.069>.
- [35] E.P. Simão, I.A.M. Frías, C.A.S. Andrade, M.D.L. Oliveira, Nanostructured electrochemical immunosensor for detection of serological alkaline phosphatase, *Colloids Surfaces B Biointerfaces*. 171 (2018) 413–418. <https://doi.org/10.1016/j.colsurfb.2018.07.056>.
- [36] C. Shen, X. Li, A. Rasooly, L. Guo, K. Zhang, M. Yang, A single electrochemical biosensor for detecting the activity and inhibition of both protein kinase and alkaline phosphatase based on phosphate ions induced deposition of redox precipitates, *Biosens. Bioelectron.* 85 (2016) 220–225. <https://doi.org/10.1016/j.bios.2016.05.025>.
- [37] QuantiFluoTM Alkaline Phosphatase Assay Kit (QFAP-100); BioAssay Systems, (n.d.). [https://www.bioassaysys.com/Alkaline-Phosphatase-Assay-Kit-\(QFAP-100\).html](https://www.bioassaysys.com/Alkaline-Phosphatase-Assay-Kit-(QFAP-100).html) (accessed August 24, 2020).
- [38] QuantiChromTM Alkaline Phosphatase Assay Kit; BioAssay Systems, (n.d.). <https://www.bioassaysys.com/Alkaline-Phosphatase-Assay-Kit.html> (accessed August 24, 2020).
- [39] C. Matellan, A.E. Del Río Hernández, Cost-effective rapid prototyping and assembly of poly(methyl methacrylate) microfluidic devices, *Sci. Rep.* 8 (2018) 1–13. <https://doi.org/10.1038/s41598-018-25202-4>.
- [40] C.W. Tsao, D.L. DeVoe, Bonding of thermoplastic polymer microfluidics, *Microfluid. Nanofluidics*. 6 (2009) 1–16. <https://doi.org/10.1007/s10404-008-0361-x>.
- [41] P. Nayak, Q. Jiang, N. Kurra, X. Wang, U. Buttner, H.N. Alshareef, Monolithic laser scribed graphene scaffolds with atomic layer deposited platinum for the hydrogen evolution reaction, *J. Mater. Chem. A*. 5 (2017) 20422–20427. <https://doi.org/10.1039/c7ta06236b>.
- [42] G. Xu, Z.A. Jarjes, V. Desprez, P.A. Kilmartin, J. Travas-Sejdic, Sensitive, selective, disposable electrochemical dopamine sensor based on PEDOT-modified laser scribed graphene, *Biosens. Bioelectron.* 107 (2018) 184–191. <https://doi.org/10.1016/j.bios.2018.02.031>.



### 3.6 Supporting Information

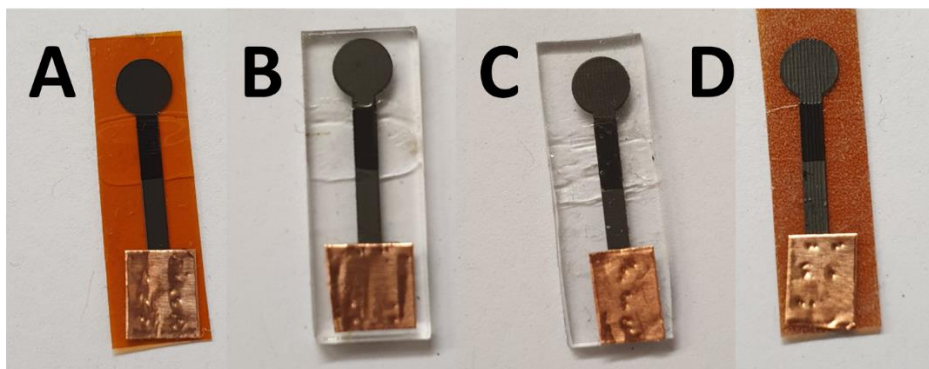


Figure S1 (A) LIG electrode on polyimide. (B) tLIG transferred to PMMA transferred with pressure transfer. (C) tLIG on PDMS transferred using the infiltration method. (D) tLIG transferred to scotch tape via delamination.

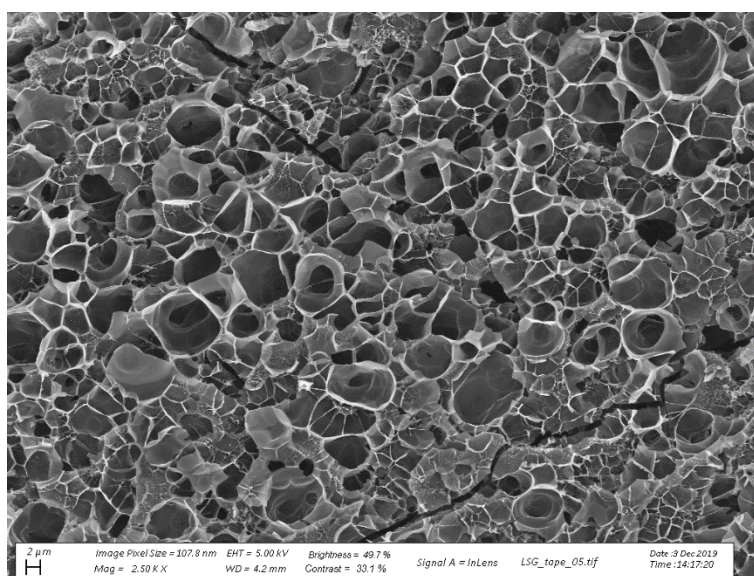


Figure S2: SEM picture of tLIG transferred to scotch tape via delamination.



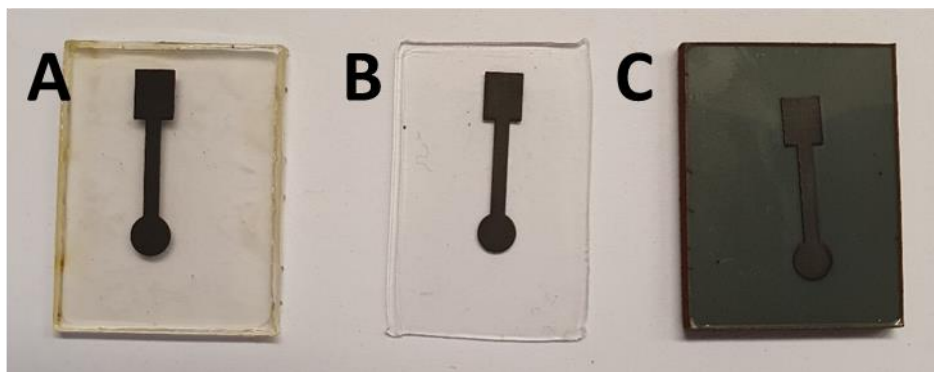


Figure S3: tLIG transferred to (A) polyethylene terephthalate (PET), (B) polystyrene (PS) and (C) polyvinyl chloride (PVC). Transfer of LIG was obtained according to the for PMMA described protocol with adjusted transfer temperatures of 77 °C (PET), 100 °C (PS) and 75 °C (PVC).

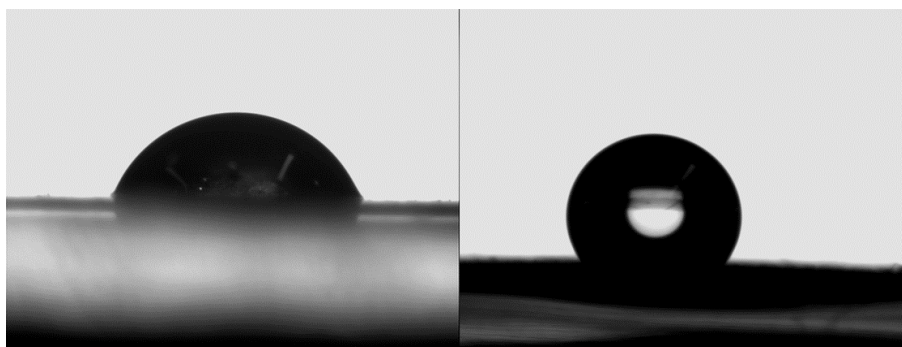


Figure S4: Contact angles of transferred laser-induced graphene. Pressure-driven tLIG on PMMA (left) and tLIG on PDMS transferred by the infiltration method (right).

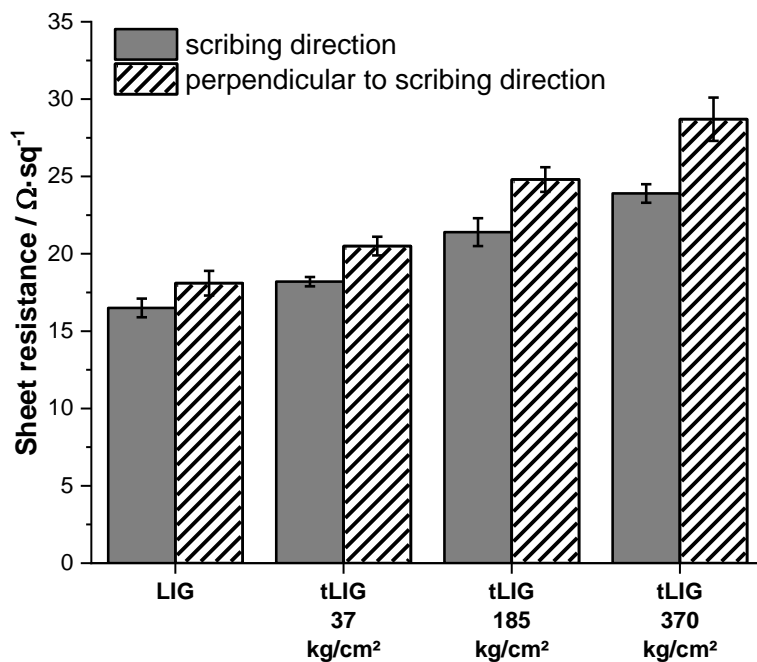


Figure S5: Sheet resistance of LIG and tLIG, transferred with varying pressure. Sheet resistance is measured in scribing direction and perpendicular towards scribing direction (n=3).

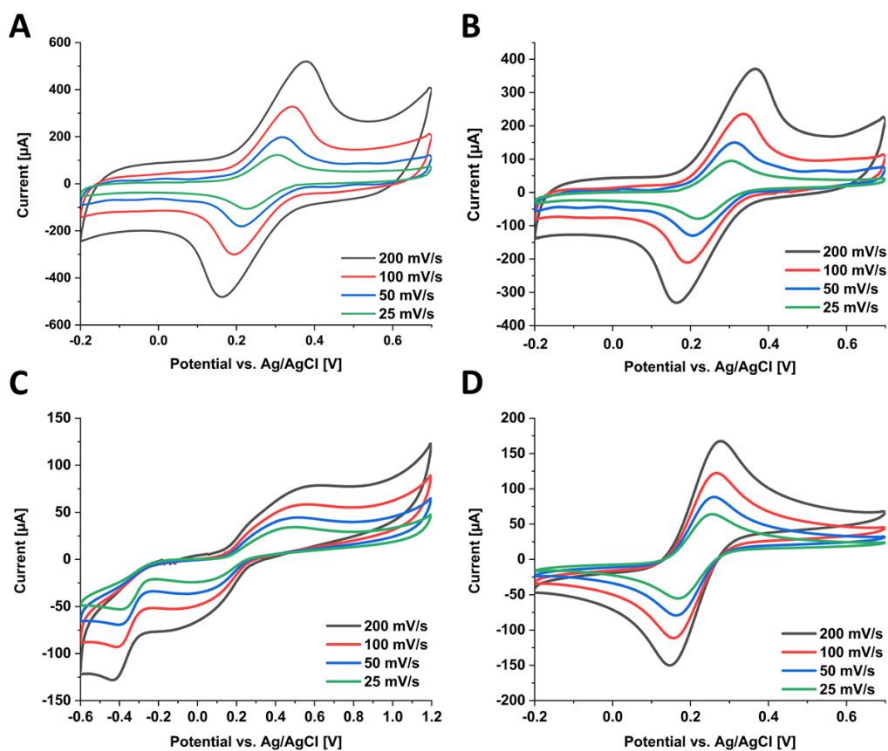


Figure S6 Cyclic voltammograms of 5 mmol L<sup>-1</sup> K<sub>4</sub>[Fe(CN)<sub>6</sub>] using LIG (A), tLIG (B), tLIG obtained with PDMS infiltration (C) and tLIG transferred by adhesive tape delamination (D).

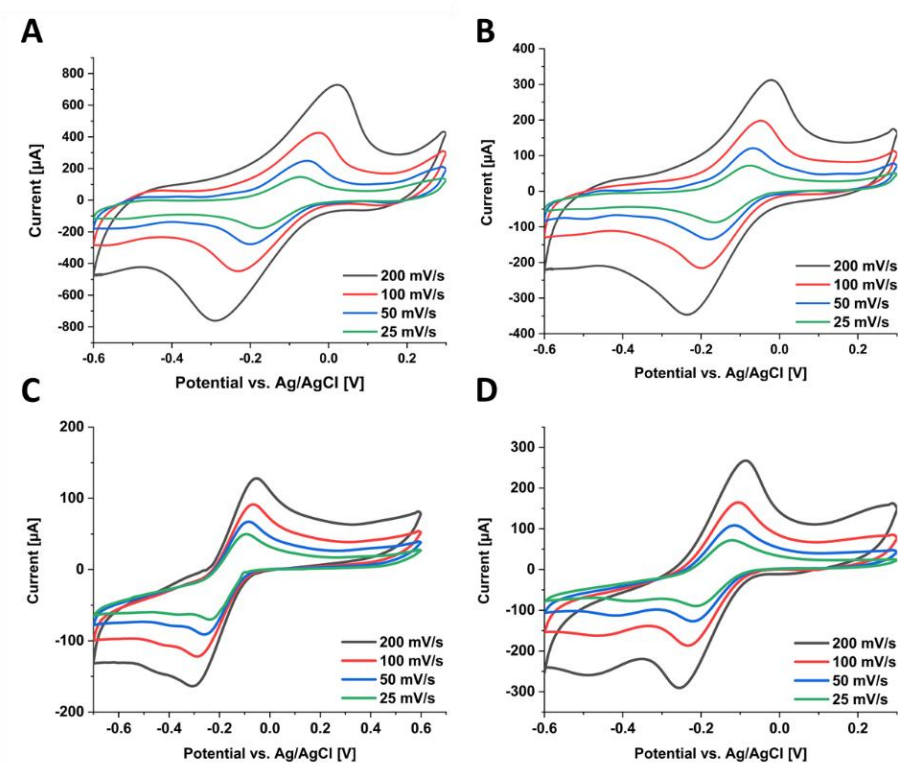


Figure S7: Cyclic voltammograms of 5 mmol L<sup>-1</sup> [Ru(NH<sub>3</sub>)<sub>6</sub>]Cl<sub>3</sub> using LIG (A), tLIG (B), tLIG obtained with PDMS infiltration (C) and tLIG transferred by adhesive tape delamination (D).

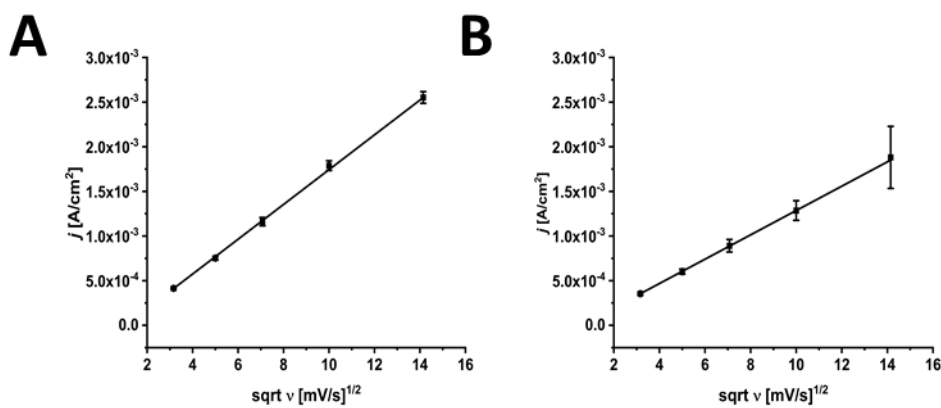


Figure S8: Plot of the wave current densities for LIG (A) and tLIG (B) versus square root of scan rate measured with cyclic voltammetry of 5 mM K<sub>4</sub>[Fe(CN)<sub>6</sub>] in PBS buffer. (n = 3)

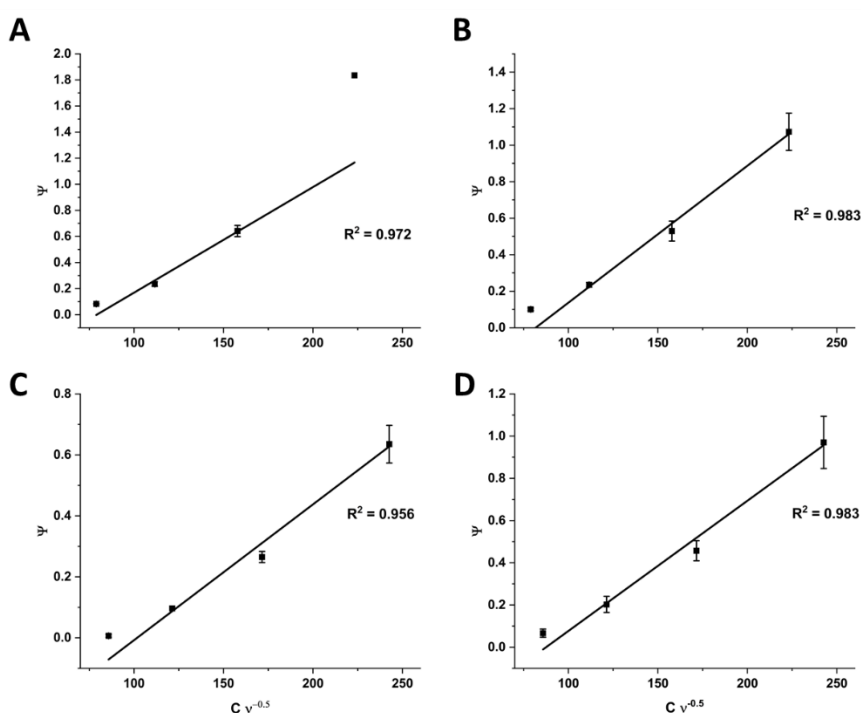


Figure S9: Plot of Nicholson's kinetic parameter  $\Psi$  versus  $C$  multiplied by reciprocal of the scan rate ( $Cv^{-0.5}$ ). The standard HET rate constant  $k^0$  is calculated by the slope of linear fitting.  $R^2$  values for the linear fit are given. (A)  $[\text{Fe}(\text{CN})_6]^{4-}$  with LIG electrode (B)  $[\text{Fe}(\text{CN})_6]^{4-}$  with tLIG electrode (C)  $[\text{Ru}(\text{NH}_3)_6]^{3+}$  with LIG electrode (D)  $[\text{Ru}(\text{NH}_3)_6]^{3+}$  with tLIG electrode. ( $n = 3$ ).

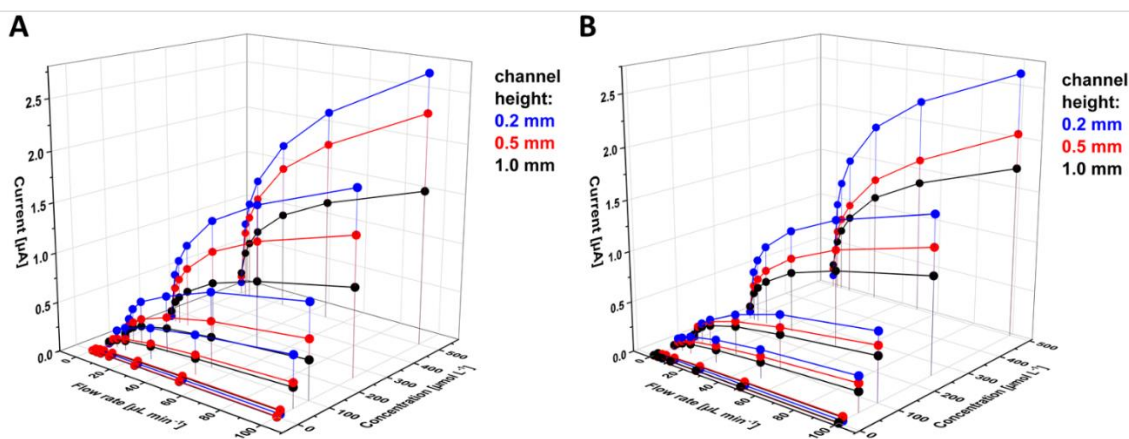


Figure S10 (A) Electrochemical response of LIG towards different concentrations of *p*-aminophenol (0; 10; 50; 100; 250; 500  $\mu\text{mol L}^{-1}$ ) with varying flow rates in microfluidic channels of different heights, 200  $\mu\text{m}$  (blue), 500  $\mu\text{m}$  (red) and 1000  $\mu\text{m}$  (black). (B) Electrochemical response of tLIG towards different concentrations of *p*-aminophenol (0; 10; 50; 100; 250; 500  $\mu\text{mol L}^{-1}$ ) with varying flow rates in microfluidic channels of different heights, 200  $\mu\text{m}$  (blue), 500  $\mu\text{m}$  (red) and 1000  $\mu\text{m}$  (black).

## Substrate-Independent Laser-Induced Graphene Electrodes for Microfluidic Electroanalytical Systems

Table S1: Heterogeneous electrochemical rate constants ( $k^0$ ) for different carbon-based graphite and graphene materials for the redox-markers  $[\text{Fe}(\text{CN})_6]^{4-}$  and  $[\text{Ru}(\text{NH}_3)_6]^{3+}$ .

Electrode	$k^0 / \text{cm s}^{-1}$		Reference
	$[\text{Fe}(\text{CN})_6]^{4-}$	$[\text{Ru}(\text{NH}_3)_6]^{3+}$	
LIG	$0.0081 \pm 0.0010$	$0.0045 \pm 0.0007$	This work
tLIG	$0.0075 \pm 0.0006$	$0.0062 \pm 0.0005$	This work
LSG (derived from graphene oxide)	0.02373	---	1
EPPG	0.002601		1
		0.00877	2
BPPG	0.00033		1
		0.00158	2
CVD-Graphene (on copper)	$0.0140 \pm 0.0005$	$0.012 \pm 0.001$	3
q-graphene (on silicon dioxide)	---	0.00158	2
m-graphene (on silicon dioxide)	---	0.00111	2
LSG (derived from polyimide)	$0.0044 \pm 0.0003$	---	4

\*LSG: laser-scribed graphene; EPPG: edge-plane pyrolytic graphite; BPPG: basal-plane pyrolytic graphite; q-graphene: quasi-graphene (ca. 4 layers); m-graphene: monolayer-graphene

## Substrate-Independent Laser-Induced Graphene Electrodes for Microfluidic Electroanalytical Systems

Table S2: Electrode sensitivity of LIG and tLIG for the detection of redox-markers using amperometry and SWV. Data are corresponding to the measurements presented in Figure 3.

Electrochemical method	Analyte	LIG	tLIG
		Sensitivity / $\mu\text{A L}\cdot\mu\text{mol}^{-1}$	Sensitivity / $\mu\text{A L}\cdot\mu\text{mol}^{-1}$
Amperometry	$\text{K}_4[\text{Fe}(\text{CN})_6]$	$0.00364 \pm 0.00003$	$0.00334 \pm 0.00004$
Amperometry	$[\text{Ru}(\text{NH}_3)_6]\text{Cl}_3$	$-0.00239 \pm 0.00014$	$-0.00135 \pm 0.00003$
SWV	$\text{K}_4[\text{Fe}(\text{CN})_6]$	$0.353 \pm 0.008$	$0.192 \pm 0.002$
SWV	$[\text{Ru}(\text{NH}_3)_6]\text{Cl}_2$	$0.937 \pm 0.073$	$0.489 \pm 0.016$

## Substrate-Independent Laser-Induced Graphene Electrodes for Microfluidic Electroanalytical Systems

Table S3: Amperometric detection of *p*-aminophenol in microfluidic channels and bulk measurements. Using tLIG and LIG as electrode material and channels of varying height. Data are corresponding to the measurements presented in Figure 4.

<b>Adhesive tape-based channels</b>			
LIG			
<b>Channel height / mm</b>	<b>Sensitivity / nA L <math>\mu\text{mol}^{-1}</math></b>	<b>Linear range / <math>\mu\text{mol L}^{-1}</math></b>	<b>R<sup>2</sup></b>
<b>0.2</b>	0.296 $\pm$ 0.017	25 - 1000	0.981
<b>0.5</b>	0.531 $\pm$ 0.016	5 - 1000	0.993
<b>1.0</b>	0.538 $\pm$ 0.017	5 -1000	0.992
tLIG			
<b>0.2</b>	0.277 $\pm$ 0.009	10 - 1000	0.992
<b>0.5</b>	0.541 $\pm$ 0.013	5 -1000	0.996
<b>1.0</b>	0.614 $\pm$ 0.006	5 -1000	0.999
<b>Solvent bonding</b>			
LIG			
<b>0.25</b>	0.251 $\pm$ 0.005	25 - 1000	0.997
<b>1.0</b>	0.673 $\pm$ 0.006	1 - 1000	0.999
<b>Bulk</b>			
<b>LIG</b>	0.588 $\pm$ 0.039 *	5 - 500	0.970
<b>tLIG</b>	0.616 $\pm$ 0.020 *	5 - 500	0.992

\* Data normalized to electrode area of electrodes in microfluidic channel measurements.

## Substrate-Independent Laser-Induced Graphene Electrodes for Microfluidic Electroanalytical Systems

Table S4: Amperometric detection of *p*-aminophenol in 0.5 mm high microfluidic channels using tLIG and LIG as electrode material under different flow rates. Data are corresponding to the measurements presented in Figure 5.

Laser-induced graphene			
Flow rate / $\mu\text{L}\cdot\text{min}^{-1}$	Sensitivity / $\text{nA L}\cdot\mu\text{mol}^{-1}$	Linear range / $\mu\text{mol L}^{-1}$	$R^2$
25	$2.68 \pm 0.06$	0.5 - 250	0.996
5	$1.74 \pm 0.08$	0.5 - 250	0.983
0*	$0.531 \pm 0.016$	5 – 1000	0.993
Transferred laser-induced graphene			
25	$2.36 \pm 0.02$	1 - 250	0.999
5	$1.73 \pm 0.05$	1 - 250	0.994
0*	$0.541 \pm 0.013$	5 -1000	0.996

\* measured in stopped-flow (cf. Table SI 2)

### 3.6.1 References

- 1 K. Griffiths, C. Dale, J. Hedley, M. D. Kowal, R. B. Kaner and N. Keegan, *Nanoscale*, 2014, **6**, 13613–13622.
- 2 D. A. C. Brownson, S. A. Varey, F. Hussain, S. J. Haigh and C. E. Banks, *Nanoscale*, 2014, **6**, 1607–1621.
- 3 C. Bosch-Navarro, Z. P. L. Laker, J. P. Rourke and N. R. Wilson, *Phys. Chem. Chem. Phys.*, 2015, **17**, 29628–29636.
- 4 C. Fenzl, P. Nayak, T. Hirsch, O. S. Wolfbeis, H. N. Alshareef and A. J. Baeumner, *ACS Sensors*, 2017, **2**, 616–620.



## 4 Electrochemical detection of *Escherichia coli* via genetically modified bacteriophages

### Abstract

Bacteriophages offer a unique opportunity for highly specific detection of viable bacteria due to their inherent host specificity. Their easy-to-manipulate genome enables rapid, sensitive and simple detection platforms. Here, we engineered the lytic T7 bacteriophage (phage) to overexpress alkaline phosphatase fused to a cellulose-specific carbohydrate-binding module (ALP-CBM). In the bioassay, a sample containing *E. coli* is infected by the phage in a 30 min. incubation period, during which large quantities of ALP-CBM are expressed and freely released into the media. Then, prior to detecting the fusion protein as a direct correlate to the original bacterial concentration, it is concentrated out of the media via its CBM function by simple filtration through a cellulose disc, followed by substrate addition and quantification via differential pulse voltammetry. This extremely simple bioassay resulted in a limit of detection of  $10^3$  CFU·mL<sup>-1</sup> within just 2 h. The simplicity and low-cost of the bioassay associated with its ruggedness against matrix interferences or reporter concentrations that typically plague antibody-based biosensors and bioassays make it a relevant inexpensive very simple detection system for viable bacteria in complex matrices especially for resource-limited settings.

### Keywords

engineered bacteriophages, electrochemical biosensor, bacterial detection, alkaline phosphatase, food safety, *E. coli*

---

**This chapter has been submitted.**

Christian Griesche, Hannah S. Zurier, Brenda G. Werner, Sam R. Nugen, Antje J. Baeumner, **2021**, submitted.

**Author contributions:** SRN and AJB developed the concept for this work. AJB and the author planned the detailed experiments. The author did most of the experimental work. HSZ prepared the *E. coli* lysate. BGW performed initial experiments on the electrochemical detection. The author wrote the first draft of the manuscript. SRN and HSZ wrote the experimental part on bacteriophages, bacterial cultures, and *E. coli* infection. HSZ, SRN, and AJB revised the manuscript. AJB is corresponding author.

## 4.1 Introduction

The World Health Organization (WHO) estimates that almost one in ten people worldwide fall sick after eating food contaminated with bacteria, viruses, parasites or chemical substances every year. With those contaminations causing over 200 diseases resulting in 420,000 annual deaths the access to safe food is essential for sustaining life and promoting good health [1,2]. Noroviruses are found to cause the largest number of foodborne illnesses in the US with bacterial contamination next to that being an increasing threat to human health [3,4]. Hence the rapid and sensitive detection of bacterial contamination in water samples and food is of great importance to ensure food safety [5].

*Escherichia coli* (*E. coli*) is one of the most studied bacteria [6]. It is found in the intestine of warm-blooded animals as well as humans. While most *E. coli* strains are harmless to humans enterohemorrhagic *E. coli* (EHEC) can cause severe intestinal diseases. Yet, even the detection of harmless *E. coli* cells is of utmost relevance, as they are a precise indicator for fecal contamination in food and water, which in turn could also indicate the presence of pathogenic intestinal strains. WHO guidelines for drinking water henceforth contain a zero tolerance of *E. coli* or thermotolerant coliform bacteria, naming *E. coli* the more precise indicator. This zero tolerance is translated into a quantitative measure by requiring that *E. coli* is not detectable in 100 mL of sample [7]. Therefore, the common detection methods for *E. coli* involve culturing and plate counting with the use of selective medium. While those methods are accurate and highly reliable they are laborious and time-consuming due to long incubation times [8]. Alternative strategies for the detection of *E. coli* include nucleic acid-based methods, like PCR, surface enhanced Raman spectroscopy or optical nanomaterials [9–11] are often unable to distinguish viable from nonviable cells. That is, neither antibody- nor DNA-based approaches can provide this distinction, unless a pre-culturing step is included. The detection of mRNA has been proposed as a strategy to overcome this hurdle [12]. Another approach for the rapid detection of bacteria, being able to distinguish viable and nonviable cells, utilizes genetically engineered bacteriophages. Bacteriophages specifically infect bacteria by their attachment to unique receptors on the cell surface. After attachment, the phage genome is injected into the host cell, altering the bacterial metabolism to predominantly replicate the bacteriophages. By altering the phage genome and including reporter genes, these become easily detectable. As such, various reporter genes were engineered in bacteriophages, including the reporter enzymes alkaline phosphatase [13],  $\beta$ -galactosidase [14] and luciferase [15,16].

Undoubtedly, these bacteriophage-based bioassays are truly promising approaches for the simple, low-cost, rapid and highly sensitive detection of viable bacteria, but many challenges to their practical operation maintain. Specifically, the reliable detection of bacteria in low concentration

needs to be carried out in large sample volumes to fulfill government requirements. Furthermore, real-world samples often consist of complex matrices containing compounds potentially interfering with the reporter enzyme itself or disabling the signal readout, e.g. signal quenching or increasing background signals. While dilution is a method used to reduce matrix effects it also affects the amounts of analytes or expressed reporter present. Thus, inevitably, long bacteria cultivation remains to be required. To shorten such incubation times to a minimum, effort has recently also focused on a better separation and pre-concentration of the target cells or reporter enzymes. The former can easily be done using filtration methods [17] or antibody coated magnetic nanoparticles [18]. For reporter enzyme pre-concentration, smart genetic engineering approaches have been demonstrated, in which the reporter enzyme is fused with a protein or peptide bearing specific affinity to synthetic polymers, cellulose or gold [19–21]. For example, this principle was successfully applied to engineer bacteriophages expressing phosphatase or luciferase fused to a cellulose-specific carbohydrate binding module and alkaline phosphatase fused to gold binding peptides [16,22].

In this study, we present a strategy for the rapid detection of *E. coli* in aqueous samples based on the electrochemical quantification of alkaline phosphatase fused with a cellulose binding peptide. This peptide allows the pre-concentration of the fusion enzyme on simple cellulose discs and hence the use of larger amounts of sample. Enzymatically generated *p*-amino phenol was detected electrochemically using screen-printed carbon electrodes requiring minimal equipment. The combination of engineered bacteriophages with electrochemical detection offers hence sensitive, low-cost detection of *E. coli*.

## 4.2 Material and Methods

### 4.2.1 Reagents and Materials

Whatman® antibiotic assay discs were obtained from Sigma-Aldrich. 1M NaOH and glycine were obtained from Merck. ZnCl<sub>2</sub> and MgCl<sub>2</sub> were obtained from Sigma. DropSens Screen-printed carbon electrodes (DRP-110) were purchased from Metrohm (Germany). *p*-aminophenyl phosphate and Luria-Bertrani broth (LB broth, 10.0 g of tryptone, 5.0 g yeast extract, 10.0 g sodium chloride in 1 L of Millipore water, pH 7.2) was obtained from Sigma (USA). A PalmSens 4 potentiostat (PalmSens, Netherlands) was used for electrochemical measurements. Electrodes were connected to the potentiostat using a boxed-connector for screen-printed electrodes to connect the electrodes (DropSens, Spain).

Glycine-NaOH buffer contains 50 mM glycine, 1 mM ZnCl<sub>2</sub> and 1 mM MgCl<sub>2</sub>. The respective pH was adjusted with 1 M NaOH.

### 4.2.2 Bacteriophage and Bacterial Cultures

The T7-based reporter bacteriophage (NRGp2) was engineered as previously described by Hinkley *et al.* [16]. Briefly, NRGp2 was engineered using the T7Select 415-1 kit (EMD Millipore, Burlington, MA, USA). A mammalianized alkaline phosphatase [23] was inserted after an inserted capsid gene stop codon and ribosome binding site (RBS) which was designed for high translation rates using an RBS calculator. [24] The alkaline phosphatase (ALP) was fused with a carbohydrate-binding module (CBM) specific to cellulose to allow for immobilization of the reporter enzyme (ALP-CBM) following infection. The assembled phage genome containing the ALP-CBM gene was transformed into *E. coli* BL21 for a reboot and subsequent progeny phages were further propagated and purified. The ALP-CBM gene was verified in an isolated phage genome via whole genome sequencing (NCBI Accession No. MH651796).

*E. coli* BL21 ATCC (Manassas, VA USA) was used for all experiments and was prepared as previously described by Hinkley *et al.* [16].

### 4.2.3 Assay Procedure

#### *E. coli* infection

*E. coli* BL21 was grown in 20 mL LB broth from a single colony to an OD<sub>600</sub> of 0.64 at 37 °C shaking constantly at 90 rpm. At this time, 10 mL of *E. coli* culture were infected with 5 × 10<sup>9</sup> plaque-forming units of NRGp2 and returned to 37 °C and 90 RPM shaking for a further 30 minutes, at which point the lysate was clear (Scheme 1-1). The initial bacterial culture was plated in triplicate to determine the concentration and the equivalent concentration of the lysate dilutions.

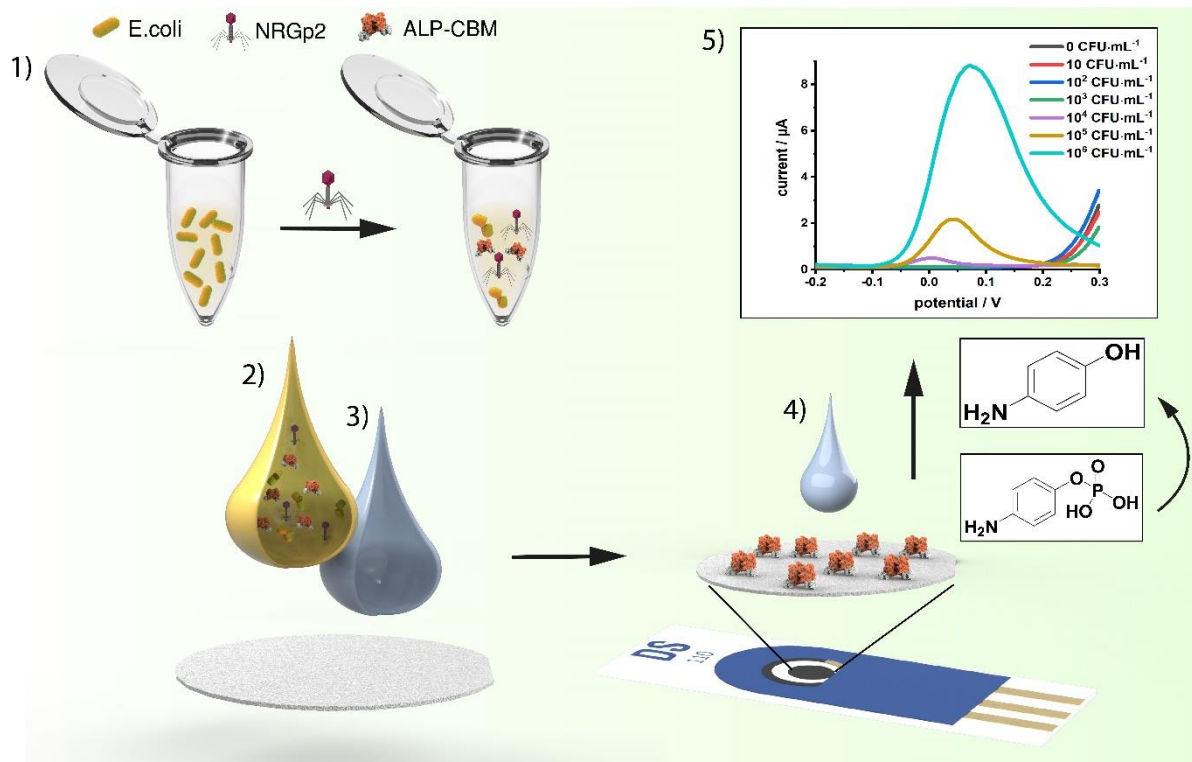
In order to capture and concentrate the ALP-CBM reporter probe due to its specific binding to cellulose, 1 mL of *E. coli* lysate was filtered through a Whatman® cellulose antibiotic assay disc (diameter 6 mm) at a flow rate of 50 µL min<sup>-1</sup> using Legato 180 syringe pumps (kd Scientific) (Scheme 1 -2). The antibiotic assay discs were washed with 200 µL of Glycine-NaOH buffer pH 10 at a flow rate of 50 µL min<sup>-1</sup> (Scheme 1 - 3). After washing, the disc was directly placed on the DropSens SPCE and 20 µL of 10 mmol L<sup>-1</sup> *p*-aminophenyl phosphate (in Glycine-NaOH buffer pH 10) were added (Scheme 1 - 4). For the enzymatic reaction the electrode was incubated for 30 min at 37 °C.

Enzymatically generated p-aminophenol was electrochemically determined using differential pulse voltammetry (DPV) from -0.2 V to 0.3 V with 5 s equilibration time (Scheme 1 - 5). Additional parameters for DPV measurements were  $E_{\text{pulse}} = 25 \text{ mV}$ ,  $t_{\text{pulse}} = 80 \text{ ms}$  and a scan rate of  $20 \text{ mV}\cdot\text{s}^{-1}$ .

For the optimization of single assay parameters (T, pH, substrate concentration and reaction time), the assay protocol was used with a single varying parameter with a negative control (LB broth) and a  $10^5 \text{ CFU mL}^{-1}$  *E. coli* sample. For data evaluation the signal—to—noise ratio of the electrochemical signals obtained for  $10^5 \text{ CFU}\cdot\text{mL}^{-1}$  *E. coli* sample vs the negative control LB broth was calculated. The electrochemical response was evaluated with varied settings ( $t_{\text{pulse}} = 60 - 100 \text{ ms}$ ,  $E_{\text{pulse}} = 10 - 40 \text{ mV}$ ; scan rate =  $10 - 20 \text{ mV s}^{-1}$ ). The best separation of the oxidation potential of pAP and pAPP and the most reliable electrochemical response were obtained with  $t_{\text{pulse}} = 80 \text{ ms}$ ,  $E_{\text{pulse}} = 25 \text{ mV}$  and a scan rate of  $20 \text{ mV s}^{-1}$ .

### 4.2.4 Statistical evaluation

The mean values ( $n = 4$ ) among different concentrations of *E. coli* were determined to be statistically different with Tukey's t-test ( $P < 0.05$ ). The lowest bacteria concentration being significantly different from the negative control was declared to be the limit of detection (LOD) of the bioassay.



Scheme 1: Assay principle for the detection of *E. coli* via genetically modified bacteriophages. (1) *E. coli* is incubated with NRGp2 bacteriophages. (2) The *E. coli* lysate is filtered through a cellulose disc and ALP-CBM is binding to cellulose followed by (3) washing of the disc. (4) The enzymatic substrate pAPP is added to the cellulose disc and enzymatically formed pAP (5) is detected electrochemically with DPV.

### 4.3 Results and Discussion

Based on prior research, a simple and sensitive, quantitative electrochemical biosensor was developed for the detection of *E. coli* in drinking water. *E. coli*-specific bacteriophages had previously been engineered to contain an alkaline phosphatase-carbohydrate binding module (ALP-CBM) fusion gene. Specifically, the enzyme is a double mutant bacterial (*E. coli*) alkaline phosphatase with a 40-fold higher activity compared to the wild-type bacteria. While the temperature stability was maintained, the pH dependency of the enzymatic activity was shifted from pH 8 to pH 10 [23]. This highly active ALP was then genetically fused to a carbohydrate binding module (CBM) being highly specific to cellulose. The binding of this genetically modified enzyme to cellulose is reported by Hinkley *et al.* within the colorimetric detection of *E. coli* [16].

Here, ALP activity was detected using differential pulse voltammetry on single-use screen-printed carbon electrodes (SPCE) with the goal of developing a stand-alone, highly quantitative simple

biosensor. Initially, the enzymatic reaction was optimized with respect to substrate, substrate concentration, pH, reaction time and incubation temperature.

Two well-known ALP substrates were evaluated for electrochemical detection, *p*-nitrophenyl phosphate (pNPP), and *p*-aminophenyl phosphate (pAPP). It was found that the LB broth had a high background signal at enzyme reaction product pNP's oxidation potential, which made the detection of concentrations below 25  $\mu\text{mol L}^{-1}$  impossible (Fig. S1A). In contrast, the lower oxidation potential of the enzyme reaction product pAP had a limit of detection of only 5  $\mu\text{mol L}^{-1}$  (Fig. S1C). However, in order to further lower the limit of detection and overcome the limited stability of pAPP in LB broth at 37 °C (Fig. S2) it was determined that a washing step between substrate addition to the cellulose disc and prior to electrochemical detection was optimal. DPV settings were optimized for the direct detection of pAP under optimized conditions for the enzymatic reaction. In Gly-NaOH buffer (0.05M, pH 10.0) a significantly more sensitive detection for both analytes (10  $\mu\text{mol L}^{-1}$  pNP and 0.5  $\mu\text{mol L}^{-1}$  pAP) (Fig. S1C and S1D) was achieved. A cellulose disc on top of the SPCE induced a higher charge transfer resistance compared to the plain electrode but still enabled the electrochemical detection with only slightly decreased sensitivity (Fig. S3). The use of alkaline phosphatase without a cellulose-affinity tag demonstrates that only bacteriophage-derived alkaline phosphatase activity is detected. Here, the washing process essentially eliminated any signal as the alkaline phosphatase is washed off the membrane (Fig. S4 and Table S1).

For the enzymatic reaction of ALP and *p*-aminophenyl phosphate within the concentration range of 5  $\text{mmol}\cdot\text{L}^{-1}$  to 20  $\text{mmol}\cdot\text{L}^{-1}$ , minimal differences were observed when considering the high standard deviations (Fig. S5). A pAPP concentration of 10  $\text{mmol}\cdot\text{L}^{-1}$  was determined to result in optimal reactions.

Furthermore, temperature, pH and incubation times were optimized (Fig. 1). The physiological temperature of 37 °C would increase the S/N only by a factor of 1.2 so that a use at room temperature is clearly a possibility. In case of the pH, as expected, a more alkaline pH was favorable, but reached an optimum at pH 10, above which background signals and standard deviations increase due to signal substrate instability (Fig. S6). Similar effects were observed with respect to the incubation time. While the S/N doubled between 15 and 30 min of incubation, additional minutes lead to increased background signals and hence overall similar S/N albeit the overall signal height increased (Fig. S6). In the end, the optimized condition was identified to incubate the ALP-CBM for 30 minutes at 37 °C at pH 10 with 10  $\text{mmol L}^{-1}$  pAPP substrate.

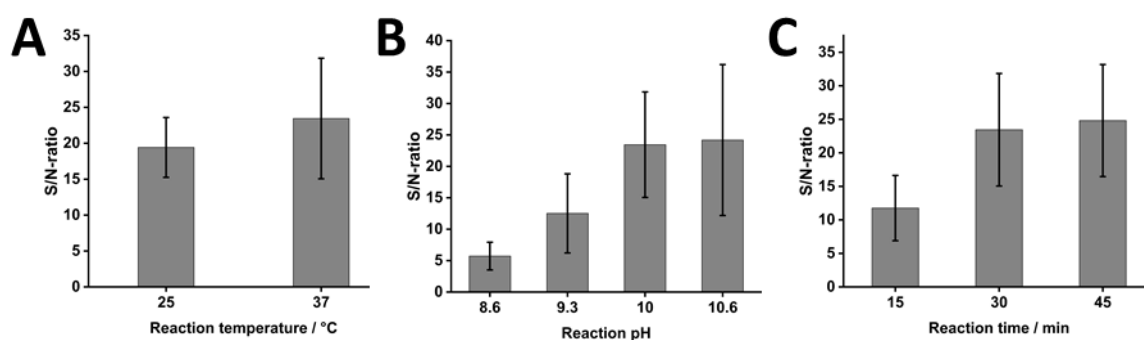


Fig. 1: Dependency of the signal-to-noise ratios for the electrochemical detection of *E. coli*. The S/N value is defined as the ratio of the current obtained for  $10^5$  CFU  $\text{mL}^{-1}$  *E. coli* divided by the current obtained for the negative control (LB broth). (A) S/N ratio obtained for varying reaction temperatures (25 °C and 37 °C) with a reaction pH of 10.0 and 30 min reaction time. (B) S/N ratio obtained for varying reaction pH values (8.6; 9.3; 10.0; 10.6) with a reaction temperature of 37 °C and 30 min reaction time. (C) S/N ratio obtained for varying reaction times (15, 30 and 45 min) with a reaction temperature of 37 °C. and reaction pH of 10.0.

Actual current signals with standard deviations of the  $n=3$  measurements are provided in Fig. S5.

The detection principle is based on the activity of alkaline phosphatase generated by *E. coli* bacteria upon phage infection. The amount of expressed alkaline phosphatase depends on the dynamic interaction of *E. coli* and the phage as well as incubation time [6]. The concentration of utilized phages  $5 \times 10^8$  PFU/mL and the incubation time of 30 min were based on earlier findings. The lytic nature of the T7 phages induces lysis of the bacterial cells at the end of the infection cycle which releases the reporter enzyme and replicated phages. Without any further sample treatment, the generated ALP was immobilized on a cellulose disc via its CBM and utilized for the enzymatic dephosphorylation of pAPP. Hence, the amount of immobilized ALP correlates with the number of *E. coli* cells and is determined by the amount of enzymatically generated pAP via DPV.

Two major aspects were optimized with respect to the design of the electrochemical biosensor. First, a method for the filtration of bacterial lysate and hence pre-concentration of ALP-CBM on cellulose filter discs had to be established. The ultimate goal is a reliable method that could be applied to various volumes in a simple format. Preliminary experiments using manually dropped solution onto the discs demonstrated, that gravity-based flow through the filter discs combined with their inherent capillarity was sufficient and no complex or slower flow was needed. Automated processing was obtained by continuous dropping through syringe pumps by setting flows that relied on the gravity and capillary-driven flow through the discs and facilitates the processing of larger sample volumes (e.g. 1 mL, 5 mL). With the use of cellulose membranes this method is adaptable to larger scale filtration as shown by the WHO for ceramic pot filters and fiber membranes [25,26].



Secondly, the combination of cellulose discs on top of SPCE for the detection of pAPP was optimized. Specifically, the smaller the volume needed, the lower ALP-CBM concentrations could be determined. It was found that volumes below 35  $\mu\text{L}$  when added to a dry disc would not result in stable electrochemical signals as in this case the solution is held within the cellulose matrix and does not allow proper wetting of the electrode surface. Ultimately, an addition of 20  $\mu\text{L}$  of enzymatic substrate to the wet cellulose disc resulted in highly reliable signals after 30 minutes incubation at 37  $^{\circ}\text{C}$ . In the future, such volumes could be minimized by integration of the electrodes and discs into microfluidic channels, which would consequently lower the limit of detection [27].

The analytical performance of the proposed electrochemical biosensor was analyzed using varying *E. coli* concentration (0, 10,  $10^2$ ,  $10^3$ ,  $10^4$ ,  $10^5$ ,  $10^6$  CFU  $\text{mL}^{-1}$ ). For concentrations above  $10^3$  CFU  $\text{mL}^{-1}$  the oxidation peak for pAP is easily discernible (Fig. 2A), and a limit of detection was accordingly established at  $10^3$  CFU  $\text{mL}^{-1}$  which is significantly different ( $P < 0.05$ ) from the negative control. (Fig. 2B).

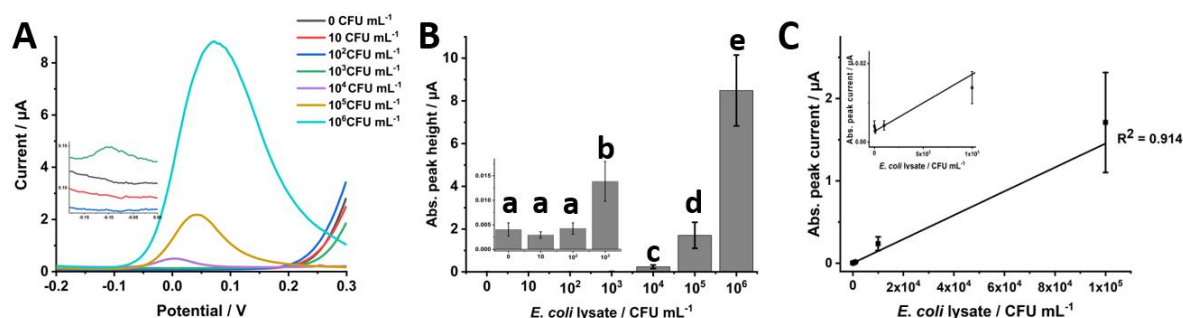


Fig. 2: **A** DPV curve for increasing concentration of *E. coli*. The inset is the amplification of the control and low *E. coli* concentrations (10,  $10^2$ ,  $10^3$  CFU  $\cdot\text{mL}^{-1}$ ). **B** Absolute peak height determined for varying concentration of *E. coli*. The inset is the amplification of the control and low *E. coli* concentrations (10,  $10^2$ ,  $10^3$  CFU  $\cdot\text{mL}^{-1}$ ). Bars with different letters (a, b, c, d, e) are significantly different ( $P < 0.05$ ). ( $n = 4$ ; error bars represent standard deviations). **C** Calibration curve for the electrochemical detection of *E. Coli* ( $n = 4$ ; error bars represent standard deviations).

Table 1: Recently published electrochemical bioassays for the bacteriophage-based electrochemical detection of *E. coli* are listed including the electrochemical detection method used, LOD and detection time.

	Detection method		LOD	Detection time	Reference
<b>Bioassays</b>	Linear	Sweep	$10^5$ CFU mL <sup>-1</sup>	4 h	[22]
	Voltammetry		1 CFU / 100 mL	12 h	
	Differential	Pulse	$10^2$ CFU mL <sup>-1</sup>	7 h	[6]
	Voltammetry				
	Potentiometry		2 CFU	>8 h	[28]
	Electrochemical		$10^3$ CFU mL <sup>-1</sup>	20 min	[29]
	Impedance Spectroscopy				
	Differential	Pulse	$10^3$ CFU mL <sup>-1</sup>	2 h	This work
	Voltammetry				

The LOD of  $10^3$  CFU mL<sup>-1</sup> is comparable to other electrochemical bioassay approaches using bacteriophages for the detection of *E. coli*. Wang *et al.* were able to detect  $10^2$  CFU·mL<sup>-1</sup> within 7 h utilizing engineered phages overexpressing  $\beta$ -galactosidase without any sample pretreatment [6]. With the use of NRGp7 phage coupled to magnetic beads for pre-concentration of bacteria and pre-concentration Wang *et al.* were able to detect 1 CFU in 100 mL within 12 h of assay time [22]. Hereby they were using overexpressed alkaline phosphatase fused to gold binding peptides enabling the immobilization of the reporter enzyme directly on the electrode. Shabani *et al.* as well utilized phage-coated magnetic beads for the separation of phages before the detection of *E. coli* with electrochemical impedance spectroscopy on phage-modified screen-printed carbon electrodes [29]. Using filtration for the sample pretreatment and pre-concentration of *E. coli* followed by preincubation before phage infection Neufeld *et al.* have shown to be able to detect *E. coli* within 8 h [30]. In a phagemid assay as well using filtration as pretreatment they were able to lower the limit of detection to 1 CFU·mL<sup>-1</sup> within 3 h [31]. The here presented approach hence falls within the same category of tests with the advantage of relying on simple SPCEs, simple filtration processes for pre-concentration and an overall low-cost approach. It can be concluded that also this assay can reach an even lower limit of detection but processing higher sample volumes. Gravitational pressure driven membrane ultrafiltration with flow rates up to 12 L/hour

are reported for household water treatment [26]. In combination with novel developments of (nano-)cellulose membranes this approach can increase the assay performance directly by the processing of larger volumes of bacterial lysate without costly equipment [25,32]. Besides the processing of larger lysate volumes the bacterial cells can be preconcentrated beforehand the phage infection using filtration techniques like vortex flow filtration or tangential flow filtration [33,34]. While filtrations are scalable to liters the rapid preconcentration of viable bacteria in the mL-range can be reached reliably with novel methods, e.g. the use of magnetic ionic liquids or superparamagnetic anion exchangers [35,36]. Alternatively, especially in order to detect concentrations as low as 1 CFU/ 100mL, preincubation of the sample prior to detection is suggested. Since incubation of cells with the bacteriophages is needed in any event, it would not further complicate the assay, but only prolong it by a few hours. With a doubling time of  $31 \pm 3$  min [37] 1 CFU/ 100 mL *E.coli* to  $10^3$  CFU mL<sup>-1</sup> within 8.5 h.

### 4.4 Conclusion

The detection of bacterial contamination in food and water is required to ensure public health. Therefore, a strategy combining engineered T7 phages with electrochemical detection was developed for the detection of *E. coli*. Without preconcentration this approach was able to detect  $10^3$  CFU mL<sup>-1</sup> *E. coli* within 2 h in a very simple mix-and-wait assay strategy. Recent research proved that phages are an excellent alternative biorecognition element to antibodies or aptamers for the specific detection of bacteria. [38] In addition to their extremely high binding affinity they can also distinguish between viable and non-viable bacteria cells, which is otherwise only possible through lengthy additional metabolic assays or mRNA detection strategies. Compared to antibodies, phage production is significantly less costly and phages are less demanding in storage, making them especially attractive for resource-limited applications as lyophilized phages have been reported to maintain viability up to 10 months when stored at 37 °C [39]. With unspecific binding and corresponding background signals being a common challenge in bioassay formats the lytic phage approach overcomes this due to the phage's inherent life cycle, i.e. reporter enzymes and phages are only replicated after the successful infection of the specific viable host bacteria cell [6]. All of those properties favor the implementation of phages into cost-efficient bioassays or biosensors which are especially needed in the developing world to ensure drinking water quality.

Most phages are highly specific toward their host bacteria, which on the one hand requires multiple engineered phages to cover an appropriate host range of *E. coli* from fecal contamination [16]. On the other hand, it suggests that the here presented principle can easily be adapted to the specific

detection of other pathogens. It thus paves the way for a new class of biosensors for the identification and quantification of bacteria by the engineering of different phages. Furthermore, multi-analyte detection strategies can be realized through the use of various engineered host-specific phages expressing different enzymes.

## 4.5 References

- [1] Foodborne diseases, [https://www.who.int/health-topics/foodborne-diseases#tab=tab\\_1](https://www.who.int/health-topics/foodborne-diseases#tab=tab_1) (accessed August 27, 2020).
- [2] Food Safety, <https://www.who.int/health-topics/food-safety/> (accessed August 27, 2020).
- [3] E. Scallan, R.M. Hoekstra, F.J. Angulo, R. V. Tauxe, M.A. Widdowson, S.L. Roy, J.L. Jones, P.M. Griffin, Foodborne illness acquired in the United States-Major pathogens, *Emerg. Infect. Dis.* 17 (2011) 7–15. <https://doi.org/10.3201/eid1701.P11101>.
- [4] R.L. Scharff, Economic burden from health losses due to foodborne illness in the united states, *J. Food Prot.* 75 (2012) 123–131. <https://doi.org/10.4315/0362-028X.JFP-11-058>.
- [5] J.W.F. Law, N.S.A. Mutalib, K.G. Chan, L.H. Lee, Rapid methods for the detection of foodborne bacterial pathogens: Principles, applications, advantages and limitations, *Front. Microbiol.* 5 (2014) 770. <https://doi.org/10.3389/fmicb.2014.00770>.
- [6] D. Wang, J. Chen, S.R. Nugen, Electrochemical Detection of *Escherichia coli* from Aqueous Samples Using Engineered Phages, *Anal. Chem.* 89 (2017) 1650–1657. <https://doi.org/10.1021/acs.analchem.6b03752>.
- [7] WHO, Guidelines for drinking-water quality, 2nd ed., Geneva, 1997.
- [8] X. Zhao, C.W. Lin, J. Wang, D.H. Oh, Advances in rapid detection methods for foodborne pathogens, *J. Microbiol. Biotechnol.* 24 (2014) 297–312. <https://doi.org/10.4014/jmb.1310.10013>.
- [9] J.B. Ludwig, X. Shi, P.B. Shridhar, E.L. Roberts, C. DebRoy, R.K. Phebus, J. Bai, T.G. Nagaraja, Multiplex PCR Assays for the Detection of One Hundred and Thirty Seven Serogroups of Shiga Toxin-Producing *Escherichia coli* Associated With Cattle, *Front. Cell. Infect. Microbiol.* 10 (2020) 378. <https://doi.org/10.3389/fcimb.2020.00378>.
- [10] S. Díaz-Amaya, L.K. Lin, A.J. Deering, L.A. Stanciu, Aptamer-based SERS biosensor for whole cell analytical detection of *E. coli* O157:H7, *Anal. Chim. Acta.* 1081 (2019) 146–156. <https://doi.org/10.1016/j.aca.2019.07.028>.
- [11] L. Zheng, G. Cai, S. Wang, M. Liao, Y. Li, J. Lin, A microfluidic colorimetric biosensor for rapid detection of *Escherichia coli* O157:H7 using gold nanoparticle aggregation and smart phone imaging, *Biosens. Bioelectron.* 124–125 (2019) 143–149. <https://doi.org/10.1016/j.bios.2018.10.006>.
- [12] J. Min, A.J. Baeumner, Highly sensitive and specific detection of viable *Escherichia coli* in drinking water, *Anal. Biochem.* 303 (2002) 186–193. <https://doi.org/10.1006/abio.2002.5593>.
- [13] A.A. Jackson, T.C. Hinkley, J.N. Talbert, S.R. Nugen, D.A. Sela, Genetic optimization of a bacteriophage-delivered alkaline phosphatase reporter to detect: *Escherichia coli*, *Analyst.* 141 (2016) 5543–5548. <https://doi.org/10.1039/c6an00479b>.
- [14] J. Chen, S.D. Alcaine, A.A. Jackson, V.M. Rotello, S.R. Nugen, Development of Engineered Bacteriophages for *Escherichia coli* Detection and High-Throughput Antibiotic Resistance Determination, *ACS Sensors.* 2 (2017) 484–489. <https://doi.org/10.1021/acssensors.7b00021>.
- [15] K.C. Sasahara, M.J. Gray, S.J. Shin, K.J. Boor, Detection of viable *Mycobacterium avium* subsp. *paratuberculosis* using luciferase reporter systems., *Foodborne Pathog. Dis.* 1 (2004) 258–266. <https://doi.org/10.1089/fpd.2004.1.258>.
- [16] T.C. Hinkley, S. Singh, S. Garing, A.L.M. Le Ny, K.P. Nichols, J.E. Peters, J.N. Talbert, S.R. Nugen, A phage-based assay for the rapid, quantitative, and single CFU visualization of *E. coli* (ECOR #13) in drinking water, *Sci. Rep.* 8 (2018) 14630. <https://doi.org/10.1038/s41598-018-33097-4>.

- [17] R. Derda, M.R. Lockett, S.K.Y. Tang, R.C. Fuller, E.J. Maxwell, B. Breiten, C.A. Cuddemi, A. Ozdogan, G.M. Whitesides, Filter-based assay for *Escherichia coli* in aqueous samples using bacteriophage-based amplification, *Anal. Chem.* 85 (2013) 7213–7220. <https://doi.org/10.1021/ac400961b>.
- [18] B. Guven, N. Basaran-Akgul, E. Temur, U. Tamer, I.H. Boyaci, SERS-based sandwich immunoassay using antibody coated magnetic nanoparticles for *Escherichia coli* enumeration, *Analyst.* 136 (2011) 740–748. <https://doi.org/10.1039/c0an00473a>.
- [19] Y. Kumada, S. Murata, Y. Ishikawa, K. Nakatsuka, M. Kishimoto, Screening of PC and PMMA-binding peptides for site-specific immobilization of proteins, *J. Biotechnol.* 160 (2012) 222–228. <https://doi.org/10.1016/j.jbiotec.2012.02.010>.
- [20] P. Tomme, A. Boraston, B. McLean, J. Kormos, A.L. Creagh, K. Sturch, N.R. Gilkes, C.A. Haynes, R.A.J. Warren, D.G. Kilburn, Characterization and affinity applications of cellulose-binding domains, *J. Chromatogr. B Biomed. Appl.* 715 (1998) 283–296. [https://doi.org/10.1016/S0378-4347\(98\)00053-X](https://doi.org/10.1016/S0378-4347(98)00053-X).
- [21] S. Ko, T.J. Park, H.S. Kim, J.H. Kim, Y.J. Cho, Directed self-assembly of gold binding polypeptide-protein A fusion proteins for development of gold nanoparticle-based SPR immunosensors, *Biosens. Bioelectron.* 24 (2009) 2592–2597. <https://doi.org/10.1016/j.bios.2009.01.030>.
- [22] D. Wang, T. Hinkley, J. Chen, J.N. Talbert, S.R. Nugen, Phage based electrochemical detection of: *Escherichia coli* in drinking water using affinity reporter probes, *Analyst.* 144 (2019) 1345–1352. <https://doi.org/10.1039/c8an01850b>.
- [23] B.H. Muller, C. Lamoure, M.H. Le Du, L. Cattolico, E. Lajeunesse, F. Lemaître, A. Pearson, F. Ducancel, A. Ménez, J.C. Boulain, Improving *Escherichia coli* alkaline phosphatase efficacy by additional mutations inside and outside the catalytic pocket, *ChemBioChem.* 2 (2001) 517–523. [https://doi.org/10.1002/1439-7633\(20010803\)2:7/8<517::aid-cbic517>3.0.co;2-h](https://doi.org/10.1002/1439-7633(20010803)2:7/8<517::aid-cbic517>3.0.co;2-h).
- [24] H.M. Salis, The ribosome binding site calculator, in: *Methods Enzymol.*, Academic Press Inc., 2011: pp. 19–42. <https://doi.org/10.1016/B978-0-12-385120-8.00002-4>.
- [25] A.W. Carpenter, C.F. De Lannoy, M.R. Wiesner, Cellulose nanomaterials in water treatment technologies, *Environ. Sci. Technol.* 49 (2015) 5277–5287. <https://doi.org/10.1021/es506351r>.
- [26] WHO, Results of round I of the WHO international scheme to evaluate household water treatment technologies, World Health Organization, 2016.
- [27] C. Griesche, K. Hoecherl, A.J. Baeumner, Substrate-Independent Laser-Induced Graphene Electrodes for Microfluidic Electroanalytical Systems, *ACS Appl. Nano Mater.* 4 (2021) 3114–3121. <https://doi.org/10.1021/acsnm.1c00299>.
- [28] J. Ettenauer, K. Zuser, K. Kellner, T. Posniecek, M. Brandl, Development of an automated biosensor for rapid detection and quantification of *E. coli* in water, in: *Procedia Eng.*, Elsevier Ltd, 2015: pp. 376–379. <https://doi.org/10.1016/j.proeng.2015.08.643>.
- [29] A. Shabani, C.A. Marquette, R. Mandeville, M.F. Lawrence, Magnetically-assisted impedimetric detection of bacteria using phage-modified carbon microarrays, *Talanta.* 116 (2013) 1047–1053. <https://doi.org/10.1016/j.talanta.2013.07.078>.
- [30] T. Neufeld, A. Schwartz-Mittelmann, D. Biran, E.Z. Ron, J. Rishpon, Combined phage typing and amperometric detection of released enzymatic activity for the specific identification and quantification of bacteria, *Anal. Chem.* 75 (2003) 580–585. <https://doi.org/10.1021/ac026083e>.

- [31] T. Neufeld, A.S. Mittelman, V. Buchner, J. Rishpon, Electrochemical phagemid assay for the specific detection of bacteria using *Escherichia coli* TG-1 and the M13KO7 phagemid in a model system, *Anal. Chem.* 77 (2005) 652–657. <https://doi.org/10.1021/ac0488053>.
- [32] P.R. Sharma, S.K. Sharma, T. Lindström, B.S. Hsiao, Nanocellulose-Enabled Membranes for Water Purification: Perspectives, *Adv. Sustain. Syst.* 4 (2020) 1900114. <https://doi.org/10.1002/adsu.201900114>.
- [33] J.H. Jiang, Sunny C.; Thurmond, Jennifer M.; Pichard, Scott L.; and Paul, Concentration of Microbial Populations from Aquatic Environments by Vortex Flow Filtration, *Mar. Ecol. Prog. Ser.* 80 (1992) 101–107. <https://doi.org/10.3354/meps080101>.
- [34] Y. Zhang, C. Xu, T. Guo, L. Hong, An automated bacterial concentration and recovery system for pre-enrichment required in rapid *Escherichia coli* detection, *Sci. Rep.* 8 (2018) 17808. <https://doi.org/10.1038/s41598-018-35970-8>.
- [35] K.D. Clark, J.A. Purslow, S.A. Pierson, O. Nacham, J.L. Anderson, Rapid preconcentration of viable bacteria using magnetic ionic liquids for PCR amplification and culture-based diagnostics, *Anal. Bioanal. Chem.* 409 (2017) 4983–4991. <https://doi.org/10.1007/s00216-017-0439-y>.
- [36] K. Yang, D.M. Jenkins, W.W. Su, Rapid concentration of bacteria using submicron magnetic anion exchangers for improving PCR-based multiplex pathogen detection, *J. Microbiol. Methods.* 86 (2011) 69–77. <https://doi.org/10.1016/j.mimet.2011.03.018>.
- [37] H.L. Lin, C.C. Lin, Y.J. Lin, H.C. Lin, C.M. Shih, C.R. Chen, R.N. Huang, T.C. Kuo, Revisiting with a relative-density calibration approach the determination of growth rates of microorganisms by use of optical density data from liquid cultures, *Appl. Environ. Microbiol.* 76 (2010) 1683–1685. <https://doi.org/10.1128/AEM.00824-09>.
- [38] Ł. Richter, M. Janczuk-Richter, J. Niedziółka-Jönsson, J. Paczesny, R. Hołyst, Recent advances in bacteriophage-based methods for bacteria detection, *Drug Discov. Today.* 23 (2018) 448–455. <https://doi.org/10.1016/j.drudis.2017.11.007>.
- [39] P. Manohar, N. Ramesh, Improved lyophilization conditions for long-term storage of bacteriophages, *Sci. Rep.* 9 (2019) 15242. <https://doi.org/10.1038/s41598-019-51742-4>.

## 4.6 Supporting Information

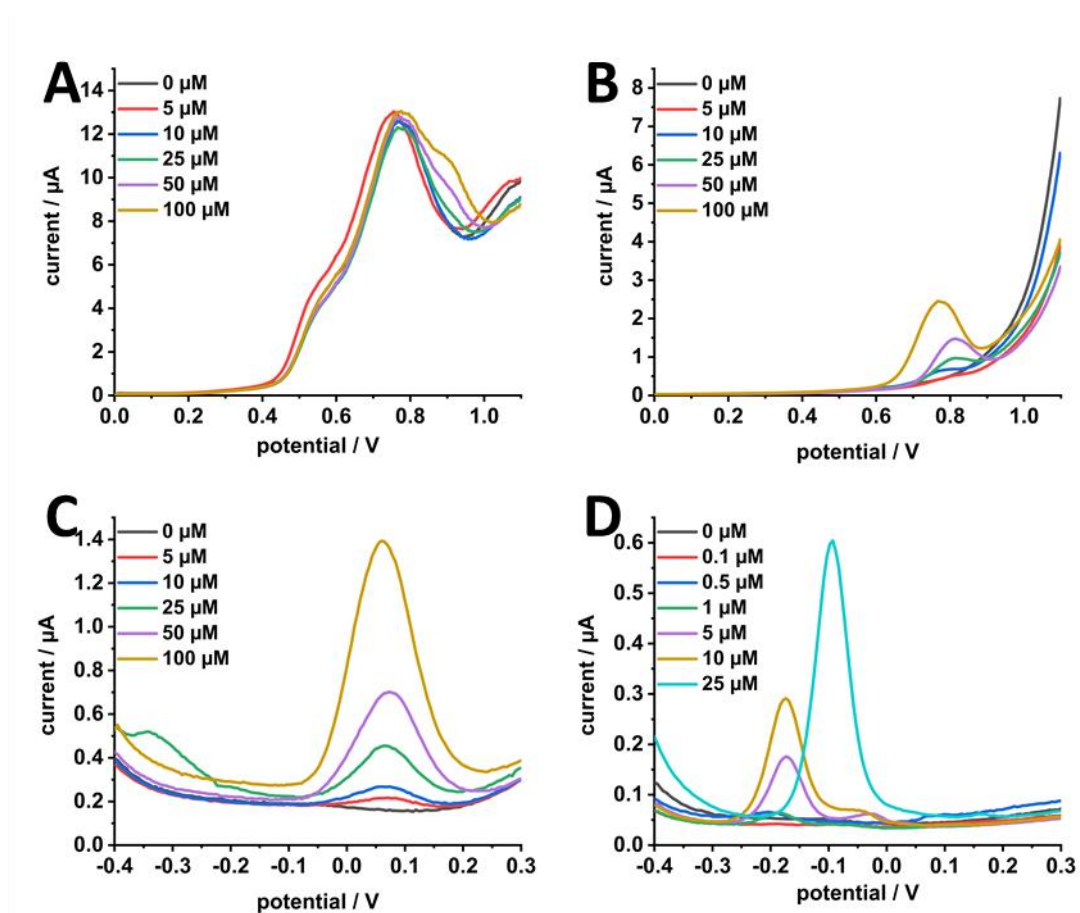


Figure S1: **(A)** Differential-pulse voltammograms for the detection of different concentration of *p*-nitrophenol (0; 5; 10; 25; 50; 100 μmol L<sup>-1</sup>) in LB broth. **(B)** Differential-pulse voltammograms for the detection of different concentration of *p*-nitrophenol (0; 5; 10; 25; 50; 100 μmol L<sup>-1</sup>) in Gly-NaOH (0.05M, pH 10.0). **(C)** Differential-pulse voltammograms for the detection of different concentration of *p*-aminophenol (0; 5; 10; 25; 50; 100 μmol L<sup>-1</sup>) in LB broth. **(D)** Differential-pulse voltammograms for the detection of different concentration of *p*-aminophenol (0; 0.1; 0.5; 1; 5; 10; 25 μmol L<sup>-1</sup>) in Gly-NaOH (0.05M, pH 10.0).



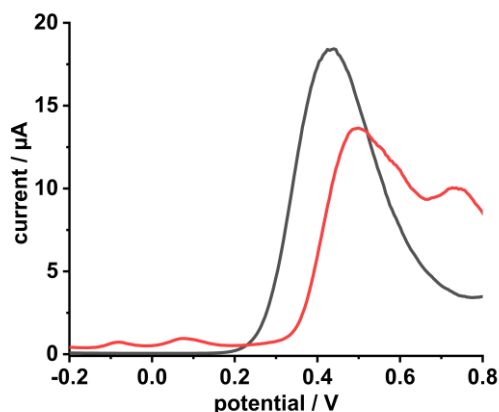


Figure S2: Differential-pulse voltammogram of 5 mmol L<sup>-1</sup> *p*-aminophenyl phosphate in Gly-NaOH (0.05M, pH 10.0) (black) and 5 mmol L<sup>-1</sup> in LB broth after incubation for 15 min at 37 °C, respectively.

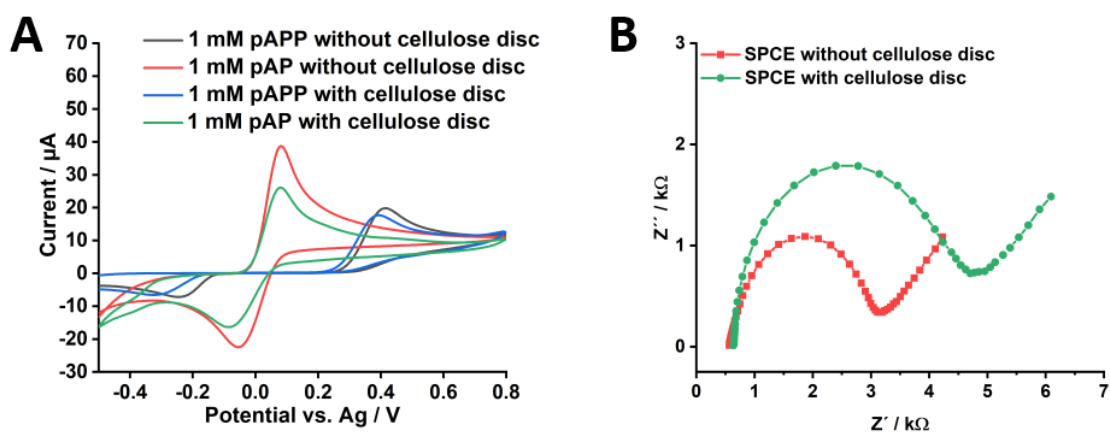


Figure S3: **A** Cyclic voltammetry of 1 mmol L<sup>-1</sup> *p*-aminophenyl phosphate and 1 mmol L<sup>-1</sup> *p*-aminophenol on screen-printed carbon electrodes with or without cellulose disc in 50 mM Gly-NaOH buffer pH 10 (scan rate 50 mV s<sup>-1</sup>). **B** Nyquist plot for electrochemical impedance spectroscopy measurements of 1 mmol L<sup>-1</sup> *p*-aminophenol on screen-printed carbon electrodes with or without cellulose disc in 50 mM Gly-NaOH buffer pH 10.8 (Fixed potential 0.01V, Max. frequency 50000 Hz, Min. frequency 0.1 Hz, n(frequencies) 57 = 9.8 dec.<sup>-1</sup>).

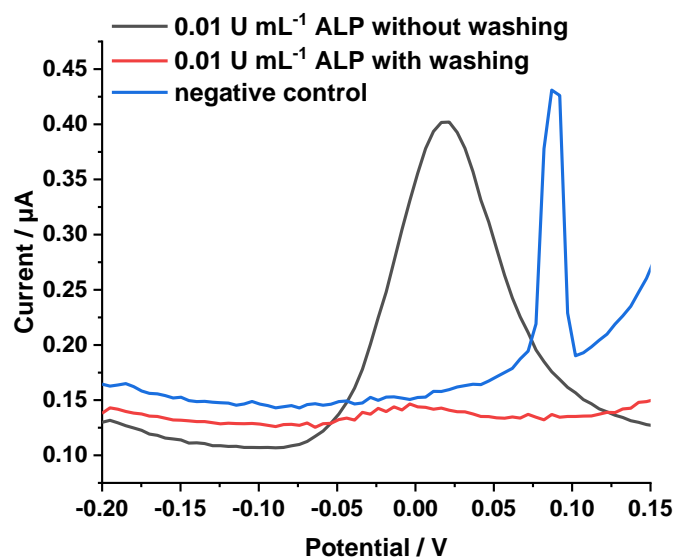


Figure S4: Differential-pulse voltammograms, from -0.2 V to 0.15 V), performing the assay with alkaline phosphatase from bovine intestinal mucosa (purchased from Sigma-Aldrich, Germany) (ALP) without a cellulose-specific carbohydrate-binding module (0.01 U mL<sup>-1</sup>) without washing of the cellulose disc, including washing of the cellulose disc and a negative control not containing alkaline phosphatase. The sharp oxidation peak for the negative control is caused by silver impurities on the SPCE.

Table S1: Results of the assay performance with and without washing, respectively, using alkaline phosphatase without a cellulose-specific carbohydrate-binding module (n =3).

Experiment	Abs. peak height / μA
0.01 U mL <sup>-1</sup> ALP without washing	0.320 ± 0.020
0.01 U mL <sup>-1</sup> ALP with washing	0.017 ± 0.003
Negative control	0.009 ± 0.004

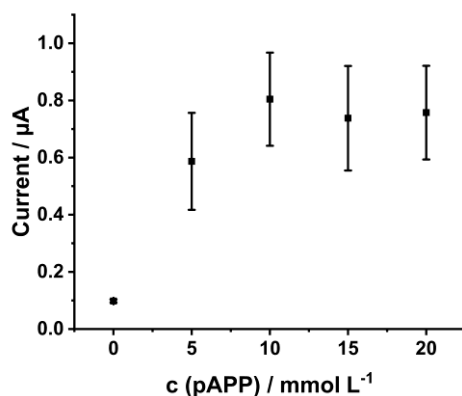


Figure S5: Dependency of the current on varying concentration of the enzymatic substrate *p*-aminophenyl phosphate (0, 5, 10, 15, 20 mmol·L<sup>-1</sup>) detecting 10<sup>5</sup> CFU/mL *E. coli* infected with the genetically engineered bacteriophage. The enzymatic reaction carried out at pH 10, 37 °C for 30 min. (n = 4; error bars represent standard deviations)

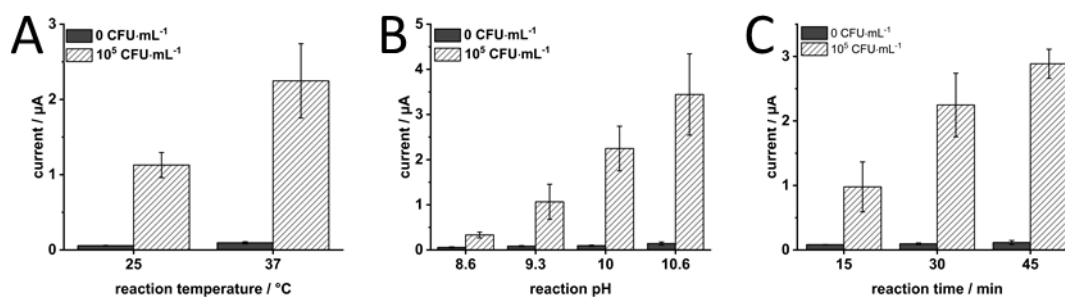


Figure S6: Dependency of the currents for the electrochemical detection of 0 and 10<sup>5</sup> CFU mL<sup>-1</sup> *E. coli*. 20 µL of 10 mM pAPP was used within all measurements. **(A)** Currents for the enzymatic reaction being performed at pH 10.0 with 30 min reaction time under varying reaction temperatures (25 °C; 37 °C). **(B)** Currents for the enzymatic reaction being performed at 37 °C with 30 min reaction time with varying pH (8.6; 9.3; 10.0; 10.6). **(C)** Currents for the enzymatic reaction being performed at 37 °C pH 10.0 with varying reaction times (15 min, 30 min, 45 min). n = 3

## 5 Liposome-based POCT sensors for the detection of beta-hemolytic *Streptococcus pyogenes*

### Abstract

A simple amperometric approach for the detection of *Streptococcus pyogenes* (*S. pyogenes*), exemplary for beta-hemolytic bacteria, was investigated using liposomes of varying sizes. Beta-hemolysis was detected electrochemically using low-cost laser-induced graphene (LIG) electrodes and liposomes encapsulation the electrochemical marker potassium ferrocyanide. Interaction of hemolysins of beta-hemolytic *S. pyogenes* releases the encapsulant. Liposomes with increasing size were found to directly correlate with higher sensitivities for the detection of *S. pyogenes* with a limit of detection of  $10^2$  CFU mL<sup>-1</sup> within 7.25 h. Liposomes were stable against non-hemolytic *Escherichia coli* (*E. coli*) and *S. pyogenes* were successfully detectable in the presence of *E. coli*. The developed sensor has the potential to outperform conventional blood agar plates for more timely results in clinical diagnostics.

---

**This chapter has not been submitted.**

**Author contributions:** Antje J. Baeumner and the author planned the experiments. The author did most of the experimental work. Michael Schaffer helped with electrochemical measurements. The author wrote the first draft of the manuscript. Antje J. Baeumner revised the manuscript.

## **5.1 Introduction**

While nonpathogenic bacteria being beta-hemolytic are rare to find beta-hemolysis is considered of highly predictive indication for the presence of pathogenic bacteria [1]. Hence a test for the detection of beta-hemolysis not only would be limited for clinical samples but could be utilized for the monitoring of food safety [2]. *Listeria monocytogenes*, *Vibrio vulnificus* and *Clostridium botulinum* are beta-hemolytic bacteria and are related with the highest hospitalization and death rates among foodborne pathogens, of 15.9 %, 34.8 % and 17.3 %, respectively. [3] A rapid beta-hemolytic test would allow to exclude those pathogens in addition to other beta-hemolytic foodborne pathogens [2]. Particularly, for multiple of these beta-hemolytic pathogens methods based on genetic or antigenic detection, e.g. antibody-antigen tests [4] or nucleic acid-based tests [5,6], and not relying on their beta-hemolytic properties. While those tests are limited to single analytes a rapid, sensitive assay for the detection of beta-hemolysis would cover multiple beta-hemolytic bacteria.

Streptococci are Gram-positive bacteria which can cause various human diseases [7]. They are characterized based on their ability of erythrocyte lysis using blood agar plates, sub-classifying them into alpha, beta and gamma hemolytic bacteria, causing partial, complete or no lysis of erythrocytes, respectively [7]. The most prominent is *Streptococcus pyogenes*, often referred to as Group A streptococcus (GAS). It causes mild to severe infections of skin, soft tissues, joints and the lower respiratory system. Scarlet fever remains a serious childhood disease and even antibiotic treatment did not decrease in several developed countries [8]. Millions of infections are caused by *S. pyogenes* each year with approximately 1100 to 1600 death per year [9] and substantial costs for health systems [7,10]. With overuse and misuse of antibiotics being identified to highly contribute to the rapid emerging of resistant bacteria it has become crucial to avoid unnecessary antibiotic treatment [11]. Even today, the 1903 invented, blood agar plates are the gold standard for the diagnosis of *S. pyogenes* in throat swab samples. Being not timely enough to supporting antibiotic treatment decisions it is yet inly used to confirm negative rapid antigen detection tests [1]. Hence, highly sensitive and timely analytical tests are required to enable fast and sufficient medical treatments. After their discovery in 1964 by Bangham *et al.* liposomes have been proven to have several practical uses, including their ability to serve as erythrocyte surrogates [13,14].

Almost all clinical isolates of *S. pyogenes* produce the potent cytolytic products Streptolysin O and Streptolysin S [15]. Interactions of those hemolysins with liposomes and their ability to not only lyse erythrocytes but also synthetic liposomes were already investigated in the 1970s and 1980s [16–18]. Hence the principle of using liposomes as erythrocyte surrogates for the quantitative and

qualitative detection of  $\beta$ -hemolysis was applied for liposomes in a proof-of-concept for pore-forming bacterial toxins [19] as well as for the direct detection of  $\beta$ -hemolytic bacteria using liposomes encapsulating electrochemical active species or fluorescent dyes, respectively [1,20].

If outperforming blood agar plates in speed this assay principle is applicable to multiple fields, e. g. food safety or diagnostics, for the rapid screening of samples for possible pathogenic bacteria. We demonstrate a simple electrochemical approach based on liposomes, encapsulating electroactive potassium ferrocyanide, and laser-induced graphene electrodes (LIG). The detection principle relies on the lysis of liposomes by beta-hemolytic *S. pyogenes* and the following electrochemical detection of released electroactive encapsulant.

## **5.2 Material and Methods**

### **5.2.1 Materials and Bacterial Strains**

1,2-dipalmitoyl-sn-glycero-3-phosphocholine (DPPC), 1,2-dipalmitoyl-sn-glycero-3-phospho-(1'-rac-glycerol) sodium salt (DPPG), as well as the liposome extrusion kit, were purchased from Avanti Polar Lipids, Inc. (United States). 2-[4-(2-hydroxyethyl)-1-piperazinyl]ethanesulfonic acid (HEPES), chloroform and sucrose were bought from VWR (Germany). Brain-Heart infusion broth (BHI), Cholesterol, methanol, sodium azide, 1 mol L<sup>-1</sup>sodium hydroxide solution, potassium ferrocyanide trihydrate, Sephadex G-50 medium and Whatman nuclepore track-etched polycarbonate membranes (1.0; 0.4; 0.2 and 0.1  $\mu\text{m}$  pore size) were obtained from Sigma-Aldrich (Germany). Sodium chloride was purchased from Roth Chemie GmbH (Germany). The dialysis tubes, Spectra/Por 4 regenerated cellulose dialysis tubing (MWCO 12 kDa), were bought from Spectrum Chemical Manufacturing Corp. (United States). Nitric acid was purchased from Fisher Scientific GmbH (Germany) and the phosphorus standard solution ( $\rho(\text{P}) = 1.000 \text{ g L}^{-1}$ ) was obtained from Bernd Kraft GmbH (Germany). Kapton HN polyimide film was purchased from cmc Klebetechnik (Germany), Busch 5900 silver conductive paint was purchased from Conrad Electronic SE (Germany). The bacterial strains *Streptococcus Pyogenes* (ATCC 12344) and *Escherichia Coli* K12 (ATCC 23716), were purchased from the DSMZ (German Collection of Microorganisms and Cell Cultures GmbH, Germany).

Single colonies of bacterial strains were inoculated into 5 mL of sterile BHI and incubated overnight at 37 °C. Overnight cultures were 1:100 diluted into 10 mL of fresh BHI and allowed to grow to an OD<sub>600</sub> of 0.8 – 1.0 at 37 °C and gently shaking (180 rpm). These bacterial cultures were freshly diluted in BHI before measurements. The number of bacteria was determined with plate counting.

### **5.2.2 Liposome preparation**

Liposomes were prepared using a slightly modified reverse-phase evaporation protocol by Edwards *et al.* DPPC (30.0 mg, 40.9  $\mu\text{mol}$ ), DPPG (15.0 mg, 20.1  $\mu\text{mol}$ ) and cholesterol (20.1 mg, 52.0  $\mu\text{mol}$ ) are dissolved in a mixture of chloroform (3 mL) and methanol (0.5 mL) at 42 °C and sonicated for 1 min in a sonication bath. A 42 °C solution (2 mL of 200 mM  $\text{K}_4[\text{Fe}(\text{CN})_6]$  in 0.1 M HEPES) was added and sonicated for additional 4 min. The organic solvents were removed at 42 °C and 400 mbar using a rotary evaporator for 30 min. After a second addition of 2 mL 42 °C 200 mM  $\text{K}_4[\text{Fe}(\text{CN})_6]$  in 0.1 M HEPES the mixture was vortexed for 5 min before additional removal of remaining organic solvents using the rotary evaporator at 42 °C (20 min at 380 mbar followed by 20 min at 280 mbar). The crude liposome dispersion is in the following extruded at 45 °C through 1.0  $\mu\text{m}$  membranes for 21 times. To synthesize liposomes of different size the dispersion is partly extruded to smaller membranes for 21 times with decreasing pore size (0.4; 0.2; 0.1  $\mu\text{m}$ ). The liposomes were purified with size-exclusion chromatography with Sephadex G-50 8medium) in a 60 x 20 mm column using HEPES-saline sucrose buffer (HSS; 10 mmol  $\text{L}^{-1}$  HEPES, 200 mmol  $\text{L}^{-1}$  NaCl, 200 mmol  $\text{L}^{-1}$  sucrose, 1.5 mmol  $\text{L}^{-1}$   $\text{NaN}_3$  at pH 7.5). Liposomes were dialyzed overnight against HSS and stored at 4 °C.

### **5.2.3 Preparation of laser-induced graphene electrodes**

Laser-induced graphene was generated of Kapton HN polyimide film (thickness 125  $\mu\text{m}$ ) using a VLS 2.30 laser cutting platform (Universal Laser Systems, USA) with a wavelength of 10.6  $\mu\text{m}$ . LIG working and counter electrode were scribed under ambient conditions with a 2 inch lens. The polyimide foil was placed in focus of the laser beam and LIG was scribed in raster mode with laser power of 1 % corresponding to 0.3 W, speed of 10 % corresponding to 12.7  $\text{cm s}^{-1}$  and image density 7 under ambient conditions. LIG was used as working electrode and counter electrode. The quasi silver reference electrode was painted with silver conductive paint. Nail polish was used to passivate electrode leads and electrode contacts were protected with conductive adhesive copper tape. (Figure S1).

### **5.2.4 Electrochemical measurements**

Electrochemical measurements were performed using a potentiostat (PalmSens4, Palmsens BV, Houten, The Netherlands). Data evaluation was performed with PStTrace 5.7 software (Palmsens BV, Houten, The Netherlands). Electrodes were connected to the potentiostat via a Palmsens SPE Connector (2 mm banana). Dilutions of the bacterial cultures were grown in BHI for varying times (0; 3; 7 h) at 37 °C under shaking (150 rpm) using an Eppendorf thermostat. Liposomes were diluted in HSS to a total lipid concentration of 2.5 mmol  $\text{L}^{-1}$ . 20  $\mu\text{L}$  of the bacteria sample were mixed with 5  $\mu\text{L}$  of the liposome solution (2.5 mmol  $\text{L}^{-1}$  total phospholipids) to yield a total lipid concentration

of 0.5 mmol L<sup>-1</sup> in the final assay and incubated for 10 min before amperometric detection of released potassium ferrocyanide by applying a potential of 340 mV for 60 s. For data evaluation the measured current of a negative control, containing 80 % BHI and 0.5 mmol L<sup>-1</sup>, was subtracted from the measured current after 60 s. For the heat-inactivated samples *S. pyogenes* was grown in BHI for 7 h before heat inactivation at 95 °C for 30 min.

### 5.3 Results and Discussion

Liposomes are spherical particles consisting of a lipid bilayer being formed by hydrophobic tails of the lipids forming the bilayer, whereby phospholipids are usually the main component. [21] The addition of cholesterol to liposomes, consisting of phospholipids, reduces the permeability of the membrane. [22] Duncan *et al.* reported on the crucial role of cholesterol for the interaction of Streptolysin O with rabbit erythrocytes as well as liposomes in 1975 [16]. More detailed studies by Rosenquist *et al.* suggest 50 mol% cholesterol to be optimal for Streptolysin O-induced lysis of egg lecithin/cholesterol liposomes [17] while Duncan *et al.* demonstrated a more complex relationship between lipids and cholesterol content with respect to Streptolysin S-induced lysis. Liposomes containing phospholipids with unsaturated fatty acids were found to get lysed irrespective of the cholesterol content. In contrast liposomes containing C16 : 0 and C18 : 0 phosphatidylcholine were stealth without cholesterol yet significantly lysed with 40 mol% cholesterol included in the liposomal membrane [18]. Due to our own experience with these phospholipids and cholesterol content with a variety of encapsulants, beside potassium ferro/ferricyanide also sulforhodamine B, NaCl or *m*-carboxy luminol [23][24–26], the hence possibility to design liposome-based bioassays and the outstanding long term stability of these liposomes of over years at 4 °C and at least 1 year at room temperature [25], such composition was chosen for the studies with hemolytic bacteria.

Liposomes of different sizes were synthesized using the reverse phase evaporation method combined with extrusion through membranes of different pore size since unilamellar liposomes produced by reverse-phase evaporation are reported to be extremely sensitive models for membrane-damaging effects of cytolytic toxins [18]. The hydrodynamic diameter of the synthesized liposomes shows an excellent correlation with pore size of the applied extrusion membranes for pore sizes of 1.0 µm and 0.4 µm. While for the additional extrusion through 0.1 µm pore size membranes did not reduce the liposome size below the pore size (Figure 1). The influence of liposome size and the time dependency towards lysis in the presence of *S. pyogenes* is investigated with liposomes of different sizes (180 nm, 340 nm and 700 nm) (Figure 1). For all liposomes a fast



lysis by *S. pyogenes* is observed reaching the maximum electrochemical response after 10 – 20 min (Figure 2).

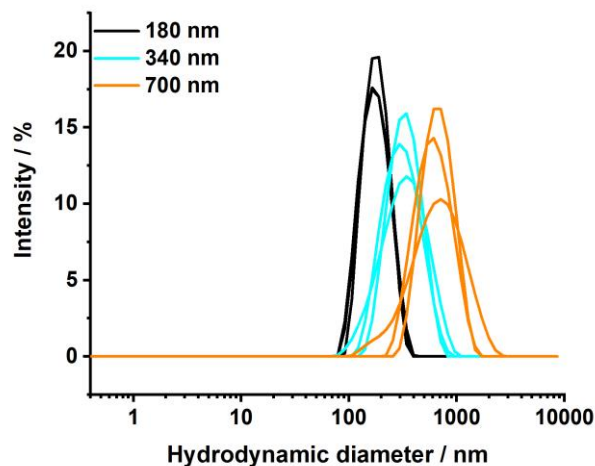


Figure 1: Hydrodynamic diameters of liposomes synthesized using membranes with different pore sizes during extrusion. 180 nm liposomes (black) extruded through membranes of 1.0  $\mu\text{m}$ , 0.4  $\mu\text{m}$ , 0.2  $\mu\text{m}$  and 0.1  $\mu\text{m}$  pore size. 340 nm liposomes (blue) extruded through membranes of 1.0  $\mu\text{m}$  and 0.4  $\mu\text{m}$  pore size. 700 nm liposomes (orange) extruded through membranes of 1.0  $\mu\text{m}$  pore size.

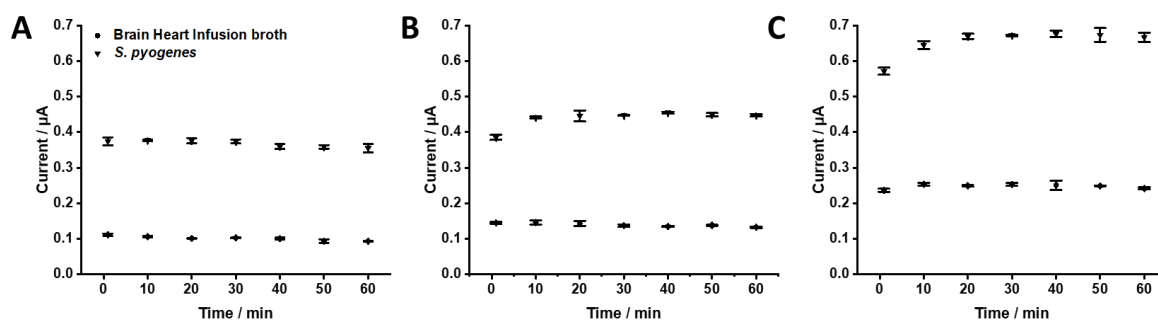


Figure 2: Time-dependent electrochemical measurements of differently-sized liposomes ( $500 \mu\text{mol L}^{-1}$  total lipid) with  $10^8 \text{ CFU mL}^{-1}$  *S. pyogenes*. Liposome hydrodynamic diameters 180 nm (A), 340 nm (B) and 700 nm (C).  $n = 3$

Higher electrochemical signals in the presence as well as in the absence of *S. pyogenes* are measured with increasing liposome size. While a higher volume-to-surface ratio for liposomes with larger hydrodynamic diameters a higher amount of encapsulated ferrocyanide enables a higher electrochemical signal with complete liposome lysis (Table S1) (1.6 : 1.4 : 1 for

700 nm : 340 nm : 180 nm liposomes). Hence a similar behavior in BHI as well as in the presence of *S. pyogenes* should be represented by this ratio if liposomes show the same lysis independently of their size. For 340 nm liposomes compared with 180 nm liposomes the encapsulant ratio of 1.4 : 1 is maintained in BHI (1.4 : 1) as well as in  $10^8$  CFU mL<sup>-1</sup> *S. pyogenes* (1.3 : 1). Contrary results are obtained for the larger 700 nm liposomes. Compared to 180 nm liposomes the determined encapsulant ratio of 1.6 : 1 increased in BHI (2.6 : 1) as well as in  $10^8$  CFU mL<sup>-1</sup> *S. pyogenes* (1.9 : 1) and hence clearly indicate a reduced stability in the BHI overlaying possible effects of beta-hemolysis.

The different-sized liposomes were tested for the detection of *S. pyogenes* (Figure 3). Interestingly, without cultivation of *S. pyogenes* the direct detection only was achieved with the larger liposomes (340 nm and 700 nm) for concentration above  $10^6$  CFU mL<sup>-1</sup> *S. pyogenes*. To enable a more sensitive detection of *S. pyogenes* samples are pre-cultivated at 37 °C before detection for 3 h or 7 h, respectively. While a pre-incubation of 3 h only slightly improves the assay's sensitivity with 7 h of pre-incubation *S. pyogenes* was detected at concentrations of  $10^3$  CFU mL<sup>-1</sup> (180 nm liposomes) or at slightly more sensitive with larger liposomes, 340 nm and 700 nm, with a limit-of-detection (LOD) of  $10^2$  CFU mL<sup>-1</sup> matching the infectious dose of  $10^3$  CFU [1]. Relatively high standard deviations hereby are causing relatively high LODs in the electrochemical detection, especially for the smaller liposomes, and hence play a crucial role for further developments.

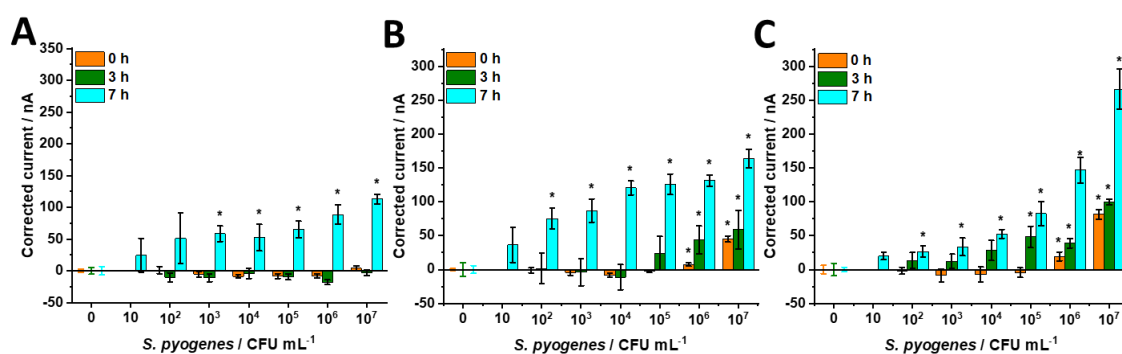


Figure 3: Electrochemical detection of *S. pyogenes* with different pre-cultivation times (0 h orange; 3 h green and 7 h blue) using liposomes of different size. Liposome hydrodynamic diameters 180 nm (A), 340 nm (B) and 700 nm (C). \* marked concentration of *S. pyogenes* are significantly different from the negative control BHI ( $P < 0.05$ ).  $n = 3$

To verify the detection of the beta-hemolytic activity of *S. pyogenes* non-hemolytic *E. coli* and heat-inactivated *S. pyogenes* were tested using the most sensitive approach identified, i.e. after 7 h pre-

cultivation (Figure 4A and 4B) using 700 nm liposomes. In both cases a current lower than that of the negative control, containing only BHI and liposomes, was determined. The same effect had been already observed earlier (Figure 3) and is assumed to be caused by metabolic products or bacterial cells settling on the electrode surfaces and blocking electron transfer and hence no additional lysis of the liposomes took place. This effect reduces the assay sensitivity as it disturbs the electrochemical reaction of the released liposome encapsulant and should be taken into consideration in real-world samples, which will involve coexistence of bacterial populations. Thus, the detection of *S. pyogenes* in the presence of  $10^4$  CFU mL<sup>-1</sup> *E. coli* was found to decrease the sensitivity of the assay by an order of magnitude to  $10^3$  CFU mL<sup>-1</sup> *S. pyogenes* (Figure 4C).

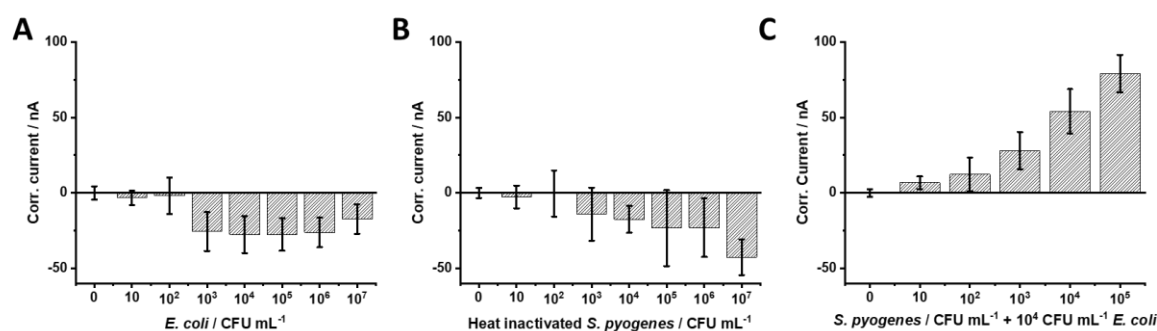


Figure 4: Electrochemical detection of (A) *E. coli*, (B) heat-inactivated *S. pyogenes* and (C) *S. pyogenes* in mixture with  $10^4$  CFU mL<sup>-1</sup> *E. coli* with 7 h pre-cultivation time using 700 nm liposomes. n = 3

With a total analysis time of 7.25 h and a LOD of  $10^2$  CFU mL<sup>-1</sup> this end-point assay is a promising approach for the detection of beta-hemolytic bacteria in a portable sensor format. While the LOD A time-resolved sensing concept for the detection of beta-hemolytic bacteria using liposomes encapsulating a fluorescence dye was published by Sum *et al.* [1]. With a higher LOD of  $10^4$  CFU mL<sup>-1</sup> they were able to detect *S. pyogenes* within 50 min and showed the selective lysis of the utilized liposomes by multiple beta-hemolytic bacteria.

## 5.4 Conclusion

The electrochemical detection of *S. pyogenes* utilizing its beta-hemolytic properties was achieved in a simple assay format utilizing lysis of liposomes in the presence of beta-hemolytic bacteria by

direct measurement in the bacteria media. The concept of using liposomes for the replacement of blood erythrocytes for the detection of beta-hemolysis is not new and the principle was applied for optical and electrochemical detection [1,20,27,28]. While earlier investigations on the interaction between liposomes and beta-hemolytic bacteria mainly focus on the lipid composition of the lipid vesicles [28] this work investigated the influence of differently sized liposomes. Whereas *S. pyogenes* was detected with slightly higher sensitivities utilizing larger liposomes. Since it was proven that the hereby used liposomes are stable against non-hemolytic *E. coli* a wider study needs to verify the assay principle by on the one hand the stability of the utilized liposomes against various non-hemolytic and alpha-hemolytic bacteria. On the other hand, the assays' suitability for numerous other beta-hemolytic bacteria needs to be verified. *Sum et al.* reported on beta-hemolysis selective liposomes with highly varying detection times for severe bacteria being caused by differently expressed hemolysins and microbial grow rates [1]. The hereby presented sensor enables the design of a portable detection system and easy execution protocols to identify the presence of beta-hemolytic pathogens. Similar to methods applied in lateral flow assays, the dehydration of liposomes on top of the electrode followed by rehydration during the addition of the bacterial sample could further simplify the sensor [29].

The interest of detecting beta-hemolysis exists in clinical diagnostics where faster detection of beta-hemolysis could replace the established blood agar plate and not only reduce costs in diagnostics but with more timely results as well avoid antibiotic overuse being a key driver for antimicrobial resistance [30]. With low costs and easy instrumentalization, the hereby presented sensor principle offers new possibilities for the future detection of pathogenic beta-hemolytic microorganisms not being limited to POCT but also for other relevant fields like food safety.

## 5.5 References

- [1] R. Sum, M. Swaminathan, S.K. Rastogi, O. Piloto, I. Cheong, Beta-Hemolytic Bacteria Selectively Trigger Liposome Lysis, Enabling Rapid and Accurate Pathogen Detection, *ACS Sensors*. 2 (2017) 1441–1451. <https://doi.org/10.1021/acssensors.7b00333>.
- [2] C. Hernández-Cortez, Food Poisoning Caused by Bacteria (Food Toxins), in: I. Palma-Martínez (Ed.), *IntechOpen, Rijeka*, 2017: p. Ch. 3. <https://doi.org/10.5772/intechopen.69953>.
- [3] E. Scallan, R.M. Hoekstra, F.J. Angulo, R. V. Tauxe, M.A. Widdowson, S.L. Roy, J.L. Jones, P.M. Griffin, Foodborne illness acquired in the United States-Major pathogens, *Emerg. Infect. Dis.* 17 (2011) 7–15. <https://doi.org/10.3201/eid1701.P11101>.
- [4] D. Schiff, H. Aviv, E. Rosenbaum, Y.R. Tischler, Spectroscopic Method for Fast and Accurate Group A Streptococcus Bacteria Detection, *Anal. Chem.* 88 (2016) 2164–2169. <https://doi.org/10.1021/acs.analchem.5b03754>.
- [5] C. Yi, K.S. J., Multiplex PCR for Simultaneous Detection of Bacteria of the Genus *Listeria*, *Listeria monocytogenes*, and Major Serotypes and Epidemic Clones of *L. monocytogenes*, *Appl. Environ. Microbiol.* 73 (2007) 6299–6304. <https://doi.org/10.1128/AEM.00961-07>.
- [6] B. Suo, Y. He, G. Paoli, A. Gehring, S.-I. Tu, X. Shi, Development of an oligonucleotide-based microarray to detect multiple foodborne pathogens, *Mol. Cell. Probes.* 24 (2010) 77–86. <https://doi.org/https://doi.org/10.1016/j.mcp.2009.10.005>.
- [7] T. Parks, L. Barrett, N. Jones, Invasive streptococcal disease: a review for clinicians, *Br. Med. Bull.* 115 (2015) 77–89. <https://doi.org/10.1093/bmb/ldv027>.
- [8] S.O. Brockmann, L. Eichner, M. Eichner, Constantly high incidence of scarlet fever in Germany, *Lancet Infect. Dis.* 18 (2018) 499–500. [https://doi.org/10.1016/S1473-3099\(18\)30210-X](https://doi.org/10.1016/S1473-3099(18)30210-X).
- [9] D.L. Stevens, A.E. Bryant, Severe Group A Streptococcal Infections, University of Oklahoma Health Sciences Center, 2016. <http://www.ncbi.nlm.nih.gov/pubmed/26866227> (accessed February 22, 2021).
- [10] G.J. Hughes, A.J. Van Hoek, S. Sriskandan, T.L. Lamagni, The cost of hospital care for management of invasive group A streptococcal infections in England, *Epidemiol. Infect.* 143 (2015) 1719–1730. <https://doi.org/10.1017/S0950268814002489>.
- [11] C.L. Ventola, The antibiotic resistance crisis: part 1: causes and threats, *P T.* 40 (2015) 277–283. <https://pubmed.ncbi.nlm.nih.gov/25859123>.
- [12] P. und K. Bundesministerium für Soziales, Gesundheit, Streptokokken-Schnelltest | Gesundheitsportal, (n.d.). <https://www.gesundheit.gv.at/labor/laborwerte/infektionen-bakterien/labor-streptokokken-a-antigen-rachenabstrich-straa1> (accessed February 12, 2021).
- [13] A.D. Bangham, R.W. Horne, Negative staining of phospholipids and their structural modification by surface-active agents as observed in the electron microscope, *J. Mol. Biol.* 8 (1964) 660–668. [https://doi.org/10.1016/S0022-2836\(64\)80115-7](https://doi.org/10.1016/S0022-2836(64)80115-7).
- [14] A.D. Bangham, Liposomes: Realizing Their Promise, *Hosp. Pract.* 27 (1992) 51–62. <https://doi.org/10.1080/21548331.1992.11705537>.
- [15] M.C. Fontaine, J.J. Lee, M.A. Kehoe, Combined contributions of streptolysin O and streptolysin S to virulence of serotype M5 *Streptococcus pyogenes* strain Manfredo, *Infect. Immun.* 71 (2003) 3857–3865. <https://doi.org/10.1128/IAI.71.7.3857-3865.2003>.

- [16] J.L. Duncan, R. Schlegel, Effect of streptolysin o on erythrocyte membranes, liposomes, and lipid dispersions: A protein-cholesterol interaction, *J. Cell Biol.* 67 (1975) 160–173. <https://doi.org/10.1083/jcb.67.1.160>.
- [17] E. Rosenqvist, T.E. Michaelsen, A.I. Vistnes, Effect of streptolysin O and digitonin on egg lecithin/cholesterol vesicles, *Biochim. Biophys. Acta - Biomembr.* 600 (1980) 91–102. [https://doi.org/10.1016/0005-2736\(80\)90414-9](https://doi.org/10.1016/0005-2736(80)90414-9).
- [18] J.L. Duncan, L. Buckingham, Effect of streptolysin S on liposomes Influence of membrane lipid composition on toxin action, *BBA - Biomembr.* 648 (1981) 6–12. [https://doi.org/10.1016/0005-2736\(81\)90119-X](https://doi.org/10.1016/0005-2736(81)90119-X).
- [19] D. Xu, Q. Cheng, Surface-Bound Lipid Vesicles Encapsulating Redox Species for Amperometric Biosensing of Pore-Forming Bacterial Toxins, *J. Am. Chem. Soc.* 124 (2002) 14314–14315. <https://doi.org/10.1021/ja027897f>.
- [20] H.J. Kim, H.P. Bennetto, M.A. Halablab, C. Choi, S. Yoon, Performance of an electrochemical sensor with different types of liposomal mediators for the detection of hemolytic bacteria, *Sensors Actuators, B Chem.* 119 (2006) 143–149. <https://doi.org/10.1016/j.snb.2005.12.013>.
- [21] Q. Liu, B.J. Boyd, Liposomes in biosensors, *Analyst.* 138 (2013) 391–409. <https://doi.org/10.1039/C2AN36140J>.
- [22] R. Bittman, L. Blau, Phospholipid-cholesterol interaction. Kinetics of water permeability in liposomes, *Biochemistry.* 11 (1972) 4831–4839. <https://doi.org/10.1021/bi00775a029>.
- [23] V.N. Goral, N. V. Zaytseva, A.J. Baeumner, Electrochemical microfluidic biosensor for the detection of nucleic acid sequences, *Lab Chip.* 6 (2006) 414–421. <https://doi.org/10.1039/b513239h>.
- [24] K.A. Edwards, A.J. Baeumner, Optimization of DNA-tagged dye-encapsulating liposomes for lateral-flow assays based on sandwich hybridization, *Anal. Bioanal. Chem.* 386 (2006) 1335–1343. <https://doi.org/10.1007/s00216-006-0705-x>.
- [25] C. Fenzl, T. Hirsch, A.J. Baeumner, Liposomes with High Refractive Index Encapsulants as Tunable Signal Amplification Tools in Surface Plasmon Resonance Spectroscopy, *Anal. Chem.* 87 (2015) 11157–11163. <https://doi.org/10.1021/acs.analchem.5b03405>.
- [26] M. Mayer, S. Takegami, M. Neumeier, S. Rink, A. Jacobi von Wangelin, S. Schulte, M. Vollmer, A.G. Griesbeck, A. Duerkop, A.J. Baeumner, Electrochemiluminescence Bioassays with a Water-Soluble Luminol Derivative Can Outperform Fluorescence Assays, *Angew. Chemie Int. Ed.* 57 (2018) 408–411. <https://doi.org/10.1002/anie.201708630>.
- [27] H.J. Kim, H.P. Bennetto, M.A. Halablab, A novel liposome-based electrochemical biosensor for the detection of haemolytic microorganisms, *Biotechnol. Tech.* 9 (1995) 389–394. <https://doi.org/10.1007/BF00160823>.
- [28] N.T. Thet, S.H. Hong, S. Marshall, M. Laabei, A. Toby, A. Jenkins, Visible, colorimetric dissemination between pathogenic strains of *Staphylococcus aureus* and *Pseudomonas aeruginosa* using fluorescent dye containing lipid vesicles, *Biosens. Bioelectron.* 41 (2013) 538–543. <https://doi.org/10.1016/j.bios.2012.09.019>.
- [29] D. Martorell, S.T.A. Siebert, R.A. Durst, Liposome dehydration on nitrocellulose and its application in a biotin immunoassay, *Anal. Biochem.* 271 (1999) 177–185. <https://doi.org/10.1006/abio.1999.4134>.
- [30] L.J. Shallcross, Editorials: Antibiotic overuse: A key driver of antimicrobial resistance, *Br. J. Gen. Pract.* 64 (2014) 604–605. <https://doi.org/10.3399/bjgp14X682561>.

## 5.6 Supporting Information

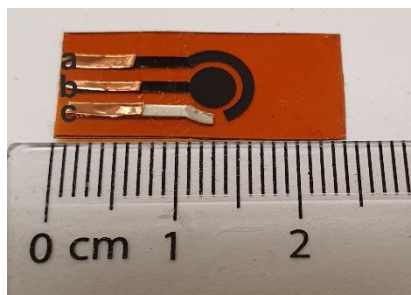


Figure S1: Three electrode system for the electrochemical detection of beta-hemolytic *S. pyogenes*, (a) Laser-induced graphene (LIG) counter electrode, (b) LIG working electrode (c) Ag quasi-reference electrode.

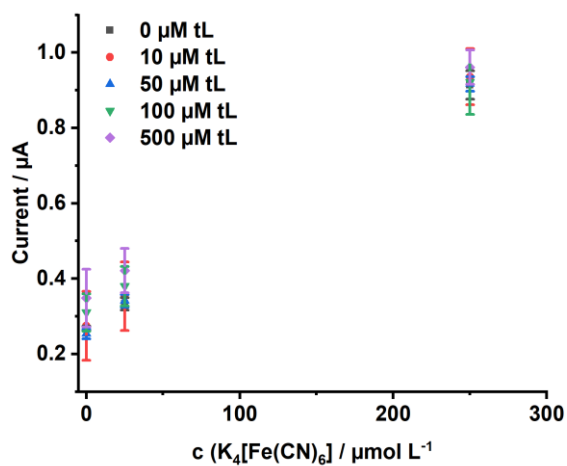


Figure S2: Electrochemical detection of  $\text{K}_4[\text{Fe}(\text{CN})_6]$  (0, 25 and 250  $\mu\text{mol L}^{-1}$ ) in the presence of liposomes (hydrodynamic diameter  $700 \pm 290$  nm) in different concentrations (0; 10; 50; 100 and 500  $\mu\text{mol L}^{-1}$  total lipids (tL)).  $n = 3$

### 6 Conclusions and Future Perspective

This thesis discusses advantageous electrochemical bioassay formats that provide analytical answers for the detection of bacteria with relevance in the fields of food safety and medical diagnostics. Furthermore, in combination with the findings on novel electrochemical microfluidic sensing systems a basis for the future development of powerful sensor technologies for the detection of microbial contamination for food safety and point-of-care-testing (POCT) is provided.

Although the convergence in the fields of biosensors, microfluidics, and electrochemistry has led to outstanding developments the latest electrochemical biosensor developments are neglecting novel concepts and mostly focus on small improvements, e.g. simple electrode modification with a large variety of nanomaterials, to reach higher sensitivities [1,2]. In the last two decades, biosensors using carbon-based electrodes with an emphasis on carbon nanotubes and graphene have received a lot of attention [3–5]. As stand-alone electrodes laser-induced graphene (LIG) is particularly interesting due to its ease-of-fabrication [6] combined with excellent electrochemical properties including small peak potential differences, high electrode transfer rates, and a good peak-current response [7]. The pressure-driven transfer of LIG to thermoplastic substrates was proven to electrochemically outperform established transfer strategies and makes high quality LIG electrode production independent from the substrate material. Consequently, this strategy dramatically expands the applicability for LIG also for electrochemical microfluidics systems as transferred LIG (tLIG) is independent of chemical and thermal properties of the polyimide substrate. A detailed characterization of the tLIG revealed differences mainly only in the surface morphology in comparison to LIG due to the non-homogeneous nature of LIG itself, i.e. with a less porous bottom of LIG, the turn-over of the electrode material due to the transfer process, reduces the electrochemically active surface area of LIG. In electrochemical applications, the sensitivity of tLIG was found to be reduced for cyclic voltammetry and square wave voltammetry, while for amperometric measurements the two materials performed equally, both off-chip and on-chip for p-aminophenol detection. Since the surface morphology of LIG is strongly dependent on the energy density of the CO<sub>2</sub>-laser during fabrication further investigations and improvements of tLIG are envisioned through optimization of the original LIG fabrication [8]. For example, with increasing scribing speed and higher laser power a fiber-like LIG structure with lower density and stiffness is obtained often correlating with higher sheet resistance [9]. The transfer process of those LIG compounds may be highly beneficial by slightly compressing the structures, hence decreasing the sheet resistance while maintaining an overall superior surface area through high porosity.



Since the transfer process adds an additional fabrication step, its commercial applications may be limited, as long as polyimide can be tolerated as substrate material. In this case, the direct use of LIG for the fabrication of microfluidic chips would be of primary interest. In addition to the substrate-independent use of double-sided adhesive tape, substantial advances for the direct bonding of polyimide with PMMA were gained with a UV/ozone assisted solvent bonding protocol. Further improvements in the bonding might be obtained by combining the developed solvent bonding with silane coupling agents, as various silane agent couplings have already been successfully applied for the bonding of polyimide to PDMS [10,11] and also to enhance the bonding of PMMA to e.g. alumina or titanium [12,13].

Electrochemical detection strategies for the bacteria *Escherichia coli* and *Streptococcus pyogenes*, as a representative of  $\beta$ -hemolytic bacteria, using bacteriophages (phages) and liposomes as biorecognition elements were developed. The detection of the bacterial species is of interest to the field of food safety or medical diagnostics, respectively. The developed bioassay strategies were designed aiming for simple, user-friendly, low-cost but highly sensitive detection strategies based on carbon electrodes.

While the use of genetically modified reporter phages, with introduced genes, for the detection of bacteria already has been described in the late 80s by Ulitzur and Kuhn [14], the number of publications on bioassay and biosensors using bacteriophages just has increased in the last years. The use of reporter phage systems has emerged as a promising strategy besides the direct detection using bacteriophages as biorecognition elements in impedance sensors [15,16]. Here, for the detection of *E. coli*, an indicator for fecal contamination in drinking and environmental water, the developed electrochemical bioassay uses genetically engineered reporter T7 phages. After infection, viable *E. coli* cells overexpress an optimized alkaline phosphatase, fused to a cellulose-specific carbohydrate-binding module. This affinity tag enables the enrichment of produced alkaline phosphatase by simple filtration through cellulose and hence overcomes limitations of the direct detection in the sample solution, e.g. low enzyme concentrations or matrix interferences. After the addition of the enzymatic substrate *p*-aminophenyl phosphate, the amount of captured enzyme, directly correlating with the number of viable *E. coli*, was successfully detected electrochemically simply by placing the cellulose filter disc on a screen-printed electrode. With this proof-of-principle further optimization for eventual application in the field relate to both the assay set-up and also pretreatment strategies. The enrichment of the bacteria before the phage infection would be a simple approach to enhance the assay performance. Pre-enrichment methods for bacteria include centrifugation, immunomagnetic separation, bacterial concentration, and cultivation [17]. Considering the often-required detection limit, for drinking water, 1 bacteria / 100 mL, cultivation

is the most suited enrichment strategy. Furthermore, within the proposed assay the filtration of the lysate is a crucial step in determining the assay's sensitivity directly by the amount of immobilized enzyme. Improvements during filtration may include the filtration of larger sample volumes and/or the more efficient enrichment due to a higher surface area. While the electrode size is a limiting factor for the cellulose disc the use of cellulose nanofibers could provide a higher surface within the same geometrical size. Finally, an obvious drawback results from the simple bioassay design with a decreased sensitivity in the electrochemical detection itself caused by the cellulose disc on top of the electrode resulting in higher charge transfer resistance. While the use of more porous cellulose nanofibers may already be an improvement an even more efficient strategy might be the direct immobilization of produced enzyme to the electrode via an affinity tag. Being already successfully developed for phages expressing gold-binding peptides fused alkaline phosphatases, [18] a promising approach may be the modification of alkaline phosphatase with graphene-binding peptides for the direct immobilization on LIG [19,20]. Hereby the integration of LIG in microfluidic chips, as presented in chapter 2, can form the basis for not only improving the sensitivity of the assay but also a reduction of manual assay steps. Furthermore, the future use of capillary microfluidics has the potential to simplify the assay protocol even more and reduce costs without the need for pumps [21]. When considering the application in on-field applications the temperature dependency of the bacterial growth, the phage infection and the enzymatic reaction must be taken into consideration. In laboratories the incubation at 37 °C can be assured while lower temperatures have an adverse effect. For in-field applications, especially in the developing world, testing at ambient temperatures would be highly advantageous to ensure the fast, reliable testing of drinking water in particularly affected rural areas. While the enzymatic reaction performed almost equally well at 25 °C the influence of lower temperature on the growth of *E. coli* growth and the T7 phage infection needs further investigation. Within a final sensor application, the integration of a temperature sensor would enable to either adjust the incubation times depending on the temperature or normalize the assay results accordingly.

Besides the specific detection of *E. coli*, a sensor for the general detection of  $\beta$ -hemolytic bacteria was developed utilizing liposomes as a biorecognition element. The proof-of-principle was performed utilizing *S. pyogenes* as a representative of  $\beta$ -hemolytic bacteria. While POCT for *S. pyogenes* is of interest in medical diagnostics the sensor principle also should be suitable to detect pathogenic  $\beta$ -hemolytic food contaminants including *Listeria monocytogenes*, *Vibrio vulnificus*, and *Clostridium botulinum* [22]. Hereby the bacteria sample was cultivated for 7 h and directly mixed with anionic liposomes encapsulating potassium ferrocyanide. The sensor was able to distinguish  $\beta$ -hemolytic *S. pyogenes* from non-hemolytic *E. coli* whereas only in the presence of

$\beta$ -hemolytic *S. pyogenes* concentration-dependent lysis of liposomes took place and the released amount of encapsulant was quantified electrochemically. Since the interaction of liposomes with hemolytic exotoxins already was reported in the 1970s the crucial role of cholesterol content and saturation of the phospholipid tails for liposome hemolytic exotoxin interaction causing liposome lysis is known. Within this thesis additionally, the correlation of liposome size to lysis induced by *S. pyogenes* was investigated. Here, larger liposomes were found to enable a more sensitive detection, whereby the liposomes show reduced stability not only against hemolytic bacteria but also in the growth medium thus increasing the background signal. Potassium ferrocyanide was chosen as encapsulant because of its good solubility in aqueous solutions and prior results in the electrochemical quantification with LIG. The complex matrix, bacteria growth medium, was limiting the sensitivity of the electrochemical detection, since the overlap of background signals at the oxidation potential of potassium ferrocyanide strongly interfered in more sensitive electrochemical techniques, e.g. square wave voltammetry and differential pulse voltammetry. Besides the interferences of the growth medium, blocking of the electrode was observed within the assay, reducing the limit of detection for *S. pyogenes* in the presence of *E. coli* which is a huge drawback as real samples most likely contain mixtures of bacteria. In this case, the large electrode area might be disadvantageous compared to planar electrodes. Furthermore, a wider sensitivity study should include additional non-hemolytic as well as  $\alpha$ -hemolytic bacteria although earlier publications demonstrated the selectivity of liposome lysis for  $\beta$ -hemolysis [22]. Even if the assay principle is applicable for the detection of  $\beta$ -hemolysis in general the results clearly showed that a preconcentration of the bacteria is required for sensitive detection and needs to be adjusted depending on the respective bacterial growth rate.

The results demonstrate the manifold potential of electrochemical biosensors with the applied bioassay concepts. Synergies of those developments with the tLIG or LIG in microfluidic chips exhibit remarkable potential. With a view to the future, electrochemistry and its favorable miniaturization, without losing performance, and minimal instrumentation requirements is the ideal tool for the design of portable low-cost microfluidic biosensors. Within an ever-evolving Internet of Things (IoT), the demand for such solutions will continuously rise as the integration of analytical chemistry is set to become one of its integral parts. Consequently, the generation of data is prone to be shifted from centralized labs to individuals, to remote sensing locations, and to the cloud [23]. With its minimal instrumentation and low power requirements electrochemistry offers the ideal platform for this approach. To date, miniaturized potentiostats for the direct connectivity to the smartphone and/or Bluetooth solutions for wireless data transfer are already commercialized and for future IoT requirements, the direct implementation of chips for the direct communication between sensors

and real-time upload to the cloud is feasible. Hence, in combination with complex lab-based techniques, electrochemical biosensors could take on a key role among analytical sensors within the IoT. Thus, besides the development of better sensors, analytical chemists must provide answers toward true long-term, autonomous, and reliable sensing functions for various environments from the vantage point of sustainability [24].

## 6.1 References

- [1] V. Naresh, N. Lee, A Review on Biosensors and Recent Development of Nanostructured Materials-Enabled Biosensors, *Sensors*. 21 (2021) 1109. <https://doi.org/10.3390/s21041109>.
- [2] D.G. Rackus, M.H. Shamsi, A.R. Wheeler, Electrochemistry, biosensors and microfluidics: a convergence of fields, *Chem. Soc. Rev.* 44 (2015) 5320–5340. <https://doi.org/10.1039/c4cs00369a>.
- [3] J. Wang, Carbon-Nanotube Based Electrochemical Biosensors: A Review, *Electroanalysis*. 17 (2005) 7–14. <https://doi.org/10.1002/elan.200403113>.
- [4] C.M. Tilmaciu, M.C. Morris, Carbon nanotube biosensors, *Front. Chem.* 3 (2015) 59. <https://doi.org/10.3389/fchem.2015.00059>.
- [5] A. Merkoci, Graphene-based biosensors, *2D Mater.* 7 (2020) 40401. <https://doi.org/10.1088/2053-1583/aba3bf>.
- [6] R. Ye, D.K. James, J.M. Tour, Laser-Induced Graphene, *Acc. Chem. Res.* 51 (2018) 1609–1620. <https://doi.org/10.1021/acs.accounts.8b00084>.
- [7] C. Fenzl, P. Nayak, T. Hirsch, O.S. Wolfbeis, H.N. Alshareef, A.J. Baeumner, Laser-Scribed Graphene Electrodes for Aptamer-Based Biosensing, *ACS Sensors*. 2 (2017) 616–620. <https://doi.org/10.1021/acssensors.7b00066>.
- [8] L.X. Duy, Z. Peng, Y. Li, J. Zhang, Y. Ji, J.M. Tour, Laser-induced graphene fibers, *Carbon N. Y.* 126 (2018) 472–479. <https://doi.org/10.1016/j.carbon.2017.10.036>.
- [9] A. Behrent, C. Griesche, P. Sippel, A.J. Baeumner, Process-property correlations in laser-induced graphene electrodes for electrochemical sensing, *Microchim. Acta.* 188 (2021) 1–14. <https://doi.org/10.1007/s00604-021-04792-3>.
- [10] M. V. Hoang, H.J. Chung, A.L. Elias, Irreversible bonding of polyimide and polydimethylsiloxane (PDMS) based on a thiol-epoxy click reaction, *J. Micromechanics Microengineering*. 26 (2016) 105019. <https://doi.org/10.1088/0960-1317/26/10/105019>.
- [11] S. Wang, S. Yu, M. Lu, L. Zuo, Microfabrication of plastic-PDMS microfluidic devices using polyimide release layer and selective adhesive bonding, *J. Micromechanics Microengineering*. 27 (2017) 055015. <https://doi.org/10.1088/1361-6439/aa66ed>.
- [12] P. Chaijareenont, H. Takahashi, N. Nishiyama, M. Arksornnukit, Effects of silane coupling agents and solutions of different polarity on PMMA bonding to alumina, *Dent. Mater. J.* 31 (2012) 610–616. <https://doi.org/10.4012/dmj.2012-040>.
- [13] K.B. May, J. Fox, M.E. Razzoog, B.R. Lang, Silane to enhance the bond between polymethyl methacrylate and titanium, *J. Prosthet. Dent.* 73 (1995) 428–431. [https://doi.org/10.1016/S0022-3913\(05\)80070-8](https://doi.org/10.1016/S0022-3913(05)80070-8).

- [14] O.A. Carmi, G.S.A.B. Stewart, S. Ulitzur, J. Kuhn, Use of bacterial luciferase to establish a promoter probe vehicle capable of nondestructive real-time analysis of gene expression in *Bacillus* spp., *J. Bacteriol.* 169 (1987) 2165–2170. <https://doi.org/10.1128/jb.169.5.2165-2170.1987>.
- [15] J. Xu, Y. Chau, Y. Lee, Phage-based Electrochemical Sensors: A Review, *Micromachines.* 10 (2019) 855. <https://doi.org/10.3390/mi10120855>.
- [16] R. Peltomaa, I. López-Perolio, E. Benito-Peña, R. Barderas, M.C. Moreno-Bondi, Application of bacteriophages in sensor development, *Anal. Bioanal. Chem.* 408 (2016) 1805–1828. <https://doi.org/10.1007/s00216-015-9087-2>.
- [17] Y. Zhang, C. Xu, T. Guo, L. Hong, An automated bacterial concentration and recovery system for pre-enrichment required in rapid *Escherichia coli* detection, *Sci. Rep.* 8 (2018) 17808. <https://doi.org/10.1038/s41598-018-35970-8>.
- [18] D. Wang, T. Hinkley, J. Chen, J.N. Talbert, S.R. Nugen, Phage based electrochemical detection of: *Escherichia coli* in drinking water using affinity reporter probes, *Analyst.* 144 (2019) 1345–1352. <https://doi.org/10.1039/c8an01850b>.
- [19] Y. Cui, S.N. Kim, S.E. Jones, L.L. Wissler, R.R. Naik, M.C. McAlpine, Chemical functionalization of graphene enabled by phage displayed peptides, *Nano Lett.* 10 (2010) 4559–4565. <https://doi.org/10.1021/nl102564d>.
- [20] Z.E. Hughes, T.R. Walsh, What makes a good graphene-binding peptide? Adsorption of amino acids and peptides at aqueous graphene interfaces, *J. Mater. Chem. B.* 3 (2015) 3211–3221. <https://doi.org/10.1039/c5tb00004a>.
- [21] A. Olanrewaju, M. Beaugrand, M. Yafia, D. Juncker, Capillary microfluidics in microchannels: From microfluidic networks to capillary circuits, *Lab Chip.* 18 (2018) 2323–2347. <https://doi.org/10.1039/c8lc00458g>.
- [22] R. Sum, M. Swaminathan, S.K. Rastogi, O. Piloto, I. Cheong, Beta-Hemolytic Bacteria Selectively Trigger Liposome Lysis, Enabling Rapid and Accurate Pathogen Detection, *ACS Sensors.* 2 (2017) 1441–1451. <https://doi.org/10.1021/acssensors.7b00333>.
- [23] M. Mayer, A.J. Baeumner, ABC Spotlight on Analytics 4.0, *Anal. Bioanal. Chem.* 410 (2018) 5095–5097. <https://doi.org/10.1007/s00216-018-1191-7>.
- [24] M. Mayer, A.J. Baeumner, A Megatrend Challenging Analytical Chemistry: Biosensor and Chemosensor Concepts Ready for the Internet of Things, *Chem. Rev.* 119 (2019) 7996–8027. <https://doi.org/10.1021/acs.chemrev.8b00719>.

## Curriculum Vitae

### Persönliche Daten

Christian Griesche | Universitätsstraße 100A | 93053 Regensburg | christian.griesche@ur.de

Geburtsdatum: 22.06.1991 | Geburtsort: Ingolstadt | Staatsangehörigkeit: Deutsch

### Ausbildung

**06/2017 – 06/2021      Promotionsstudium, Chemie – Universität Regensburg**

Dissertation: „Development of electrochemical microfluidic biosensing strategies for microbial detection“

Institut für Analytische Chemie, Chemo – und Biosensorik

(Prof. Antje. J. Bäumner)

**10/2014 – 03/2017      Master of Science, Chemie – Universität Regensburg**

Masterarbeit: „Development of surface modified liposomes and dendrimers for signal amplification“

Institut für Analytische Chemie, Chemo – und Biosensorik

(Prof. Antje. J. Bäumner)

**10/2011 – 01/2014      Bachelor of Science, Chemie – Universität Regensburg**

Bachelorarbeit: „Untersuchungen zur Stöchiometrie und Interferenzen eines neuen photometrischen Reagens für Palladium auf Basis eines Ruthenium-Komplexes“

Institut für Analytische Chemie, Chemo – und Biosensorik

(PD Dr. Axel Dürkop)

**09/2001 – 06/2010      Allgemeine Hochschulreife – Apian Gymnasium Ingolstadt**

Leistungskurse: Mathematik, Chemie

### Sonstige Qualifikationen

1. **„Polymer Chemistry: from physical basics to microencapsulation and fiber applications, modules I and II ” – Kurs**

Prof. Margret Frey, Universität Regensburg, 2017

2. **„Qualitätsmanagement in der Analytischen Chemie“ – Kurs**

Dr. Robert Schupfner, Universität Regensburg, 2019.

## Publications

1. Nongnoot Wongkaew, Marcel Simsek, **Christian Griesche**, and Antje J. Baeumner, *Chem. Rev.* **2019**, 119, 1, 120–194. DOI: <https://doi.org/10.1021/acs.chemrev.8b00172>
2. **Christian Griesche** and Antje J. Baeumner, *Trends. Anal. Chem.*, **2020**, 128, 115906. DOI: <https://doi.org/10.1016/j.trac.2020.115906>
3. Cornelia A. Hermann, Michael Mayer, **Christian Griesche**, Franziska Beck, and Antje J. Baeumner, *Analyst* **2021**, 146, 997 – 1003. DOI: <https://doi.org/10.1039/D0AN02027C>
4. **Christian Griesche**, Kilian Hoecherl, and Antje J. Baeumner, *ACS Appl. Nano Mater.* **2021**, 4, 3, 3114–3121. DOI: <https://doi.org/10.1021/acsanm.1c00299>
5. Arne Behrent, **Christian Griesche**, Paul Sippel, and Antje J. Baeumner, *Microchimica Acta* **2021**, 188, 159. DOI: <https://doi.org/10.1007/s00604-021-04792-3>



## **Presentations**

### **Oral Presentations**

- 2017** 13<sup>th</sup> International Students Conference, Prague, Czech Republic
- 2019** 2<sup>nd</sup> European BioSensor Symposium, Florence, Italy
- 2021** Virtual Pittcon 2021, Pittsburgh Conference & Exposition on Analytical Chemistry and Applied Spectroscopy

### **Poster Presentations**

- 2017** 1<sup>st</sup> European / 10<sup>th</sup> German BioSensor Symposium, Potsdam, Germany
- 2018** Gordon Research Conference & Seminar "Bioanalytical Sensors", Newport, RI, USA
- 2021** Virtual Pittcon 2021, Pittsburgh Conference & Exposition on Analytical Chemistry and Applied Spectroscopy

## **Eidesstattliche Erklärung**

Ich erkläre hiermit an Eides statt, dass ich die vorliegende Arbeit ohne unzulässige Hilfe Dritter und ohne Benutzung anderer als der angegebenen Hilfsmittel angefertigt habe; die aus anderen Quellen direkt oder indirekt übernommenen Daten und Konzepte sind unter Angabe des Literaturzitats gekennzeichnet.

Weitere Personen waren an der inhaltlich-materiellen Herstellung der vorliegenden Arbeit nicht beteiligt. Insbesondere habe ich hierfür nicht die entgeltliche Hilfe eines Promotionsberaters oder anderer Personen in Anspruch genommen. Niemand hat von mir weder unmittelbar noch mittelbar geldwerte Leistungen für Arbeiten erhalten, die im Zusammenhang mit dem Inhalt der vorgelegten Dissertation stehen.

Die Arbeit wurde bisher weder im In- noch im Ausland in gleicher oder ähnlicher Form einer anderen Prüfungsbehörde vorgelegt.

---

Ort, Datum

Unterschrift